

# HYBRID MESON DECAY FROM THE LATTICE

by

Ziwen Fu

A dissertation submitted to the faculty of  
The University of Utah  
in partial fulfillment of the requirements for the degree of

Doctor of Philosophy

Department of Physics

The University of Utah

December 2006

## ABSTRACT

Besides the conventional hadrons containing valence quarks and valence antiquarks, quantum chromodynamics (QCD) suggests the existence of the hybrid hadrons containing valence gluons in addition to the quarks and antiquarks, and some experiments may have found some. A decisive experimental confirmation of its existence, however, is still needed. At present, lattice simulations have offered the practicable ways of theoretically guiding us to search for the hybrid states.

In this dissertation, we study the spectroscopy and the decay rate of the heavy hybrid mesons with a heavy  $b$  quark, a heavy  $\bar{b}$  antiquark and a gluon ( $b\bar{b}g$ ) to the chosen channels, and use lattice methods to calculate the transition matrix elements in full QCD. We are particular interested in the spin-exotic hybrid mesons.

For sufficiently heavy quarks (e.g.,  $b$  quark), we use the leading Born-Oppenheimer (LBO) approximation to calculate the static potential energy at all  $b\bar{b}$  separations. Then, by solving the Schrödinger equation with this potential, we reconstruct the motion of the heavy quarks. In a similar way we can determine decay rates. In this dissertation, we use the lattice method to calculate the mass of the  $f_0$  meson at a single lattice spacing and light quark mass, namely,  $m_{f_0} = (768 \pm 136)$  MeV. Most of all we consider the decay channels involving the production of a scalar meson. We obtain the partial decay rate ( $\Gamma$ ) for the channel  $H \rightarrow \chi_b + \pi + \pi$ , namely,  $\Gamma = 3.62(98)$  MeV. All of our results are consistent with those of other researchers. Knowledge of the masses and the decay rates should help us considerably in experimental searches for the hybrid mesons.

# CONTENTS

<b>ABSTRACT</b> .....	ii
<b>ACKNOWLEDGEMENTS</b> .....	v
<b>CHAPTERS</b>	
<b>1. INTRODUCTION</b> .....	1
<b>2. INTRODUCTION TO PARTICLE PHYSICS</b> .....	4
2.1 Quark model .....	4
2.2 Some conservation laws .....	8
2.2.1 Parity .....	9
2.2.2 Isospin .....	9
2.2.3 Charge conjugation .....	11
2.3 Quarkonium .....	12
<b>3. LATTICE QCD</b> .....	14
3.1 Overview of continuum QCD .....	14
3.1.1 Continuum gauge field theory in QCD .....	15
3.1.2 Continuum QCD formalism .....	19
3.2 QCD on a lattice .....	23
3.2.1 Pure gauge action on lattice .....	24
3.2.2 Fermion action on lattice .....	27
3.2.3 Tastes of Kogut-Susskind staggered fermions .....	31
3.3 Simulation algorithm .....	33
3.3.1 Numerical simulation and upadating process .....	33
3.3.2 Hybrid-molecular dynamics “R algorithm” .....	36
<b>4. LEADING BORN-OPPENHEIMER (LBO)</b> .....	40
4.1 Notation from molecular physics .....	40
4.2 Born-Oppenheimer approximation .....	41
4.3 APE smearing .....	43
4.4 Computation of the static potentials .....	44
4.4.1 $C_{AA}$ Correlator .....	45
4.4.2 $C_{HH}$ Correlator .....	47
4.4.3 The results for the static potentials .....	49
4.4.4 Setting the scale .....	50
4.4.5 Fitting procedure .....	51
4.5 Hybrid quarkonium .....	54

<b>5. HYBRID MESON DECAY CHANNEL</b>	60
5.1 Hybrid states on the lattice	60
5.2 Hybrid meson decay model	61
<b>6. OUR CALCULATIONAL METHOD</b>	63
6.1 $C_{BB}$ correlator	63
6.1.1 Replica trick in lattice	63
6.1.2 The operator for the $C_{BB}$ correlator	64
6.1.3 Direct method	66
6.1.4 Random source method	67
6.2 $C_{HAB}$ correlator	68
<b>7. HYBRID MESON DECAY FROM THE LATTICE</b>	72
7.1 Perturbation expansion for $C_{HAB}$ correlator	72
7.2 Decays from the lattice	75
<b>8. OUR NUMERICAL RESULTS</b>	79
8.1 $f_0$ meson	79
8.1.1 Operator for $f_0$ meson	79
8.1.2 Procedures for determining the $f_0$ mass	80
8.2 Lattice transition matrix element	83
8.2.1 The wave function of the excited gluonic states	83
8.2.2 Simulation procedure	83
8.2.3 Our numerical results for decay rate	84
<b>9. CONCLUSION</b>	94
9.1 Evidence for $f_0$ meson	94
9.2 Evidence for light-quark hybrid exotic mesons	95
9.3 Hybrid exotic quarkonium decay	96
9.4 Summary	97
<b>APPENDICES</b>	
<b>A. THE <math>PC</math> OF THE HYBRID MESON</b>	98
<b>B. BUBBLE CONTRIBUTION FOR <math>a_0</math> CORRELATOR</b>	101
<b>C. BUBBLE CONTRIBUTION FOR <math>f_0</math> CORRELATOR</b>	108
<b>D. LBO TREATMENT OF DECAY CHANNEL FOR HYBRID</b>	111
<b>E. THREE-BODY PHASE SPACE</b>	117
<b>REFERENCES</b>	120

## ACKNOWLEDGEMENTS

First of all, I would like to thank the MILC collaboration, which has developed a parallel computer code for the simulation of  $SU(3)$  lattice gauge theory. Most of the computer code that I used for my Ph.D study was adapted or modified from the MILC code. Moreover, I was a user of MILC collaboration's lattice configurations during my Ph.D study.

I thank Urs Heller for his data of lattice Coulombic correction term. I thank C. Bernard and Sasa Prelovsek for their help in understanding the chiral perturbation theory and the bubble contribution to the scalar correlator.

Finally, I thank especially my advisor, Carleton DeTar. This project is quite difficult. We encountered many problems. Throughout, Prof. DeTar always found ways to solve the problem, and allow my studies to continue. Beyond that, Prof. DeTar is not only an expert in physics and math, but also in computer science. The computer codes I use in this dissertation were developed under his guidance. I could not have finished this dissertation without his help, encouragement, and extraordinary patience. Also Prof. DeTar's personality and enthusiasm for physics will inspire me to continue to pursue a career in physics.

An allocation of computer time from the Center for High Performance Computing at the University of Utah is gratefully acknowledged. During the development of this dissertation, I devoted my life to CHPC's ICEBOX system. I experienced happiness and bitterness on this machine. ICEBOX now is retired; I will miss her.

# CHAPTER 1

## INTRODUCTION

Besides the conventional hadrons, quantum chromodynamics (QCD) predicts the existence of the hybrid hadrons, which are hadrons but also contain the excited gluon fields. Early results in  $e^+e^-$  annihilation cross section from the CUSB and CLEO collaborations [1, 2] showed that there exists a complex resonance structure in the energy region above the  $\Upsilon(4S)$  (near 10.7 GeV), where the possible lowest hybrid states ( $b\bar{b}g$ ) are predicted in Ref. [3]. However, because it is difficult to differentiate a resonance from a threshold effect, we just have a “hint” of the existence of the hybrid states, a decisive experimental confirmation is still needed.

We need some theoretical guidance to search efficiently for the hybrid states. Due to the nonperturbative nature of the gluons, however, a perturbative theory in this field is still not available. Hence, a clear understanding the hybrid states by analytical methods is very difficult. At present, the lattice simulations have offered practical ways of theoretically guiding us to search for the hybrid states.

The heavy hybrid mesons can be investigated directly by the leading Born-Oppenheimer (LBO) approximation. The results from our LBO approximation can compare with the corresponding results from other people’s experiments. We focus on the heavy hybrid mesons ( $Q\bar{Q}g$ ), which consist of a heavy quark ( $Q$ ) and a heavy antiquark ( $\bar{Q}$ ) plus a gluon ( $g$ ). We study its spectroscopy and the decay amplitude from the heavy hybrid meson to  $(Q\bar{Q})(q\bar{q})$ , and use lattice methods to calculate the transition matrix elements in full QCD [4]. Finally, we study its phenomenological implications. We are particular interested in the spin-exotic hybrid meson, which is the meson with  $J^{PC}$  quantum numbers which are not permitted in the current quark model. The lightest one is believed to be with quantum numbers  $J^{PC} = 1^{-+}$  [5],

which does not mingle with a nonhybrid  $Q\bar{Q}$  bound state [4].

The spectroscopy of the hybrid mesons (including spin-exotic hybrid mesons) has been extensively studied over the past years [5, 6]. The BO approximation was proposed for the study of the hybrids states in Refs. [7, 8]. For sufficiently heavy quarks (e.g.,  $b$  quark), the LBO approximation justifies a treatment in which the heavy quark ( $Q$ ) and antiquark ( $\bar{Q}$ ) are regarded as approximately static, and we assume that the gluon field adjusts rapidly to their movement. Hence, for various gluonic excitations of the flux tube of  $Q\bar{Q}$ , we compute its corresponding static potential energy at  $Q\bar{Q}$  separation  $R$ . Then by numerically solving the Schrödinger equation with this potential, we reproduce the motion of the heavy quarks. In a similar way we can calculate the decay rate.

Decay modes are also intensively investigated in Ref. [4]. However, at present, our knowledge about the decay channels is still limited. We make a contribution to the understanding of the spectroscopy of the hybrid mesons and its decay model. There are many new features in our simulation: (1) We adopt gauge configurations with improved actions, which include the Symanzik improvements at 1-loop level, and “Asqtad” fermion action [9]. (2) We choose the improved wave functions for the spin-exotic gluon channels, which are used to integrate all the decay rate at all  $Q\bar{Q}$  separation  $R$ . (3) We consider decay channels  $H \rightarrow \chi_b + \pi + \pi$  involving the emission of two pions (here  $H$  stands for hybrid exotic state). (4) The mass of the dynamical sea quark we choose is closer to the physical value.

Our project needs three classes of adjustable input parameters: 1) lattice spacing:  $a$ , 2) light quark masses ( $u, d, s$  quarks), 3) the mass of the bottom quark ( $b$  quark). These input parameters are obtained from experiment. We obtain the masses of  $u, d, s$  quarks from the masses of  $\pi, K$  mesons, and we obtain the lattice spacing  $a$  from the splittings of  $\Upsilon(2S) - \Upsilon(1S)$  and  $\Upsilon(1P) - \Upsilon(1S)$  in  $\Upsilon$  spectrum. And from the  $B$  meson, we obtain the mass of the bottom quark [10]. This project help us gain the knowledge about “soft gluons.” Furthermore, we can predict the mass of some mesons, e.g., the  $f_0$  meson. Most importantly, we can calculate the partial transition rate  $\Gamma$ , which has been poorly understood. Knowledge of the

masses and decay rates helps us in experimental searches for the hybrid mesons.

In this dissertation, we use the MILC version of the Kogut-Susskind staggered quark action, and the gauge action is the Lüscher Symanzik improved action. Also we use gauge configurations, which were generated by the hybrid-molecular dynamics “R algorithm” [11]. These configurations contain three flavors: two light quark ( $u$ ,  $d$ ), and a strange ( $s$ ) quark. In our simulation, the light quarks are degenerate in mass, and we choose the bare strange quark mass and up, down quarks mass to be close to the corresponding physical values (i.e.,  $am_u = 0.005$ , and  $am_s = 0.05$ ). From Ref. [12] we find the physical mass of the pion meson is about 140 MeV, from our lattice calculation, we get the mass of the pion meson is about 230 MeV. The lattice space  $a$  is in our simulation of around 0.12 fm [10].

This dissertation is organized as follows: In Chapter 2, we provide background material on particle physics. We first give a brief review of the quark model. Then we briefly discuss a few conservation laws. Finally, we discuss about the quarkonium (heavy quark, antiquark states). In Chapter 3, we provide background material about QCD. First we give an overview of continuum QCD. Then we give an overview of lattice QCD. In Chapter 4, we use the LBO approximation to study the spectroscopy of the hybrid mesons. We first study the method of the LBO approximation. Then we introduce the static potential. Finally, we calculate hybrid quarkonium states through the LBO approximation. In Chapter 5, we first briefly review the hybrid states on the lattice. Then we give an overview of hybrid meson decays. Finally, we give a overview of the decays from the lattice. In Chapter 6, we explain our calculational method in detail. In Chapter 7, we first use time-dependent perturbation theory to study the  $C_{HAB}$  correlator. Then we introduce a method to extract transition amplitude  $x$  directly from lattice. In Chapter 8, we give all the lattice numerical simulation results. First we present the calculation of the mass of the  $f_0$  meson. Then we show the detailed procedure to obtain lattice transition amplitude  $x$ , and calculate the decay rate. In Chapter 9, we first discuss the evidence for the  $f_0$  meson and the hybrid exotic mesons. Then we discuss hybrid exotic quarkonium decay. Finally, we summarize our results.



## CHAPTER 2

### INTRODUCTION TO PARTICLE PHYSICS

Particle physics is the study of the fundamental particles that make up matter, and how they interact with each other [13]. At present, the “quarks,” along with “leptons,” are believed to be fundamental, and the quark model is a popular theory in this field.

In this chapter, we provide background material about particle physics. We first give a brief review of the quark model. Then briefly discuss a few conservation laws. Finally we discuss about quarkonium (i.e., the bound states of heavy quarks and antiquarks). We focus on just a few details needed for this dissertation. Several good textbooks [13][14] provide comprehensive background material.

#### 2.1 Quark model

In particle physics, we define a hadron as a subatomic particle which takes part in the strong nuclear force. In the current quark model, hadrons are made up of quarks, antiquarks, and gluons. Usually hadrons are further classified into many types (e.g., baryons and mesons, etc). In this dissertation we are interested only in baryons and mesons.

In 1961 Murray Gell-Mann [13] introduced the Eightfold way to arrange the hadrons which were discovered at that time. The eight lightest baryons ( $n$ ,  $p$ ,  $\Sigma^+$ ,  $\Sigma^-$ ,  $\Sigma^0$ ,  $\Lambda$ ,  $\Xi^-$ ,  $\Xi^0$ ) and the eight lightest mesons ( $K^0$ ,  $K^+$ ,  $K^-$ ,  $\bar{K}^0$ ,  $\pi^0$ ,  $\pi^+$ ,  $\pi^-$ ,  $\eta$ ) fill a hexagonal array, with two particles at the center, according to their charge and strangeness. They are called a baryon octet, and meson octet, respectively. <sup>1</sup>

---

<sup>1</sup>See the figures on page 33, 34 in Ref. [13].

In order to explain and understand the Eightfold way, in 1964, Murray Gell-Mann and George Zweig independently proposed [13] that just three fundamental constituents (and their antiparticles) combined in different ways could explain the Eightfold way. Murray Gell-Mann called these elementary constituents “quarks,” and the three types (or “flavors”) of quarks were named up ( $u$ ), down ( $d$ ), and strange ( $s$ ), respectively [13].

In the late 1960s the evidence for the existence of “quarks” became clear. In 1974 a new particle  $J/\Psi$  [13] was discovered, which was later understood to be a bound state of a new quark-antiquark pair ( $c\bar{c}$ ). The new fourth quark is known as charm ( $c$ ). In 1977 another new meson called the Upsilon ( $\Upsilon$ ) [13] was discovered at Fermilab, which was later shown to be the bound state of the new quark-antiquark pair ( $b\bar{b}$ ). The new fifth quark was called bottom ( $b$ ). Finally, in 1995, the evidence for the existence of the “top” ( $t$ ) quark was obtained at Fermilab. Hence, the current quark model with six “flavors” was fulfilled.

In the current quark model, we have the six quarks: up, down, strange, charm, bottom and top. By convention we usually label them by their first letters:  $u$ ,  $d$ ,  $s$ ,  $c$ ,  $b$  and  $t$ . Moreover, each quarks has its partner antiquarks. We label them  $\bar{u}$ ,  $\bar{d}$ ,  $\bar{s}$ ,  $\bar{c}$ ,  $\bar{b}$ ,  $\bar{t}$ , respectively. The charges of up, down, strange, charm, bottom (or beauty), and top (or truth) quarks are  $\frac{2}{3}e$ ,  $-\frac{1}{3}e$ ,  $-\frac{1}{3}e$ ,  $\frac{2}{3}e$ ,  $-\frac{1}{3}e$ ,  $\frac{2}{3}e$  respectively, where  $e$  is the charge of the electron. For each quark ( $q$ ), the corresponding antiquark ( $\bar{q}$ ) has the opposite charge. Hence, the charges of antiup ( $\bar{u}$ ), antidown ( $\bar{d}$ ), antistrange ( $\bar{s}$ ), anticharm ( $\bar{c}$ ), antibottom ( $\bar{b}$ ), antitop ( $\bar{t}$ ) quarks are  $-\frac{2}{3}e$ ,  $\frac{1}{3}e$ ,  $\frac{1}{3}e$ ,  $-\frac{2}{3}e$ ,  $\frac{1}{3}e$ ,  $-\frac{2}{3}e$ , respectively [13].

The six types of quarks (plus their six antiquarks) are classified into three pairs, which are listed in Table 2.1. They are the up-down, the charm-strange, and the top-bottom multiplets. The top block is the first generation, the middle block is the second generation, and the bottom block is the third generation [13].

Like quarks, there are six types of the leptons [13], which also are classified into three pairs: electron-neutrino ( $e - \nu_e$ ), muon-neutrino ( $\mu - \nu_\mu$ ), and tau-neutrino ( $\tau - \nu_\tau$ ). The electron, muon, and tau each carry a negative charge, but the three

**Table 2.1.** Three quark generation. Where  $Q$  is the electric charges,  $D$  is the “downness,”  $U$  is the “upness,”  $S$  is the “strangeness,”  $C$  is the “charm,”  $B$  is the “beauty,” and  $T$  is the “truth.”

Flavor	Mass( $GeV/c^2$ )	$Q$	$D$	$U$	$S$	$C$	$B$	$T$
$d$	0.08	$-\frac{1}{3}$	-1	0	0	0	0	0
$u$	0.004	$+\frac{2}{3}$	0	1	0	0	0	0
$s$	0.15	$-\frac{1}{3}$	0	0	-1	0	0	0
$c$	1.5	$+\frac{2}{3}$	0	0	0	1	0	0
$b$	4.7	$-\frac{1}{3}$	0	0	0	0	-1	0
$t$	176	$+\frac{2}{3}$	0	0	0	0	0	1

neutrinos ( $\nu_e, \nu_\mu, \nu_\tau$ ) carry no charge.

The quark model assumes [13] that the quarks bind with each other to form the particles. There are two basic types of the combination. The first type of the combination is “baryons,” which are made up of three quarks. (Similarly, an antibaryon is made up of three antiquarks). Listing all the combination of three quarks gives the baryon decuplet [13]. One example of a baryon is the proton ( $p$ ), the proton is made up of “ $uud$ .”<sup>2</sup> whose charge is +1.

Another type is the meson, which is made up of a quark and an antiquark. Counting all the quark-antiquark combinations yields the mesons in which we are especially interested. We list these mesons in Table 2.2, the top block is the meson nonet, the middle block contains “charmed mesons” [12], and the bottom block contains “bottom mesons” [12]. The “charmed mesons” and “bottom mesons” are heavy.

The quarks and antiquarks carry spin  $\frac{1}{2}$ . When a quark and an antiquark bind to form the mesons in a state of zero orbital angular momentum ( $L = 0$ ), there are spin-0 combinations that are called “pseudoscalar meson” (i.e.,  $\pi^+$ ,  $\pi^-$ ,  $\pi^0$ ,  $K^0$ ,  $K^+$ ,  $K^-$ ,  $\bar{K}^0$ ,  $\eta$ ,  $\eta'$ ), and spin-1 combinations that are called “vector meson” (i.e.,  $\rho^+$ ,  $\rho^-$ ,  $\rho^0$ ,  $K^{*0}$ ,  $K^{*+}$ ,  $K^{*-}$ ,  $\bar{K}^{*0}$ ,  $\phi$ ,  $\omega$ ). In the language of group theory, each quark can occur as spin-up ( $m_s = \frac{1}{2}$ ) or spin-down ( $m_s = -\frac{1}{2}$ ) states, and two spin states belong to the fundamental representation of spin  $SU(2)$  (**2**). Similarly, each

---

<sup>2</sup>Here we just include the valence quark. Later in this chapter we will consider the sea quark,

**Table 2.2.** The top block is the meson nonet, the middle block is “charmed mesons,” and the bottom block is “bottom mesons.” Here we just include the mesons which we are interest in this dissertation. Where the  $Q$  stand for charge, and  $S$  is strangeness, the  $C$  stand for charm, and  $B$  is bottom (or beauty).

$q\bar{q}$	$Q$	$S$	$C$	$B$	Meson
$u\bar{u}$	0	0	0	0	$\pi^0$
$u\bar{d}$	1	0	0	0	$\pi^+$
$d\bar{u}$	-1	0	0	0	$\pi^-$
$d\bar{d}$	0	0	0	0	$\eta$
$u\bar{s}$	1	1	0	0	$K^+$
$d\bar{s}$	0	1	0	0	$K^0$
$s\bar{u}$	-1	-1	0	0	$K^-$
$s\bar{d}$	0	-1	0	0	$\bar{K}^0$
$s\bar{s}$	0	0	0	0	$\eta'$
$c\bar{d}$	1	0	1	0	$D^+$
$c\bar{u}$	0	0	1	0	$D^0$
$\bar{c}u$	0	0	-1	0	$\bar{D}^-$
$\bar{c}d$	-1	0	-1	0	$D^-$
$u\bar{b}$	1	0	0	-1	$B^+$
$d\bar{b}$	0	0	0	-1	$B^0$
$\bar{d}b$	0	0	0	1	$\bar{B}^0$
$\bar{u}b$	-1	0	0	1	$B^-$

antiquark can also occur as spin-up ( $m_s = \frac{1}{2}$ ) or spin-down ( $m_s = -\frac{1}{2}$ ) states, and two spin states belong to the complex conjugate fundamental representation of spin  $SU(2)$  ( $\bar{\mathbf{2}}$ ). We combine two two-dimensional fundamental representations ( $\mathbf{2}$ , and  $\bar{\mathbf{2}}$ ) of spin  $SU(2)$  to obtain a spin triplet ( $\mathbf{3}$ , spin  $s = 1$ ) and a spin singlet ( $\mathbf{1}$ , spin  $s = 0$ ),

$$\mathbf{2} \otimes \bar{\mathbf{2}} = \mathbf{3} \oplus \mathbf{1}. \quad (2.1)$$

Hence, the spin singlet state is pseudoscalar mesons (namely, the total spin  $s = 0$ ), and the spin triplet state is vector mesons (namely, the total spin  $s = 1$ ) [13].

In addition to the electric charge, quarks also carry “color charge” [13]. In the language of group theory, each quark takes “red” ( $r$ ), “green” ( $g$ ), or “blue” ( $b$ ), and the three color states belong to the fundamental representation of color  $SU(3)$  ( $\mathbf{3}$ ). Similarly, each antiquark occurs as “antired” ( $\bar{r}$ ), “antigreen” ( $\bar{g}$ ), or “antiblu” ( $\bar{b}$ ), and three anticolor states belong to the complex conjugate fundamental repre-

sentation of color  $SU(3)$  ( $\bar{\mathbf{3}}$ ). We combine two three-dimensional fundamental representations ( $\mathbf{3}$ , and  $\bar{\mathbf{3}}$ ) of color  $SU(3)$  to form a color octet ( $\mathbf{8}$ ) and a color singlet ( $\mathbf{1}$ ),

$$\mathbf{3} \otimes \bar{\mathbf{3}} = \mathbf{8} \oplus \mathbf{1}. \quad (2.2)$$

The quark model asserts that all macroscopically isolated particles must be “color singlet.” For example, mesons are the combinations of a quark of color and a quark of its anticolor to form a neutral color charge.

The force between color charged particles is the “strong force.” The carriers of the strong force are gluons [13], which carry no electrical charge, but have both a color and an anticolor charge. According to Eq. (2.2), the gluon can exist as color octet states or color singlet state. However if the gluon of color  $SU(3)$  singlet state exists as mediator, it can also occur as a free particle. An interesting fact about quarks and gluons is that we have never been observed a macroscopically isolated quark or gluon. For this reason, the color-charged quarks (or gluons) are believed to be confined within a hadron [13]. Hence, we have eight physical gluon states.

By convention valence quarks for a given hadron are the quarks (or antiquarks) that give rise to the quantum numbers of the given hadron. For example: the proton’s quantum numbers are characterized by two “ $u$ ” and one “ $d$ ” quark valence quark. At any given momentum the proton may contains extra  $u\bar{u}$  pairs, or  $d\bar{d}$  pairs, or even  $s\bar{s}$  pairs,  $c\bar{c}$  pairs, etc. We call these extra quarks sea quarks [13].

## 2.2 Some conservation laws

The study of the interactions and the decays has resulted in a few conservation laws. For the strong interactions and decay, the conserved quantities include baryon number ( $A$ ), lepton number ( $L$ ), upness ( $U$ ), downness ( $D$ ), strangeness ( $S$ ), charm ( $\bar{C}$ ), bottom ( $B$ ), top ( $T$ ), isospin ( $I$ ), parity ( $P$ ), and charge-conjugation ( $C$ ). These conservation laws, together with the classical conservation laws (such as the conservation of energy, momentum, charge) should apply in the strong interactions and decays.

In this section, we just focus on the conservation laws of parity ( $P$ ), isospin ( $I$ ), and charge-conjugation ( $C$ ), which are needed for this dissertation.

### 2.2.1 Parity

Many physical processes like strong interactions have a property of parity invariance (or “mirror symmetry”). This means that the mirror image of any physical process can also occur with the same probability. In this subsection, we repeat some discussion in Sec. 4.6 in Ref. [13].

In physics, the parity basic operator is an inversion operation, in which the object is flipped to the opposite location through the origin [13].

Quarks have an intrinsic parity, which is defined to be  $+1$ , and for an antiquark the parity is  $-1$  [13]. Since the quantum number parity for the composite system is multiplicative, the intrinsic parity of the baryon octet and decuplet is  $+1$ , and the intrinsic parity of the meson is  $-1$  [13]. For the excited states of the mesons, the parity is given by [13]

$$P = (-1)^{l+1}, \quad (2.3)$$

where  $l$  is the orbital angular momentum of the meson.

The parity is not conserved by the weak force, with the result that all the neutrinos are found to be “left-handed” [13].

### 2.2.2 Isospin

Isospin is a physical term that was introduced to describe a group of particles that has almost the same mass [13]. For example, the doublet of the proton and the neutron is said to have isospin  $\frac{1}{2}$  ( $I = \frac{1}{2}$ ), with the third component  $I_3 = +\frac{1}{2}$  for the proton and  $-\frac{1}{2}$  for the neutron. Another example is the three pions ( $\pi^+, \pi^0, \pi^-$ ), which compose a triplet. Hence, its isospin is 1. The third components are  $+1$  for the  $\pi^+$ ,  $0$  for  $\pi^0$ , and  $-1$  for  $\pi^-$ , respectively.

In 1932 Heisenberg suggested that isospin is conserved in strong interactions. In the language of group theory, we can declare that strong interactions are invariant under an internal  $SU(2)$  symmetry (or internal isospin symmetry) [13]. Hence, nucleon ( $p$ , and  $n$ ) is the two-dimensional representation of the  $SU(2)$  ( $I = \frac{1}{2}$ ), and

pion meson ( $\pi^+$ ,  $\pi^0$ , and  $\pi^-$ ) is the three-dimensional representation of the  $SU(2)$  ( $I = 1$ ).

Isospin for the particles is related to other quantum numbers for the particles by general Gell-Mann-Nishijima formula [13]

$$Q = \frac{A + U + D + S + C + B + T}{2}, \quad (2.4)$$

where  $Q$  is the charge of the particle,  $A$  is baryon number,  $U$  is upness,  $D$  is downness,  $S$  is strangeness,  $C$  is charm,  $B$  is bottom, and  $T$  is the top [14].

At the current quark model, the bare masses of the up and down quarks are close. Hence, the “up” and “down” quarks can form an isospin doublet ( $I = \frac{1}{2}$ ), and all the other flavors ( $s, c, b, t$ ) carry isospin zero [13]. By convention the third component of isospin of the up( $u$ ) quark is assigned to be  $\frac{1}{2}$ , and the third component of isospin of the down ( $d$ ) quark is assigned to be  $-\frac{1}{2}$  (like proton and neutron) [13]:

$$u = \left| \frac{1}{2} \quad \frac{1}{2} \right\rangle, \quad d = \left| \frac{1}{2} \quad -\frac{1}{2} \right\rangle. \quad (2.5)$$

The antiup ( $\bar{u}$ ) and antidown ( $\bar{d}$ ) quarks also form an isospin doublet [13]:

$$\bar{u} = \left| \frac{1}{2} \quad -\frac{1}{2} \right\rangle, \quad \bar{d} = -\left| \frac{1}{2} \quad \frac{1}{2} \right\rangle. \quad (2.6)$$

By convention the third component of the isospin of  $\bar{u}$  quark is assigned to be  $-\frac{1}{2}$  and the third component of the isospin of the  $\bar{d}$  quark is assigned to be  $\frac{1}{2}$  [13].

If we add two particles whose isospins are  $I = \frac{1}{2}$ , we obtain an “isotriplet” [13]

$$|1 \quad 1\rangle = -u\bar{d}, \quad |1 \quad 0\rangle = \frac{u\bar{u} - d\bar{d}}{\sqrt{2}}, \quad |1 \quad -1\rangle = d\bar{u}, \quad (2.7)$$

and an “isosinglet”

$$|0 \quad 0\rangle = \frac{u\bar{u} + d\bar{d}}{\sqrt{2}}. \quad (2.8)$$

In the language of group theory, the  $u, d$  quarks belong to the fundamental representation of isospin  $SU(2)$  ( $\mathbf{2}$ ), and the  $\bar{u}, \bar{d}$  quarks belong to the complex conjugate fundamental representation of spin  $SU(2)$  ( $\bar{\mathbf{2}}$ ). We combine two two-

dimensional representations ( $\mathbf{2}$ , and  $\bar{\mathbf{2}}$ ) of spin  $SU(2)$  to obtain an “isotriplet” ( $\mathbf{3}$ , isospin  $I = 1$ ) and an “isosinglet” ( $\mathbf{1}$ , isospin  $I = 0$ ),

$$\mathbf{2} \otimes \bar{\mathbf{2}} = \mathbf{3} \oplus \mathbf{1}. \quad (2.9)$$

For the pseudoscalar mesons the isotriplet is the pion. For the vector mesons the isotriplet is the  $\rho$  meson. Hence, the quark content (or the wave function of “flavor”) for  $\pi^0$ (or  $\rho^0$ ) meson is given by [13]

$$\pi^0, \rho^0 = \frac{u\bar{u} - d\bar{d}}{\sqrt{2}}. \quad (2.10)$$

Isospin is connected with a conservation law, as shown by the strong process

$$\begin{array}{ccc} p + p & \longrightarrow & d + \pi^+ \\ I \quad \frac{1}{2} \quad \frac{1}{2} & & 0 \quad 1 \end{array} \quad (2.11)$$

Here we assume the isospin of the deuteron ( $d$ ) is consistent with the observation that there are no other bound state of two nucleons [14]. It is obvious that the above process conserves charge, angular momentum, baryon number, and isospin.

### 2.2.3 Charge conjugation

Charge conjugation is a physical operation that replaces each particle in a process with its the corresponding antiparticle [13]. It changes the sign of the charge, baryon number, lepton number, strangeness number, charm number, beauty number, and truth number of the particle. It does not, however, change the mass, energy, momentum, and spin of the particle [13].

We can show that for a system of a quark (spin- $\frac{1}{2}$  particle) and its antiquark, the charge conjugation( $C$ ) is given by [14]

$$C = (-1)^{l+s}, \quad (2.12)$$

where  $l$  is total orbital angular momentum of the meson, and  $s$  is total spin of the meson.

If we consider the ground states ( $l = 0$ ) of mesons, then for the pseudo-scalar mesons ( $s = 0$ ), hence  $C = +1$ ; for the vector mesons ( $s = 1$ ), thus  $C = -1$ .



One kind of the notation for these states is to indicate their total angular momentum ( $j = l + s$ ), parity, and charge conjugation explicitly. For the ground states ( $l = 0$ ) of the pseudoscalar meson, the total angular momentum is zero (i.e.,  $j = 0 + 0 = 0$ ), and they have negative parity and positive charge conjugation ( $C$ ). Hence

$$J^{PC} = 0^{-+}. \quad (2.13)$$

For the ground states of the vector mesons,  $s = 1$ , we obtain  $j = 1$ , and they have negative parity and negative charge conjugation ( $C$ ). Hence

$$J^{PC} = 1^{--}. \quad (2.14)$$

Charge conjugation is conserved for strong and electromagnetic interactions, but not for weak interactions. We know that charge conjugation turns a left-handed neutrino into a left-handed antineutrino, and changes right-handed neutrino into a right-handed antineutrino. In weak processes, there exist only left-handed neutrinos and only right-handed antineutrinos. Hence, it is obvious that charge conjugation is not conserved in weak processes [13, 14].

### 2.3 Quarkonium

In the quark model, we regard all the mesons ( $q_1\bar{q}_2$ ) as two-particle bound states [13]. The potential model works well for hydrogen and positronium. It is reasonable to ask whether the potential model works for the mesons or not [13]?

After the discovery of the bound state  $c\bar{c}$  (or charmonium states), potential models of QCD have become an important tool in understanding quarkonium (i.e., the bound state of a heavy quark and heavy antiquark, e.g.,  $\Upsilon(b\bar{b})$ ,  $c\bar{b}$ , etc.) [13].

In hydrogen and positronium model, there exists only Coulombic potential [13]. (In QED, the force between electrical charges is mediated by the exchange of photons.) However, for the meson, we know that the force between color charged particles through gluon exchange is very powerful. Thus, the short distance behavior of QCD is dominated by this “strong force.” Hence, the potential of a meson should be Coulombic potential at short range [13]. However, due to quark

confinement, the potential can increase indefinitely when the distance  $r$  between quark and antiquark becomes large. Here we assume no  $q\bar{q}$  pair production. At this range, it is standard to choose a linear fit (i.e.,  $V(r) \sim r$ ) (and it is confirmed in numerical simulation). Thus, in this dissertation, we choose the overall potential to be [13, 14]. In Chapter 4, we will note that for the  $\Pi_u$  potential, we choose a different model.

$$V(r) = -\frac{k_1}{r} + k_2 r, \quad (2.15)$$

where  $k_1, k_2$  are just two constants.

The mesons, which are made up of light quarks (i.e.,  $u, d, s$ ), are intrinsically relativistic [13]. The mesons, which are made up of heavy quarks (i.e.,  $b, t$ ), are intrinsically nonrelativistic [13]. The classical quantum mechanics can describe these systems pretty well. From Fig. 5.7 in [13], we can see that potential model describe the charmonium very well. For the bound state  $b\bar{b}$  (also called bottomonium), the potential model describes it very well also. Please see Fig. 5.9 in [13].

In this dissertation we study the hybrid quarkonium (or hybrid meson). Hybrid mesons are the bound state of  $Q\bar{Q}$  with nontrivial excited gluonic components ( $Q\bar{Q}g$ ), where  $Q$  is a heavy quark (e.g.,  $b, t$  quark), and  $\bar{Q}$  is a heavy antiquark. A hybrid spin-exotic state is a hybrid meson whose  $J^{PC}$  value is permitted in the quark model [4]. From the current quark model, the quantum numbers for  $Q\bar{Q}$  composites are given in Table 2.3.

Because the quantum numbers  $J^{PC} = 1^{-+}, 0^{+-}$  and  $2^{+-}$  cannot exist for the meson in the quark model, they are hybrid spin-exotic mesons. In Chapter 4, we give more details about hybrid spin-exotic mesons and the potential model.

**Table 2.3.** The  $^{2S+1}L_J$  or  $J^{PC}$  for  $Q\bar{Q}$ .

$L$	Singlet( $S = 0$ )	Triplet( $S = 1$ )
0	$^1S_0(0^{-+})$	$^3S_1(0^{--})$
1	$^1P_1(1^{+-})$	$^3P_{0,1,2}(0^{++}, 1^{++}, 2^{++})$
2	$^1D_2(2^{-+})$	$^3D_{1,2,3}(1^{--}, 2^{--}, 3^{--})$
3	$^1F_3(3^{+1})$	$^3F_{2,3,4}(2^{++}, 3^{++}, 4^{++})$

## CHAPTER 3

### LATTICE QCD

It is well known that quantum electrodynamics (QED) describes the interaction of the charged particles and photons. In the same way, quantum chromodynamics (QCD) is the popular theory of the strong interactions of the colored particles, which is formulated in terms of the quarks and gluons. QCD has been very successful in predicting the phenomena of high energy hadron physics.

Quantum chromodynamics is a well-developed theory, but calculations are very difficult, particularly at energies below about 1 GeV, where the strong coupling constant is of the order of unit, so perturbation methods fail. Fortunately, lattice QCD provides a nonperturbative method in this field. Lattice QCD is a quantum field theory that formulates QCD on a discrete Euclidean spacetime grid. We explain later. The main benefits are that many calculations in QCD take on forms familiar in classical statistical mechanics. Since lattice QCD does not introduce new field variables, it inherits the basic characters of QCD.

In this chapter we provide background material about QCD. We first give an overview of continuum QCD. Then we give an overview of lattice QCD and some special ways to incorporate fermion fields. Finally, we explain how to generate the configurations. We focus on some details needed for this dissertation. Several textbooks [15, 16] provide comprehensive background material.

### 3.1 Overview of continuum QCD

In this section, we first introduce the full gauge invariant classical Minkowski Lagrangian for QCD by directly starting from the Minkowski Lagrangian of a free Dirac field for a given flavor, and then introducing the gluon field through the help of the parallel transport. Then we write the path integral representation for

the physical vacuum expectation values of any observables. Later we change this path integral representation to the corresponding path integral in the Euclidean space-time. Also we associate the path integral formulation of the partition function in QCD with the corresponding partition function of quantum statistical mechanics.

### 3.1.1 Continuum gauge field theory in QCD

On the lowest level, QCD describes the interactions of the quarks and gluons. In Chapter 1, we explained that the quarks ( $u, d, s, c, b, t$ ) and the antiquarks ( $\bar{u}, \bar{d}, \bar{s}, \bar{c}, \bar{b}, \bar{t}$ ) are fermions of fractional electric charge and color charge. Each of the quarks carries a  $SU(3)$  color index. According to the current colored quark model, the three colors of a given flavor have the same mass, although different flavors have different masses [13]. Hence, the wave function  $\psi_c$  of each quark contains a triplet of fields ( $c = 1, 2, 3$ ). The wave function  $\bar{\psi}_c$  of each antiquark also contains a triplet of fields [16][13].

Now we introduce the gauge-invariant Lagrangian in continuum QCD in the Minkowski space. The starting point is the Minkowski Lorentz invariant Lagrangian of the free Dirac field for a given flavor [13][15]

$$\mathcal{L}_{\mathcal{F}} = \sum_{c=1}^3 \bar{\psi}_c(x)(i\gamma^\mu \partial_\mu - m)\psi_c(x), \quad (3.1)$$

where  $c$  is the quark color index,  $m$  is the mass of the given flavor quark, and  $\gamma^\mu$  are the Minkowski Dirac matrices. The Lagrangian in Eq. (3.1) is invariant under the  $SU(3)$  rotation [15]

$$\psi(x) \rightarrow \psi'(x) = \Lambda \psi(x), \quad \bar{\psi}(x) \rightarrow \bar{\psi}'(x) = \bar{\psi}(x) \Lambda^\dagger, \quad (3.2)$$

where  $\Lambda \in SU(3)$  is independent of  $x$ . The above transformation is called a global gauge transformation [15]. If  $\Lambda$  depends on  $x$ , that is,  $\Lambda(x)$  is a function of  $x$ , the Lagrangian in Eq. (3.1) is not invariant under the gauge transformation

$$\psi(x) \rightarrow \psi'(x) = \Lambda(x)\psi(x), \quad \bar{\psi}(x) \rightarrow \bar{\psi}'(x) = \bar{\psi}(x)\Lambda(x)^\dagger, \quad (3.3)$$

where  $\Lambda(x)$  is an element of  $SU(3)$ . The above transformation is known as local gauge transformation [15]. We will modify the Lagrangian in Eq. (3.1), so it is invariant under a local gauge transformation.

For each space-time point  $x$ , there is a space  $V_x$  allowed values of  $\psi(x)$  at that point. How do we compare  $\psi(x)$  on one vector space  $V_x$  with  $\psi(y)$  at another vector space  $V_y$ . In the gauge theory of QCD it is the parallel transporter that connects a point on one vector space with the corresponding point on another vector space. The parallel transport is generated infinitesimally [17] along a smooth curve. First let  $\mathcal{C}_{yx}$  be a smooth curve in space-time from point  $x$  to point  $y$ . Then we define a mapping from vector space  $V_x$  to vector space  $V_y$ , that is,

$$U(\mathcal{C}_{yx}) : V_x \rightarrow V_y, \quad (3.4)$$

for  $U(\mathcal{C}_{yx}) \in SU(3)$  such that  $U(\mathcal{C}_{yx})\psi(x)$  is an element of the vector space  $V_y$ . That is, vector  $U(\mathcal{C}_{yx})\psi(x)$  is regarded as the vector  $\psi(x)$  at the point  $x$ , parallel transported along the smooth curve  $\mathcal{C}_{yx}$  to the point  $y$  [15]. We say  $U(\mathcal{C}_{yx})$  is a “parallel transporter” [15] along the smooth curve  $\mathcal{C}_{yx}$ .

We can prove that [15, 17], under the local gauge transformation

$$\psi(x) \rightarrow \psi'(x) = \Lambda(x)\psi(x), \quad \bar{\psi}(x) \rightarrow \bar{\psi}'(x) = \bar{\psi}(x)\Lambda^\dagger(x), \quad (3.5)$$

$$\psi(y) \rightarrow \psi'(y) = \Lambda(y)\psi(y), \quad \bar{\psi}(y) \rightarrow \bar{\psi}'(y) = \bar{\psi}(y)\Lambda^\dagger(y), \quad (3.6)$$

a parallel transporter transforms as [15]

$$U(\mathcal{C}_{yx}) \rightarrow U'(\mathcal{C}_{yx}) = \Lambda^\dagger(y)U(\mathcal{C}_{yx})\Lambda(x). \quad (3.7)$$

Now we consider the straight smooth curve  $\mathcal{C}_{x+dx,x}$  from point  $x$  to point  $x+dx$ . The Lie algebra of  $SU(3)$  is generated by  $\frac{\lambda^a}{2}$ , the eight Gell-Mann matrices satisfy the commutation relations

$$[\lambda^a, \lambda^b] = 2if_{abc}\lambda^c, \quad (3.8)$$

where  $f^{abc}$  are the structure constants of  $SU(3)$ . Hence, the corresponding infinitesimal parallel transporter can be written as [15]

$$U(\mathcal{C}_{x+dx,x}) = \mathbf{1} + igA_\mu^a(x)\frac{\lambda^a}{2}dx^\mu, \quad (3.9)$$

where  $\mathbf{1}$  is the  $3 \times 3$  unit matrix,  $g$  is the color coupling constant, which is just introduced conventionally,  $A_\mu^a(x)$  is the gluon gauge field, and  $a$  is the gluon color

index ( $a = 1, \dots, 8$ ). The parallel transporter in Eq. (3.9) has a vector index  $\mu$  that gets contracted between  $A_\mu^a(x)$  and  $dx^\mu$ . For notational simplicity, we define the gauge field  $A_\mu(x)$  in the Lie algebra of  $SU(3)$  [15]

$$A_\mu(x) \equiv ig A_\mu^a(x) \frac{\lambda^a}{2}. \quad (3.10)$$

Then we can rewrite Eq. (3.9) as

$$U(\mathcal{C}_{x+dx,x}) = \mathbf{1} + A_\mu(x) dx^\mu. \quad (3.11)$$

Now we perform a longer distance parallel transport along smooth path  $\mathcal{C}_{yx}$ , where the points  $x, x_1, x_2, x_3 \dots, x_{n-1}, x_n, y$  form a series of infinitesimally separated points along the path  $\mathcal{C}_{y,x}$ . Then the parallel transport of  $\psi(x)$  to the end of the path (i.e., point  $y$ ) in space-time is constructed by taking a series of infinitesimal transports along path  $\mathcal{C}_{yx}$  [15, 18, 19]. That is,

$$U(\mathcal{C}_{y,x})\psi(x) = [\mathbf{1} + A_\mu(x)(x_1^\mu - x^\mu)] \times [\mathbf{1} + A_\mu(x_1)(x_2^\mu - x_1^\mu)] \times \dots \times \\ [\mathbf{1} + A_\mu(x_{n-1})(x_n^\mu - x_{n-1}^\mu)] \times [\mathbf{1} + A_\mu(x_n)(y^\mu - x_n^\mu)]\psi(y), \quad (3.12)$$

here  $U(\mathcal{C}_{y,x})$  is the parallel transporter along smooth curve  $\mathcal{C}_{y,x}$ . This product of a series of infinitesimal parallel transports, with  $x$  (the path's beginning) on the left and  $y$  (the path's end) on the right, results in Dyson's formula [20, 15]

$$U(\mathcal{C}_{yx}) = P \exp \left\{ \int_{\mathcal{C}_{yx}} A_\mu dx^\mu \right\}, \quad (3.13)$$

where the symbol  $P$  denotes the path ordering of the integrand. The parallel transporter  $U(\mathcal{C}_{yx})$  is called the Wilson line from point  $y$  to point  $x$  along path  $\mathcal{C}_{yx}$ , and when the path  $\mathcal{C}_{yx}$  is a closed loop, the trace of the parallel transporter  $U(\mathcal{C}_{yx})$  is referred to as a Wilson loop by convention.

Since now the parallel transporter can relate different vector spaces ( $V_x$ ), we can define the covariant derivative of  $\psi(x)$  by the formula

$$D_\mu \psi(x) dx^\mu = U(\mathcal{C}_{x+dx,x})\psi(x+dx) - \psi(x). \quad (3.14)$$

After some algebra, we arrive at [15]

$$D_\mu = \partial_\mu + A_\mu. \quad (3.15)$$

We can prove that, under the local gauge transformation, the covariant derivative transforms as [15]

$$D_\mu \psi(x) \rightarrow D'_\mu \psi'(x) = \Lambda^\dagger(x) D_\mu \psi(x). \quad (3.16)$$

Next we introduce the field tensor  $F_{\mu\nu}$  through the commutator of two covariant derivatives [15]:

$$F_{\mu\nu}(x) \equiv [D_\mu, D_\nu] = \partial^\mu A_\nu(x) - \partial^\nu A_\mu(x) + [A_\mu(x), A_\nu(x)]. \quad (3.17)$$

Since the field tensor  $F_{\mu\nu}$  is also an element in the Lie algebra of color  $SU(3)$ , it can be written in the form [15]

$$F_{\mu\nu}(x) = ig F_{\mu\nu}^a(x) \frac{\lambda^a}{2}, \quad (3.18)$$

where  $F_{\mu\nu}^a = \partial^\mu A_\nu^a - \partial^\nu A_\mu^a - gf^{abc} A_\mu^b A_\nu^c$  is the gluon field strength tensor. We can prove that, under the local gauge transformation, the field strength tensor transforms as [15]

$$F_{\mu\nu}(x) \rightarrow F'_{\mu\nu}(x) = \Lambda^\dagger(x) F_{\mu\nu}(x) \Lambda(x). \quad (3.19)$$

If we replace the ordinary four-derivative  $\partial^\mu$  by the covariant derivative  $D^\mu$ , the resulting new Lagrangian [13]

$$\mathcal{L}_{\mathcal{F}} = \sum_{c=1}^3 \bar{\psi}_c(x) (i\gamma^\mu D_\mu - m_f) \psi_c(x) \quad (3.20)$$

is invariant under the local gauge transformations.

Since we have already introduced the gauge field  $A_\mu$ , we should add its own free Lagrangian to Eq. (3.20). This term is given by the Yang-Mills Lagrangian (or pure gauge Lagrangian) [13]

$$\mathcal{L}_{\mathcal{YM}} = -\frac{1}{4} F_a^{\mu\nu} F_{\mu\nu}^a, \quad (3.21)$$

which is obviously invariant under the local gauge transformations. Hence, we finally arrive at the full gauge invariant classical Minkowski Lagrangian for QCD (here we consider the case of various flavors)

$$\mathcal{L} = -\frac{1}{4} F_a^{\mu\nu} F_{\mu\nu}^a + \sum_{f=1}^{n_f} \sum_{c=1}^3 \bar{\psi}_c^f (i\not{D} - m_f) \psi_c^f, \quad (3.22)$$

where  $\not{D} = \gamma_M^\mu D_\mu$ ,  $f$  is the quark flavor index,  $m_f$  is the mass of the quark with flavor  $f$ ,  $\psi_c^f$  and  $\bar{\psi}_c^f$  are the spin quark fields,  $n_f$  is the number of the fermion

flavors, and  $\gamma_M^\mu$  are the Minkowski Dirac matrices. For brevity, we have omitted the quark spin index.

### 3.1.2 Continuum QCD formalism

We calculate the physical vacuum expectation values of any observables  $F(U, \psi, \bar{\psi})$  which are function of the field variables. For QCD in the Minkowski space [16], the expectation values can be written as a path integral <sup>1</sup>

$$\langle 0 | F(U, \psi, \bar{\psi}) | 0 \rangle = \frac{1}{Z} \int \mathcal{D}U \mathcal{D}\psi \mathcal{D}\bar{\psi} F(U, \psi, \bar{\psi}) e^{i\mathcal{S}_{\mathcal{M}}}, \quad (3.23)$$

where  $\psi$  and  $\bar{\psi}$  are Grassmann variables <sup>2</sup>,  $|0\rangle$  stands for the ground state of the system (or physical vacuum states), and

$$Z = \int \mathcal{D}U \mathcal{D}\psi \mathcal{D}\bar{\psi} e^{i\mathcal{S}_{\mathcal{M}}}. \quad (3.24)$$

Here  $\mathcal{S}_{\mathcal{M}} = \int d^4x \mathcal{L}$  is the action of QCD,  $\mathcal{L}$  is described by Eq. (3.22), and

$$\mathcal{D}U = \prod_{x,\mu} dA_\mu(x) \quad (3.25)$$

$$\mathcal{D}\psi \mathcal{D}\bar{\psi} = \prod_{x,\alpha} d\psi_\alpha(x) \prod_{y,\beta} d\bar{\psi}_\beta(y), \quad (3.26)$$

where  $\psi$  and  $\bar{\psi}$  are Grassmann variables, and  $\alpha, \beta$  are the indices including color, flavor, and spin.

Hence, in Minkowski space the paths are weighted by a function  $e^{iS}$  ( $S$  is action) [16], which is oscillating. Therefore, it is not suitable for numerical calculations. For a numerical simulation, it is very convenient to calculate in imaginary time (i.e.,  $t \rightarrow -i\tau$ ), where the variable  $\tau$  is called “Euclidean time.” This means that we change the Minkowski spacetime metric to Euclidean spacetime

---

<sup>1</sup>The path integral (PI) was introduced by Feynman in quantum mechanics in Ref. [21], For example, we replace the matrix element  $\langle x | e^{-iHt} | y \rangle$  by an infinite-dimensional integration over all classical paths, which were weighted by the exponential of  $i$  times the classical action  $\int Dx e^{iS}$ , where the  $|y\rangle$  is the eigenstate of Hamiltonian operator  $H$ , and  $S$  is the classical action. Hence, the Hamiltonian operator has been removed [15, 16].

<sup>2</sup>In Ref. [15] the authors give the detailed discussion of the properties of Grassmann variables. Please see Ref. [15] for details.



metric, then use the Minkowski Lagrangian in Eq. (3.22) for QCD to create the corresponding classical Euclidean action for QCD. First of all, we should understand the difference between these two metrics. We know that the Minkowski spacetime is a four-dimensional space (i.e.,  $x_0, x_1, x_2, x_3$ ), whose metric is  $g_{\mu\nu}$ .<sup>3</sup> Hence, the Minkowski scalar product is

$$x * y \equiv g_{\mu\nu} x^\mu y^\nu = x^0 y^0 - x^1 y^1 - x^2 y^2 - x^3 y^3. \quad (3.27)$$

Euclidean spacetime (or Cartesian space) is the space of 4-tuples of real numbers (i.e.,  $x_1, x_2, x_3, x_4$ ), where  $x_4$  (or  $t$ ) is time and  $x_1, x_2, x_3$  is space. In Euclidean spacetime, we use the metric  $\delta_{\mu\nu}$ . Hence, the Euclidean scalar product is

$$x \cdot y \equiv \delta_{\mu\nu} x^\mu y^\nu = x^1 y^1 + x^2 y^2 + x^3 y^3 + x^4 y^4. \quad (3.28)$$

In fact, Minkowski spacetime can be considered to have a Euclidean metric but with imaginary time  $x^0 = -icx_4$ , where  $c$  is the speed of light. By convention in high energy physics, we choose  $c=1$  (so,  $x^0 = -ix_4$ ).

Now we first make following substitutions:  $x_0 \rightarrow -ix_4$  (or  $t \rightarrow -i\tau$ ) and  $A_0 \rightarrow -iA_4$ , where  $t \equiv x_0$ , and  $x_4 \equiv \tau$ . Second we adopt the Euclidean Dirac matrices  $\gamma^\mu$ . They are related to the Minkowski Dirac matrices  $\gamma_M^\mu$  through [15]

$$\gamma_M^\mu = i\gamma^\mu \quad \mu = 1, 2, 3 \quad (3.29)$$

$$\gamma_M^\mu = \gamma^\mu \quad \mu = 0. \quad (3.30)$$

Therefore, we obtain the classical Euclidean action [16] for QCD<sup>4</sup>

$$\mathcal{S} = \int d^4x \left\{ \frac{1}{4} F_a^{\mu\nu} F_{\mu\nu}^a + \sum_{f=1}^{n_f} \sum_{c=1}^3 \bar{\psi}_c^f M_f \psi_c^f \right\}, \quad (3.31)$$

where

---

<sup>3</sup>The definition of  $g_{\mu\nu}$  is in Ref. [22].

<sup>4</sup>In principle we can relate Minkowski space observable to Euclidean space through analytic continuation. This is a trivial for static quantities such as masses [15, 22, 23]. In Chapter 5, we will discuss some problems (e.g., the energy conservation) due to this continuation.

$$M_f = \not{D} + m_f \quad (3.32)$$

$$\not{D} = \gamma^\mu D_\mu, \quad (3.33)$$

and  $M_f$  is the Dirac operator. Then Eq. (3.24) can be rewritten as [16]

$$Z = \int \mathcal{D}U \mathcal{D}\psi \mathcal{D}\bar{\psi} e^{-\mathcal{S}}. \quad (3.34)$$

Therefore, Eq. (3.23) can be rewritten as [16]

$$\langle 0 | F(U, \psi, \bar{\psi}) | 0 \rangle = \frac{1}{Z} \int \mathcal{D}U \mathcal{D}\psi \mathcal{D}\bar{\psi} F(U, \psi, \bar{\psi}) e^{-\mathcal{S}}, \quad (3.35)$$

where  $\mathcal{S}$  is the action in Euclidean space. We note that the weighting factor in path integral now is  $e^{-\mathcal{S}}$ .

Now we associate the path integral formula of the partition function described by Eq. (3.34) and Eq. (3.35) with the ones of quantum statistical mechanics. In quantum statistical mechanics, we define the partition function as

$$Z(\tau) = \text{Tr} e^{-\tau H}. \quad (3.36)$$

In terms of the eigenvectors and eigenvalues of the operator  $H$  which satisfies  $H|n\rangle = E_n|n\rangle$ , where  $H$  is the Hamiltonian,  $\tau$  is the “Euclidean time.” If we consider the following equation [15]

$$\text{Tr}(e^{-\tau H} F) = \sum_{n=0}^{\infty} e^{-E_n \tau} \langle n | F | n \rangle \quad (3.37)$$

$$Z(\tau) = \text{Tr}(e^{-\tau H}) = \sum_{n=0}^{\infty} e^{-E_n \tau}, \quad (3.38)$$

We obtain that the thermal expectation values of any observables ( $F$ ) through [15]

$$\langle F \rangle = \lim_{\tau \rightarrow \infty} \frac{\text{Tr}(F e^{-\tau H})}{Z(\tau)}. \quad (3.39)$$

Hence, many calculations in QCD take on forms familiar in classical statistical mechanics. In Euclidean space the definition of the partition function described by Eq. (3.34) and the definition of the expectation value described by Eq. (3.35) are consistent with what we define in quantum statistical mechanics. Therefore, from now on we can reasonably call the  $Z$  in Eq. (3.34) “partition function.”

We usually separate the action  $S$  into two parts

$$\mathcal{S} = S_g + S_f. \quad (3.40)$$

The first term,  $S_g$ , depends on only the gauge fields. We call this term the pure gauge action (or Yang-Mills action)

$$\mathcal{S}_g = \int d^4x \frac{1}{4} F^{\mu\nu} F_{\mu\nu}. \quad (3.41)$$

The second term,  $S_f$ , depends on both the gluon and fermion fields. We refer to this term as fermion action,

$$\mathcal{S}_f = \int d^4x \bar{\psi} M \psi, \quad (3.42)$$

where, for brevity, the flavor index and color index have been suppressed.

For  $n_f$  degenerate fermion flavors, the QCD partition function in Euclidean space time is described by [16]

$$Z = \int \mathcal{D}U \mathcal{D}\psi \mathcal{D}\bar{\psi} e^{-(S_g + S_f)}. \quad (3.43)$$

Integrating the fermion field for degenerate flavors gives [16]<sup>5</sup>

$$\int \mathcal{D}\psi \mathcal{D}\bar{\psi} e^{-S_f} = (\det M)^{n_f}. \quad (3.45)$$

Thus

$$Z = \int \mathcal{D}U (\det M)^{n_f} e^{-S_g} = \int \mathcal{D}U e^{-S_{eff}}, \quad (3.46)$$

where the effective gauge action  $S_{eff}$  is denoted as [16][24]

$$S_{eff} \equiv S_g - n_f \ln (\det M). \quad (3.47)$$

The quark determinant  $\det M$  generates quark loops. In the quenched approximation, we set this determinant to a constant. In effect, in this approximation

<sup>5</sup>For the  $n_f$  nondegenerate fermion flavors,

$$\int \mathcal{D}\psi \mathcal{D}\bar{\psi} e^{-S_f} = \prod_{f=1}^{n_f} \det M_f, \quad (3.44)$$

where  $f$  is the index of flavor, and  $M_f$  is Dirac operator for flavor  $f$ .

we ignore the interaction between fermions and gauge fields. This approximation introduces a 5–15% error in the lattice calculations of the light hadron masses [25]. It greatly simplifies the computation.

The expectation value of any physical observable  $\mathcal{O}$  that depends on the quark and gluon fields is [16]

$$\langle \mathcal{O} \rangle = \frac{\int \mathcal{D}U \mathcal{D}\psi \mathcal{D}\bar{\psi} \mathcal{O} e^{-S}}{\int \mathcal{D}U \mathcal{D}\psi \mathcal{D}\bar{\psi} e^{-S}}. \quad (3.48)$$

The above integral is a Feynman functional integral over all configurations of the gauge field. Usually the fermion fields are integrated out analytically, leading to a numerical path integral over only the gauge fields.

### 3.2 QCD on a lattice

In QED, a perturbative expansion gives quite accurate results for many physical problems. At very high energies, a perturbative expansion in QCD also gives quite accurate results for some physical systems. However in a low energy physical system, perturbation theory in QCD is not suitable, due to a large coupling constant. To overcome this, numerical techniques (namely, Monte Carlo techniques and a lattice discretization) were proposed to study QCD nonperturbatively.

Numerical techniques require discretizing the continuum QCD theory on a Euclidean space time grid ( $a$  is lattice spacing). At the same time we should retain as many properties of the continuum QCD action as possible, and we require that the continuum theory be recovered in the physical continuum limit (i.e.,  $a \rightarrow 0$ ). Such a lattice QCD action is then used to generate a biased sample of gauge field configurations. Our observables are calculated on each of these configurations, and our observables are averaged on these configurations to get their expectation values.

In this discretization, we optionally choose periodic boundary conditions for the gauge fields in space. That means that the first and last points along any straight line in the lattice are considered nearest neighbors (e.g.,  $\phi(x_0) = \phi(x_N)$ , where  $\phi$  is any function which depend on lattice site  $x$ . However in the time direction, periodic boundary conditions for the gauge fields are not optional.

In QCD perturbation theory, we encounter various divergent integrals. We deal with them by modifying the original integral. A “regulator” parameter characterizes the modification. The physical limit involves removing the regulator. The lattice is a natural regulator of ultraviolet divergence. In lattice regularization, we assume that our physical system is not a continuum space, but a discrete lattice. The lattice spacing  $a$  serves to limit the highest possible momentum (namely,  $\frac{\pi}{a}$ ) of particles defined on the lattice. Due to this cutoff, all of the volume integrals of interest are sums:

$$\int d^4x = \sum_x a^4. \quad (3.49)$$

Hence, we never integrate the momentum to infinity. This shows that, in order to get the theory in the continuum, after performing the finite sums, we should take the limit  $a \rightarrow 0$ .

In this section, we first give an overview of the pure gauge action in lattice QCD. Then we give three methods to incorporate the fermion, namely, the naïve fermion, the Wilson fermion, and the staggered fermion. Finally, we discuss the taste interpretation of the staggered fermion.

### 3.2.1 Pure gauge action on lattice

In order to explain confinement, in 1974, Wilson [26] proposed a lattice method. We now called it lattice QCD (LQCD). From then on, LQCD become a fundamental tool for the studies of QCD, and it is still in intensive use. The starting point for LQCD is to define fermion fields only on the sites of a four-dimensional grid with four spacetime dimensions of finite extent,  $N_x, N_y, N_z, N_t$ , and lattice spacing  $a$ . Here  $N_x, N_y, N_z$  are space dimensions, and  $N_t$  is the time dimension.

A crucial point in his paper [26] is the introduction of the gauge link matrices that connect nearest neighbor lattice sites. Here we follow the procedures in Sec. 3.1.1 and Sec. 3.2.2 in Ref. [15]. But in some places we choose different convention.

For the lattice, let  $x$  be any point on the lattice, and lattice spacing be  $a$ . Then  $x + a\hat{\mu}$  is the neighboring point in the direction of the lattice axis  $\mu = 1, 2, 3, 4$ .

where  $\hat{\mu}$  is the unit vector in the  $\mu$  direction. The parallel transporter that moves  $A_\mu$  along the straight path line from point  $x$  to point  $x + a\hat{\mu}$  is [15]

$$U_\mu(x) = \exp \left\{ \int_{\mathcal{C}_{x+a\hat{\mu},x}} A_\mu dx^\mu \right\} \approx e^{aA_\mu}. \quad (3.50)$$

Here we make the approximation

$$\int_{\mathcal{C}_{x+a\hat{\mu},x}} A_\mu(x) dx^\mu \longrightarrow A_\mu(x)a. \quad (3.51)$$

We call  $U_\mu(x)$  the link matrix linking site  $x$  to its nearest neighbor in the  $\mu$  direction,  $x + a\hat{\mu}$ . A link matrix is an element of the gauge group  $SU(3)$  between pairs of nearest neighbor lattice points. The gauge field configuration is just the set of all such link matrices between pairs of the nearest neighbor sites.

An important property in lattice QCD is that the trace of any product of link matrices around any closed loop is gauge invariant. This property provides a way to translate some gauge invariant quantities onto the lattice. For example, the smallest closed loop on the lattice is the unit square (see Fig. 3.1), which contains four points,  $x$ ,  $x+a\hat{\mu}$ ,  $x+a\hat{\nu}$ ,  $x+a\hat{\mu}+a\hat{\nu}$ . The corresponding product of four link matrices [15],

$$U_P = U_\nu(x)U_\mu(x+a\hat{\nu})U_\nu^\dagger(x+a\hat{\mu})U_\mu^\dagger(x) = U_{x\nu}U_{x+a\hat{\nu},\mu}U_{x+a\hat{\mu},\nu}^\dagger U_{x\mu}^\dagger, \quad (3.52)$$

is called the plaquette variable in the  $\mu - \nu$  plane at lattice point  $x$ .

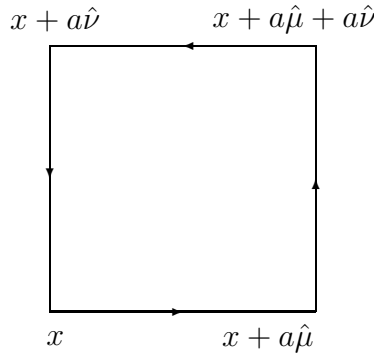


**Figure 3.1.** A plaquette on a hypercubic lattice.

The Wilson gauge action, expressed in terms of the plaquettes, is [15]

$$S_G(U) = \sum_P \beta \left\{ 1 - \frac{1}{6} \left( \text{Tr } U_P + \text{Tr } U_P^{-1} \right) \right\} = \sum_P \beta \left\{ 1 - \frac{1}{3} \text{Re Tr } U_P \right\}, \quad (3.53)$$

where the sum over  $P$  stands for the sum over all plaquettes, including each plaquette with only one orientation [15], that is,

$$\sum_P = \sum_x \sum_{1 \leq \mu < \nu \leq 4}. \quad (3.54)$$

In Wilson action  $\beta = \frac{6}{g^2}$ , where  $g$  is the bare coupling constant. The Taylor expansion of the link matrix  $U_\mu(x)$  is [15]

$$U_\mu(x) = 1 + aA_\mu(x) + \frac{a^2}{2}A_\mu(x)^2. \quad (3.55)$$

The Taylor expansion of the gauge fields is [15]

$$A_\nu(x + a\hat{\mu}) = A_\nu(x) + a\Delta_\mu^f A_\nu(x), \quad (3.56)$$

where  $\Delta_\mu^f$  is the forward lattice derivative. That means

$$\Delta_\mu^f A_\nu(x) = \frac{A_\nu(x + a\hat{\mu}) - A_\nu(x)}{a}. \quad (3.57)$$

If we use the well-known Campbell-Baker-Hausdorff identity [15]

$$e^x e^y = e^{x+y+\frac{1}{2}[x,y]+\dots} \quad (3.58)$$

and the formula [15]

$$F_{\mu\nu} \equiv igF_{\mu\nu}^a \frac{\lambda^a}{2} \quad (3.59)$$

$$F_{\mu\nu} = \Delta_\mu^f A_\nu(x) - \Delta_\nu^f A_\mu(x) + [A_\mu(x), A_\nu(x)] \quad (3.60)$$

$$\text{Tr}(F^{\mu\nu} F_{\mu\nu}) = -\frac{g^2}{2} F_a^{\mu\nu} F_{\mu\nu}^a, \quad (3.61)$$

we find, after some algebra, that as  $a \rightarrow 0$ , the action in Eq. (3.53) can be changed into [15]

$$S_G = \frac{1}{4} \sum_x a^4 F_a^{\mu\nu} F_{\mu\nu}^a + \mathcal{O}(a^6). \quad (3.62)$$

Therefore, we indeed reproduce continuum QCD action as  $a \rightarrow 0$ , and it is the correct QCD action for the gauge fields in the lattice.

If we add some terms around larger loops than plaquettes, as in the Symanzik improved gauge action [27], the  $\mathcal{O}(a^6)$  error in the gauge action can be eliminated. The gauge action used in this dissertation was a Symanzik improved action [28],

$$S_G = \frac{\beta_{imp}}{3} \left\{ \sum_{x;\mu<\nu} P_{\mu\nu} - \frac{1}{20u_0^2} (1+0.4805\alpha_s) \sum_{x;\mu\neq\nu} R_{\mu\nu} - \frac{1}{u_0^2} 0.03325\alpha_s \sum_{x;\mu<\nu<\sigma} C_{\mu\nu\sigma} \right\}, \quad (3.63)$$

where  $P$  is the standard plaquette in the  $\mu, \nu$  plane,  $R$  is the real part of the trace of the ordered product of  $SU(3)$  link matrices along  $1 \times 2$  rectangles (see Eq. (3.64)),  $C$  is the real part of the trace of the ordered product of  $SU(3)$  link matrices around  $1 \times 1 \times 1$  paths (see Eq. (3.65)),

$$R_{\mu\nu} \equiv \frac{1}{3} \text{Re Tr} \left[ \text{Diagram of a } 1 \times 2 \text{ rectangle with arrows indicating a loop} \right] \quad (3.64)$$

$$C_{\mu\nu\sigma} \equiv \frac{1}{3} \text{Re Tr} \left[ \text{Diagram of a } 1 \times 1 \times 1 \text{ cube with arrows indicating a loop} \right] \quad (3.65)$$

and here  $\beta_{imp} = \frac{10}{g^2}$ ,  $\alpha_s = -\frac{4 \log(u_0)}{3.0684}$ . The symbol  $u_0$  is the tadpole improvement factor

$$u_0 = \left( \frac{1}{3} \text{Re Tr} \langle P \rangle \right)^{\frac{1}{4}}. \quad (3.66)$$

In lattice perturbation theory, there exists ultraviolet (UV) divergence from tadpole-type graphs [28]. This contribution can be partially removed by absorbing them in lattice coupling constants. The common method is to replace lattice gauge matrix  $U(x)$  by  $U(x)/u_0$  [28]. In this dissertation, we also use this method.

### 3.2.2 Fermion action on lattice

The naïve approach to formulate the fermion action is simply to replace the symmetric derivative in the Dirac operator with a symmetric difference. Here we follow the procedure and convention as in Ref. [16]. We can change the continuum action in Eq. (3.42) into the naïve lattice fermion action [16], that is,

$$S_N = a^4 \sum_x \left\{ \frac{1}{2a} \sum_{\mu=1}^4 \bar{\psi}(x) \gamma^\mu \left[ U_\mu(x) \psi(x+a\hat{\mu}) - U_\mu^\dagger(x-a\hat{\mu}) \psi(x-a\hat{\mu}) \right] + m \bar{\psi}_x \psi_x \right\}, \quad (3.67)$$



where the symmetric difference is denoted as [16]

$$D_\mu = \frac{1}{2a} \left[ U_\mu(x) \psi(x+a\hat{\mu}) - U_\mu^\dagger(x-a\hat{\mu}) \psi(x-a\hat{\mu}) \right]. \quad (3.68)$$

This is called the naïve fermion action.

Unfortunately, in the continuum limit, the naïve action brings out an unphysical doubling of the fermion modes in each lattice direction. This mean that for every physical mode at momentum  $k_\mu = 0$ , there is a degenerate mode at momentum  $k_\mu = \frac{\pi}{a}$ , where  $\frac{\pi}{a}$  is the cutoff momentum of the lattice. Hence, in four space-time dimensions, there are 16 degenerate modes [15]. Several methods have been proposed to solve this “doubling problem.”

Wilson added a second order derivative term to the naïve action to break this degeneracy. This term includes a coefficient factor  $r$ , usually chosen to be 1. For the physical  $k_\mu = 0$  mode, this term does not change the continuum limit, but this term suppresses the remaining 15  $k_\mu = \frac{\pi}{a}$  doubler modes [15]. The Wilson fermion action is [16]

$$S_W = S_N - \frac{r}{2a} \sum_x a^4 \sum_{\mu=1}^4 \bar{\psi}(x) \left\{ U_\mu^\dagger(x) \psi(x+a\hat{\mu}) + U_\mu(x-a\hat{\mu}) \psi(x-a\hat{\mu}) - 2\psi(x) \right\}. \quad (3.69)$$

After some algebra, we get [16]

$$\begin{aligned} S_W = a^4 \sum_x \left\{ \left( m + \frac{4}{a} \right) \bar{\psi}(x) \psi(x) + \frac{1}{2a} \sum_{\mu=1}^4 \bar{\psi}(x) [r + \gamma_\mu] U_\mu(x) \psi(x+a\hat{\mu}) \right. \\ \left. + \frac{1}{2a} \sum_{\mu=1}^4 \bar{\psi}(x) [r - \gamma_\mu] U_\mu^\dagger(x-a\hat{\mu}) \psi(x-a\hat{\mu}) \right\}. \end{aligned} \quad (3.70)$$

For brevity, we define the hopping parameter  $\kappa$

$$\kappa \equiv \frac{1}{2am + 8r}. \quad (3.71)$$

Also we rescale the fermion fields with

$$\psi \rightarrow \psi \sqrt{2\kappa}. \quad (3.72)$$

Then the action can be rewritten as

$$S_W = \sum_{xy} \bar{\psi}_x M_{xy} \psi_y, \quad (3.73)$$

where  $M_{xy}$  are the matrix elements of the fermion matrix [16], that is,

$$M_{xy} = \delta_{xy} - \kappa \sum_{\mu=1}^4 \left\{ [r + \gamma_\mu] U_\mu(x) \delta_{x,y-a\hat{\mu}} + [r - \gamma_\mu] U_\mu^\dagger(x - a\hat{\mu}) \delta_{x-a\hat{\mu},y} \right\}. \quad (3.74)$$

From above equation, we can note that the diagonal term in  $M_{xy}$  is unit.

For the naïve fermion action, due to the doubling problem, a single quark in fact describes 16 identical replicas of the quark. Each of these replication is called a “taste” [24].

Kogut and Susskind [29] developed another approach to solve the doubling problem called the staggered fermion Kogut Susskind action. In this approach, the 16-fold doubling problem of the naïve fermion action given in Eq. (3.67) can be reduced to a factor of four if we keep only a single fermion field component on each lattice site. This procedure reduces the number of tastes per quark fermion from 16 to 4. We use another trick (discussed later in Sec. 3.3.2) to reduce the remaining 4 fermions tastes to 1 in the determinant.

To keep just one single fermion field component on each lattice site, we do spin-diagonalization [15]. Staggered fermions  $\chi$  are defined by the local transformation.

$$\psi(x) = \Gamma_x \chi(x) \quad \bar{\psi}(x) = \bar{\chi}(x) \Gamma_x^\dagger \quad \Gamma_x = \gamma_1^{x_1} \gamma_2^{x_2} \gamma_3^{x_3} \gamma_4^{x_4}. \quad (3.75)$$

where  $\Gamma_x$  is a  $4 \otimes 4$  unitary matrix, which diagonalizes all the  $\gamma$  matrices in the action. In terms of the staggered fermions  $\chi$  the quark action can be written as <sup>6</sup>

$$\begin{aligned} \mathcal{S}_S &= \sum_{x,t} \left\{ am_t \bar{\chi}_t(x) \chi_t(x) + \frac{1}{2} \sum_{\mu=1}^4 \alpha_{x\mu} \left[ \bar{\chi}_t(x) U_\mu(x) \chi_t(x+a\hat{\mu}) - \bar{\chi}_t(x+a\hat{\mu}) U_\mu^\dagger(x) \chi_t(x) \right] \right\} \\ &\equiv \sum_{x,y,t} \bar{\chi}_t(x) M^t[U]_{x,y} \chi_t(y), \end{aligned} \quad (3.76)$$

where the  $t$  is the taste index of a given flavor, and the matrix  $M^t$  is given by [16]

$$M^t[U]_{x,y} = am_t \delta_{xy} + \frac{1}{2} \sum_{\mu} \alpha_{x\mu} \left[ U_\mu(x) \delta_{x,y-a\hat{\mu}} - U_\mu^\dagger(x - a\hat{\mu}) \delta_{x,y+a\hat{\mu}} \right]. \quad (3.77)$$

The  $\gamma_\mu$  matrices have been replaced by the phase factors

$$\alpha_{x\mu} = (-)^{x_1 + \dots + x_{\mu-1}}, \quad (\mu = 1, 2, 3, 4). \quad (3.78)$$

---

<sup>6</sup>This formula is similar to Eq. (6.26) [16], but we use different notation and add a taste index.

From Eq. (3.76), and Eq. (3.77), we note that the different spin components of  $\chi$  are decoupled, because the phase factor  $\alpha_{x,\mu}$  depends only on the site index and direction index and does not have a spin index. Here we drop the spin index on  $\chi$ , keeping only the color and taste degrees of freedom at each site. So this trick reduces the original 16-fold degeneracy of naïve fermions by a factor of four.

The fermion action used in this dissertation is the “Asqtad” action [9]. The link paths of “Asqtad” action are illustrated in Fig. 3.2. The first term is the simple link. The second term is three link staple, and the third term is five link staple. The second term and third term are to reduce the flavor symmetry [9]. The fourth term (or seven link staple) removes tree level couplings at the momentum  $\frac{\pi}{a}$  [9]. The fifth term (or Lepage term) is the correction to the form factor at small momentum [9]. The sixth term (or Naik term, the third nearest neighbor) is to improve the quark dispersion relation [9]. If we set the zero momentum coupling to one and all the other momentum couplings to zero, and we introduce the tadpole factors  $(\frac{1}{u_0})^{L-1}$ , where  $L$  is the length of path, we obtain the coefficients  $\frac{5}{8}, \frac{1}{16}u_0^{-2}, \frac{1}{64}u_0^{-4}, \frac{1}{384}u_0^{-6}, -\frac{1}{16}u_0^{-4}, -\frac{1}{24}u_0^{-2}$ , [9] respectively.

The fermion action in Eq. (3.76) is first term in the “Asqtad” action. Here is the second term:

$$\mathcal{S}_{S2} = \sum_{x,t} \left\{ am_t \bar{\chi}_t(x) \chi_t(x) + \frac{1}{12} \sum_{\mu=1}^4 \sum_{\nu \neq \mu}^4 \alpha_{x\mu} \left[ \bar{\chi}_t(x) U_\nu(x) U_\mu(x+\hat{\nu}) U_\nu^\dagger(x+\hat{\mu}) \chi_t(x+a\hat{\mu}) \right. \right. \\ \left. \left. - \bar{\chi}_t(x+a\hat{\mu}) U_\nu(x+\hat{\mu}) U_\mu^\dagger(x+\hat{\nu}) U_\nu^\dagger(x) \chi_t(x) \right] \right\}. \quad (3.79)$$

The rest are constructed similarly.

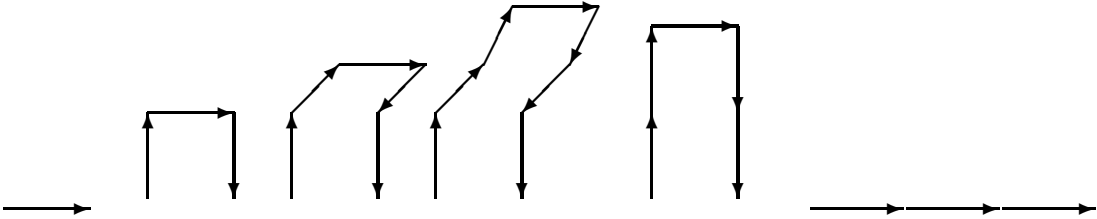


**Figure 3.2.** The simple link, three link staple, five link staple, seven link staple, Lepage term, and Naik term of Asqtad action.

### 3.2.3 Tastes of Kogut-Susskind staggered fermions

Due to the phase factors  $\alpha_{x,\mu}$  the Kogut-Susskind staggered fermion action has translational invariance under shift by  $2a$ . Therefore, in the continuum limit, we can map a  $2^4$  hypercube into a single lattice point [15]. For simplicity, we just discuss the free Kogut-Susskind Staggered fermions.

In position space [15], we can easily understand the taste identification. For some purpose it is convenient to represent the 16 degrees of freedom in a hypercube by a new field  $q$  called a hypercubic field, which in the continuum limit represents the four spin components of four degenerate tastes.

Let us first assume that the number of the points in a hypercubic lattice is even in every direction:  $L_\mu = 2L'_\mu$  ( $\mu = 1, 2, 3, 4$ ). The coordinates of the lattice points lie in the interval  $0 \leq x_\mu \leq L_\mu - 1$ . The coordinates of the hypercubic blocks  $y_\mu$  [15] are denoted by

$$x_\mu = 2y_\mu + A_\mu, \quad (3.80)$$

where  $A_\mu = 0, 1$ . Therefore, it is convenient to divide the lattice into the hypercubes identified by a 4-vector  $y$ , that is,  $y$  is defined on a lattice of spacing  $2a$ . The set of 16 vectors  $\{A\}$  identify the points within the hypercube, and they are called hypercube vectors. The sum over lattice points can be written as

$$\sum_x = \sum_y \sum_A. \quad (3.81)$$

The new fields with definite taste are written as  $q_y^{\alpha a}$  and  $\bar{q}_y^{\alpha a}$ , that is,

$$q_y^{\alpha a} = \frac{1}{4} \sum_A \Gamma_{A;\alpha a} \chi(2y + A), \quad \bar{q}_y^{\alpha a} = \frac{1}{4} \sum_A \bar{\chi}(2y + A) \Gamma_{A;a\alpha}^\dagger, \quad (3.82)$$

where  $\alpha$  is the Dirac spin index,  $a$  is the taste index, and

$$\Gamma_A = \gamma_1^{A_1} \gamma_2^{A_2} \gamma_3^{A_3} \gamma_4^{A_4}. \quad (3.83)$$

The inverse expressions are

$$\chi(2y + A) = \text{Tr}(\Gamma_A^\dagger q_y), \quad \bar{\chi}(2y + A) = \text{Tr}(\bar{q}_y \Gamma_A). \quad (3.84)$$

Then the free staggered fermion action can be written in terms of the new fields as

$$\mathcal{S}_S = 4m_q \sum_y \bar{q}_y (\mathbf{1} \otimes \mathbf{1}) q_y + 4 \sum_{y,\mu} \bar{q}_y \left[ \gamma_\mu \otimes \mathbf{1} \Delta_\mu - \gamma_5 \otimes (\gamma_\mu \gamma_5)^T \square_\mu \right] q_y, \quad (3.85)$$

where we define two different lattice derivatives on the block lattice,

$$\begin{aligned} \Delta_\mu &\equiv \frac{1}{4} (f_{y+\hat{\mu}} - f_{y-\hat{\mu}}) \longrightarrow a \partial_\mu f_y \\ \square_\mu &\equiv \frac{1}{4} (f_{y+\hat{\mu}} + f_{y-\hat{\mu}} - 2f_y) \longrightarrow a^2 \partial_\mu^2 f_y. \end{aligned} \quad (3.86)$$

In the continuum limit, the first term tends to the usual kinetic term. The second term is a lattice artifact of order  $\mathcal{O}(a)$ , which disappears in continuum limit [15]. At finite lattice spacing  $a$ , the 16 degrees of staggered fermions in the hypercube are a mixture of spin and taste.

We can write the general bilinear operator as

$$\mathcal{O}_{SF} = \bar{q}_y (\gamma_S \otimes \xi_T) q_y = \sum_{A,B} \bar{\chi}(y+A) \text{Tr}(\Gamma_A^\dagger \gamma_S \Gamma_B \xi_T) \chi(y+B), \quad (3.87)$$

where  $\xi_T \equiv \Gamma_T^\dagger$ . The matrices  $\gamma_S$  determine the angular momentum and parity of the operator [30] and the matrices  $\xi_T$  label the taste. Each of these can be one of the standard 16 elements of the Dirac Clifford algebra.

The notation  $\gamma_S \otimes \xi_T$  stands for the direct product of the matrix  $\gamma_S$  and  $\xi_T$ , where the former acts on the Dirac indices, and the later acts on the taste indices. The bilinear operators are identified as follows [31][30]

$$\begin{aligned} V_\mu &= \bar{q}(\gamma_\mu \otimes \xi_T) q \\ A_\mu &= \bar{q}(\gamma_\mu \gamma_5 \otimes \xi_T) q \\ P &= \bar{q}(\gamma_5 \otimes \xi_T) q \\ S &= \bar{q}(1 \otimes \xi_T) q, \end{aligned} \quad (3.88)$$

where  $V_\mu$  is a vector,  $A_\mu$  is an axial vector,  $P$  is a pseudoscalar, and  $S$  is a scalar meson [32].

We use these operators as interpolating operators to create and annihilate mesons. In the continuum, the mesons are in the taste  $SU(4)$  representations  $\mathbf{1}$  and  $\mathbf{15}$ , while

on the lattice the action has a reduced symmetry and these representations break into many smaller representations [30]. For example, the continuum **15**-plet of pion mesons breaks into seven lattice representations (four 3-dimensional and three 1-dimensional) on the lattice.

$$\begin{aligned}
\mathbf{15} &\rightarrow (\gamma_5 \otimes \gamma_i) \oplus (\gamma_5 \otimes \gamma_i \gamma_4) \oplus (\gamma_5 \otimes \gamma_i \gamma_5) \oplus (\gamma_5 \otimes \gamma_i \gamma_4 \gamma_5) \oplus \\
&\quad (\gamma_5 \otimes \gamma_4) \oplus (\gamma_5 \otimes \gamma_5) \oplus (\gamma_5 \otimes \gamma_4 \gamma_5), \\
\mathbf{1} &\rightarrow (\gamma_5 \otimes 1).
\end{aligned} \tag{3.89}$$

In the first line of Eq. (3.89),  $i = 1, 2, 3$ , the representations are three-dimensional. The other representations are one-dimensional [30]. Hence, when we measure the mass of the pion meson on lattice, there exists many different types of the mass for pion meson. In Chapter 8, we can see this in detail.

### 3.3 Simulation algorithm

In this dissertation, we use the configurations which were generated by the hybrid-molecular dynamics “R algorithm” [11]. In order to explain this algorithm clearly, we first introduce the process of generating gauge configurations. Then we discuss the hybrid-molecular dynamics “R algorithm.”

#### 3.3.1 Numerical simulation and updating process

One of the main aims of numerical simulations in lattice QCD (LQCD) is to calculate the expectation values of some observables  $F[\phi]$  which are the functions of the field variables  $[\phi] \equiv \{\phi_{x\alpha}\}$ , where  $\phi_{x\alpha}$  is a real field component with index  $\alpha$  at lattice site  $x$ , where the index  $\alpha$  includes flavor, color, spin [15]. For brevity we often omit  $\alpha$ . For simplicity we assume that the variables for the fermions are integrated out analytically.

$$\langle F[\phi] \rangle = \frac{\int [d\phi] e^{-S[\phi]} F[\phi]}{\int [d\phi] e^{-S[\phi]}}, \tag{3.90}$$

where  $e^{-S[\phi]}$  is an action suitable for simulation. The above equation involves a multidimensional integral over all the field variables  $[\phi]$  on the lattice. But the

number of the integration variables in  $[d\phi] = \prod_{x,\alpha} d\phi_{x\alpha}$  is typically very large (in this dissertation, it is over  $10^6$ ). Hence, a Monte Carlo integration is used to calculate the integral efficiently [15].

For a given lattice with field variables  $[\phi]$ , a configuration (i.e.,  $[\phi]$ ) is just one point in the space (or domain) of the field variables. Fortunately, due to the factor  $e^{-S[\phi]}$ , only those paths for which the action  $S[\phi]$  has the values close to minimum dominate the path integrals [15]. Hence, the efficient Monte Carlo simulation uses an importance sampling [15][16], which generates a series of configurations with the density  $W[\phi]$  proportional to the Boltzmann factor  $e^{-S[\phi]}$  [15]. That is,

$$W[\phi] \propto e^{-S[\phi]}. \quad (3.91)$$

We can call this series of configurations an ensemble of configurations. Then we can use these configurations to calculate the integral like Eq. (3.90) [15].

The configurations are generated  $\{[\phi_n], 1 \leq n \leq N\}$  in a sequential manner by creating from one configuration to the previous configuration,  $[\phi] \rightarrow [\phi']$ , with a given transition probability. The transition probability,  $P([\phi] \rightarrow [\phi'])$ , specifies the probability that the configuration  $\phi$  becomes to a configuration  $\phi'$ . The above procedure of creating configurations is called “updating” [15]. For the numerical simulation, we have a variety of schemes to get from one configuration to others.

As in statistical mechanics, we want the density  $W[\phi]$  of the configuration. We also set the equilibrium density,  $W_c[\phi]$ , to be proportional to the  $e^{-S[\phi]}$ , where  $S[\phi]$  is the action for a configuration. To achieve this result, a single step causes the density  $W$  to evolve as follow [15]

$$W'[\phi'] = \sum_{[\phi]} P([\phi'] \leftarrow [\phi]) W[\phi]. \quad (3.92)$$

The transition probability  $P$  satisfies [15]

$$\sum_{[\phi']} P([\phi'] \leftarrow [\phi]) = 1 \quad (3.93)$$

$$P([\phi'] \leftarrow [\phi]) > 0. \quad (3.94)$$

The normalization condition for the density  $W$  is [15]

$$\sum_{[\phi']} W[\phi'] = 1, \quad (3.95)$$

and we require the detailed balance condition [15]

$$P([\phi'] \leftarrow [\phi]) W_c[\phi] = P([\phi] \leftarrow [\phi']) W_c[\phi']. \quad (3.96)$$

Different choices of the transition probability  $P([\phi] \rightarrow [\phi'])$  generate different ensembles. Here we discuss one common updating algorithm: the Metropolis method [15][16]. Briefly, the Metropolis proceeds as follows [15][16]: we first randomly choose a possible new configuration (i.e.,  $[\phi']$ ) from  $N$  possible new configurations, then calculate the new action ( $S[\phi']$ ). If the new action is less than the original action ( $S[\phi]$ ), we accept the configuration  $[\phi']$ . If the new action  $S[\phi']$  is greater than the original action  $S[\phi]$ , we accept the configuration  $[\phi']$  with probability  $\frac{e^{-S[\phi']}}{e^{-S[\phi]}}$ . We can simplify this algorithm for the transition probability  $P([\phi] \rightarrow [\phi'])$  as follows [15][16]

$$P([\phi'] \leftarrow [\phi]) = N^{-1} \min \left\{ 1, \frac{W_c[\phi']}{W_c[\phi]} \right\}. \quad (3.97)$$

This method results in  $W_c[\phi] \propto e^{-S[\phi]}$ , which means that the probability that any particular gauge configuration is included in the sample (or an ensemble of gauge configuration) is proportional to  $e^{-S[\phi]}$ .

With an ensemble of the sample gauge configurations, the average value of any operator ( $\mathcal{O}$ ) is simply calculated according to its average [16]

$$\overline{\mathcal{O}} = \frac{1}{N} \sum_{n=1}^N \mathcal{O}[\phi_n] + O\left(\frac{1}{\sqrt{N}}\right). \quad (3.98)$$

If we have a large number of the sample configurations (i.e.,  $N$  large), the average value that we measure is very close to the operator expectation value  $\langle \mathcal{O} \rangle$ .



### 3.3.2 Hybrid-molecular dynamics “R algorithm”

The Metropolis method is simple. However, it usually updates the gauge link matrix locally (i.e., each step updates one gauge link matrix). Hence, we need a more efficient algorithm to update the gauge link matrix globally (i.e., each step updates the entire lattice). The hybrid-molecular dynamics (HMD) “R algorithm” [11] is an example. It was used to generate the configurations for this dissertation.

The basic idea of the HMD “R algorithm” can be stated as follows: by introducing a set of conjugate momenta  $H$  for the gauge link matrices  $U$ , the Euclidean path integral associated with QCD theory can be rewritten in the form of a partition function for a classical statistical mechanical system in space-time, and the motion of gauge link matrix ( $U$ ) is governed by a classical Hamiltonian in the simulation time. Therefore, the configurations are generated in a deterministic way.

In Sec. 3.3.1, we assume that the variables for the fermions are integrated out analytically. In some cases, we cannot analytically integrate out the variables for fermions. Hence, we consider the general case. The starting point for this algorithm [11] is to consider the following path integral for the partition function for  $N_f$  degenerate staggered fermion flavors in Eq. (3.46).<sup>7</sup>

$$\begin{aligned} Z &= \int \mathcal{D}U e^{-S_g} [\det(M(U))]^{\frac{N_f}{4}} \\ &= \int \mathcal{D}U e^{-S_{eff}}, \end{aligned} \quad (3.100)$$

where, as we explain below,

$$S_{eff} = S_g - \frac{N_f}{4} \ln \det[M(U)^\dagger M(U)]. \quad (3.101)$$

---

<sup>7</sup>In Sec. 3.2.2, when we discuss Kogut-Susskind fermions, we keep only a single fermion field component on each lattice site. This procedure reduces the number of tastes from 16 to 4. The factor  $\frac{1}{4}$  (fourth root trick [33]) is used to reduce the remaining four fermions tastes to one taste in the determinant. In this dissertation, we use the configurations [10] with three flavors: two light quarks ( $u$ ,  $d$ ), and a strange ( $s$ ) quark with  $m_u = m_d \neq m_s$ . Then Eq. (3.100) becomes

$$Z = \int \mathcal{D}U e^{-S_g} [\det(M_u(U))]^{\frac{1}{2}} [\det(M_s(U))]^{\frac{1}{4}}, \quad (3.99)$$

where  $M_u[U]_{x,y}$  is the quark matrix for  $u$  or  $d$  quark, and  $M_s[U]_{x,y}$  is the quark matrix for  $s$  quark. Hence, only two masses of KS quarks are included (i.e., the square root of  $u$  or  $d$  determinant, and the fourth root of  $s$  determinant).

Here  $S_g(U)$  is the pure gauge action on lattice, and the quark matrix  $M[U]_{x,y}$  is given by Eq. (3.77). From Eq. (3.77), we obtain  $\det[M(U)] = \det[M(U)^\dagger]$ . The factor of  $\frac{1}{4}$  comes from the fact that  $\det[M(U)]$  stands for four tastes per quark fermion. Here, in Eq. (3.101), we considered the fact that the determinants of the submatrices on the even sites of  $M(U)^\dagger M(U)$  and the submatrices on the odd sites of  $M(U)^\dagger M(U)$  are equal [34].

In order for the matrix  $U_{x,\mu}$  still to be an element of  $SU(3)$ , the molecular dynamics equation <sup>8</sup> of the motion for  $U_{x,\mu}$  at site  $x$  should obey [11]

$$\dot{U}_{x,\mu}(t) = iH_{x,\mu}(t)U_{x,\mu}(t), \quad (3.102)$$

where  $H_{x,\mu}(t)$  is a traceless Hermitian matrix, and  $\dot{U}_{x,\mu}(t)$  is the derivative of  $U_{x,\mu}(t)$  with respect to the simulation time ( $t$ ). Hence, as we promised above, we introduce the auxiliary field  $H$  conjugate to the gauge field  $A$  into the partition function [11]

$$\begin{aligned} Z &= \int \mathcal{D}U \mathcal{D}H e^{-\frac{1}{2} \text{Tr}(H^2) - S_g(U) + \frac{N_f}{4} \text{Tr} \ln[M(U)^\dagger M(U)]} \\ &= \int \mathcal{D}U \mathcal{D}H e^{-\mathcal{H}}, \end{aligned} \quad (3.103)$$

leading to the effective Hamiltonian  $\mathcal{H}$  [11]

$$\mathcal{H} = \frac{1}{2} \text{Tr}(H^2) + S_g(U) - \frac{N_f}{4} \text{Tr} \ln[M(U)^\dagger M(U)], \quad (3.104)$$

and  $\text{Tr}(H^2) = \sum_{x,\mu} \text{Tr}(H_{x,\mu}^2)$ .

Now we briefly illustrate the algorithm to generate a set of gauge field configurations with a probability distribution proportional to  $e^{-\mathcal{H}}$ , that is,

$$P[U, H] \propto e^{-\mathcal{H}}. \quad (3.105)$$

To this end, we adopt two types of updating steps. First, the  $H$  field is initialized by the heat bath method [35][36], that is, we construct a random  $H$  field [11]

$$H_{x,\mu} = \lambda_a h_{x,\mu}^a, \quad (3.106)$$

---

<sup>8</sup>The general Hamiltonian equations of motion are

$$\dot{\phi}_i = \frac{\partial H[\phi, \pi]}{\partial \pi_i}, \quad \dot{\pi}_i = -\frac{\partial H[\phi, \pi]}{\partial \phi_i},$$

where  $\phi_i$  is field variable,  $\pi_i$  is the momenta canonically conjugate to  $\phi_i$ , and  $H[\phi, \pi]$  is the hamiltonian.

by setting each  $h_{i,\mu}^a$  to a complex Gaussian random number with standard deviation  $< |h_{x,\mu}^a|^2 > = 1$ . Thus, the  $H$  field is first updated globally.

Second, the  $U$  field is updated by the equation of the molecular dynamics. From Eq. (3.102), if we first update the  $H_{x,\mu}$ , then we can easily obtain  $U$ . Since the  $H_{x,\mu}$  is updated globally, the  $U$  field is updated at the whole lattice. Because it is very difficult to calculate the inverse of the matrix  $M(U)^\dagger M(U)$ , it is standard to use a noisy estimator method [37][36] to compute it. The integration of the equations of motion proceeds by the leapfrog method. It generates the sequence  $U(t + i\Delta t)$  and  $H(t + i\Delta t)$ , where  $i = 1, 2, \dots, N$ . we take about  $N = \frac{1}{\Delta t}$  molecular-dynamics steps. The result is called a molecular dynamics trajectory. If we repeat two types of updating steps (namely, the heat bath steps and molecular dynamics steps) many times, we obtain an ensemble of configurations.

In hybrid-molecular dynamics “R algorithm,” since  $P[U, H] \propto e^{-\mathcal{H}}$ , the expectation value of an observable  $F[U]$  can be written in the form

$$\langle F[U] \rangle = \frac{\int [dU][dH] e^{-\mathcal{H}} F[U]}{\int [dU][dH] e^{-\mathcal{H}}}. \quad (3.107)$$

Because  $F[U]$  does not depend on the momentum  $H$ , and  $\int [dH] e^{-\mathcal{H}} \propto e^{-S_{eff}}$ . Eq. (3.107) can be rewritten in the form

$$\langle F[U] \rangle = \frac{\int [dU] e^{-S_{eff}} F[U]}{\int [dU] e^{-S_{eff}}}, \quad (3.108)$$

which mean that the probability distribution  $P[U] \propto e^{-S_{eff}}$ .

This algorithm is applicable to any kind of fermions [11]. For example, in this dissertation, we use configurations [10] with three flavors: two light quarks ( $u, d$ ), and a strange ( $s$ ) quark. In our simulation, the light quarks are degenerate in mass, and we choose the different mass for strange quark. Hence, we replace the effective Hamiltonian  $\mathcal{H}$  described by Eq. (3.104) by

$$\mathcal{H} = \frac{1}{2} \text{Tr}(H^2) + S_g(U) - \frac{1}{2} \text{Tr} \ln[M_l(U)^\dagger M_l(U)] - \frac{1}{4} \text{Tr} \ln[M_s(U)^\dagger M_s(U)], \quad (3.109)$$

where  $M_l(U)$  is the quark matrix for the light quark, and  $M_s(U)$  is the quark matrix for the strange quark. The calculation is similar to what we discussed

before. The only difference is that we generate two gaussian random vectors, and use two conjugate-gradient<sup>9</sup> calculations (i.e., one for the light quark, one for the strange quark) for each molecular dynamics step.

From the above algorithm, we can see that there are two sources of systematic errors. The first error is due to the nonzero time step (i.e.,  $\Delta t \neq 0$ ) in the integration, which results in the quadratic dependence of the error [11] (i.e., the error is of the order  $(\Delta t)^2$ ). This is because that we integrate the molecular dynamics equation (i.e., Eq. (3.102), Eq. (46) and Eq. (47) in Ref. [11]) with an error of order  $(\Delta t)^3$  at each time step. The second error comes from the conjugate gradient residual [11] (i.e., the required accuracy of conjugate gradient calculation), which we choose in the conjugate gradient calculation. If we choose the conjugate gradient residual to be small, we will take too much *CPU* time. Otherwise, if we prefer it to be the large, the accuracy is not what we want. So in the simulation, we choose a suitable value for conjugate gradient residual.

Another error comes from our measurements. Because the conjugate gradient calculation consumes too much *CPU* time, we measure the potential (or the spectrum) at the physical time separation  $\delta t$ . In our simulation, we make a measurement at intervals of six simulation time units (namely,  $\delta t = 6\Delta t$ ). So our measurements are not entirely statistically independent (i.e., our measurement is autocorrelated). We can reduce the effect of this autocorrelation of measurements by blocking several consecutive measurements before fitting [38]. In the latter chapter, when we fit the mass of the  $f_0$  meson, we will consider the effect of autocorrelation.

---

<sup>9</sup>In mathematics, the conjugate gradient is an algorithm for the numerical solution of linear systems. For example, we want to solve the following linear system

$$Ax = b,$$

where  $A$  is the  $n \times n$  matrix, which is symmetric and positive definite,  $b$  is  $1 \times n$  matrix, and  $x$  is the solution. The conjugate gradient method is an iterative method. In this dissertation, we solve many systems like this.

## CHAPTER 4

### LEADING BORN-OPPENHEIMER (LBO)

The heavy hybrid mesons can be investigated directly by the numerical simulation, and by the Born-Oppenheimer (BO) approximation, which was proposed for the study of the hybrids states in Refs. [7, 8]. Here we focus on the leading order in the BO approximation, and ignore the higher-order terms. We use the Leading Born-Oppenheimer (LBO) approximation to study the spectroscopy of the heavy hybrid mesons ( $Q\bar{Q}g$ ), which consist of a heavy quark ( $Q$ ) and a heavy antiquark ( $\bar{Q}$ ) plus a gluon. We are particularly interested in the spin-exotic hybrid mesons with  $J^{PC}$  quantum numbers, which is not permitted in the quark model. The lightest one is believed to be with  $J^{PC} = 1^{-+}$  [5], which does not mingle with a nonhybrid  $Q\bar{Q}$  bound state [4].

In this chapter, we use the LBO approximation to study the spectroscopy of the hybrid mesons. We first introduce some notations from molecular physics. Then we study the LBO approximation. Next we review the APE smearing algorithm, and introduce the static potentials. Finally, we calculate the hybrid quarkonia through the LBO approximation.

#### 4.1 Notation from molecular physics

We borrow the standard notation from diatomic molecular physics to classify the static potential (i.e., gluonic energies). Here we describe the gluon wave function in analogy with the electron wave function [4, 5]. The symmetries of the gluons include:

- $J_z$  : The magnitude (denoted by  $\Lambda$ ) of eigenvalues of the projection of the projection  $\mathbf{J}_g \cdot \mathbf{n}$  of the total angular momentum  $\mathbf{J}_g$  of the gluon field onto the separation axis  $\mathbf{R}$  of the quark  $Q$  and antiquark  $\bar{Q}$  with unit vector  $\mathbf{n} = \mathbf{R}/R$ .

The states with  $\Lambda = 0, 1, 2, \dots$  are typically denoted by the capital Greek letters  $\Sigma, \Pi, \Delta, \dots$ , respectively.

- $CP$  : The combined operations of the charge conjugation ( $C$ ) and spatial inversion ( $P$ ) about the midpoint between quark  $Q$  and antiquark  $\bar{Q}$  is also a symmetry. Its eigenvalue is usually defined by  $\eta$ . States which are even ( $\eta = 1$ ) or odd ( $\eta = -1$ ) under the above parity-charge-conjugation operation ( $CP$ ) are denoted by the subscripts  $g$ , and  $u$ , respectively.
- $R$  : For the  $\Sigma$  states ( $\Lambda = 0$ ), there is an extra symmetry. The wave function of the  $\Sigma$  states which are even (odd) under reflection in any plane passing through the separation axis (i.e., the plane contains the separation axis) are specified by a superscript  $+$ ( $-$ ).

For the states with  $\Lambda \neq 0$ , the energy of the gluons is not changed by operation  $R$ . Hence, those states are degenerate (namely,  $\Lambda$  doubling). We can list the low-lying levels of the gluon field as  $\Sigma_g^+$ ,  $\Sigma_g^-$ ,  $\Sigma_u^+$ ,  $\Sigma_u^-$ ,  $\Pi_g$ ,  $\Pi_u$ ,  $\Delta_g$ ,  $\Delta_u$ , etc [5]. In this dissertation, we only consider the states  $\Sigma_g^+$  and  $\Pi_u$ .

## 4.2 Born-Oppenheimer approximation

The hydrogen molecule ion,  $H_2^+$ , consists of a single electron in the Coulombic field of two protons (see Fig. 4.1). Here we make the approximation that the nuclei (i.e., two protons) are at rest. Since the nuclear motion is much slower than the motion of the electron, the electronic wave function depends on the nuclear positions. The Hamiltonian is

$$H = -\frac{1}{2m} \nabla^2 - e^2 \left( \frac{1}{R_1} + \frac{1}{R_2} \right), \quad (4.1)$$

where  $R_1$  and  $R_2$  are the distances to the electron from the respective protons, and  $e$  is the charge of the electron [39].

For each fixed  $R$ , we can use some methods (e.g., the trial wave function in the variational principle) [39] to solve for the motion of the electron, obtaining the ground state energy  $V(R)$  of the system of  $H_2^+$  as a function of  $R$ . We solve the

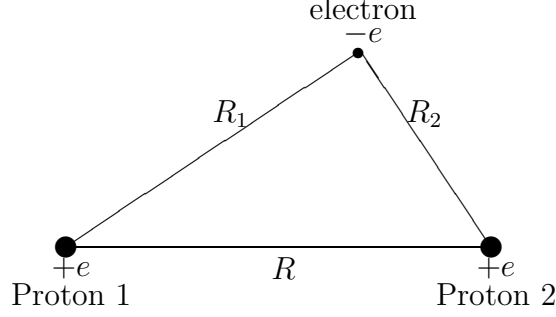


**Figure 4.1.** The hydrogen molecule ion,  $H_2^+$

Schrödinger equation for the motion of the nuclei using  $V(R)$  as the interacting potential. Then we can recover information about the positions and motions (e.g., rotation, vibration) of the nuclei [39]. In molecular physics this method is called the BO approximation.

The heavy hybrid mesons can be studied similarly with the BO approximation (see Fig. 4.2). The slow heavy quarks  $Q\bar{Q}$  correspond to the nuclei in the diatomic molecule while the fast gluons correspond to the electrons [7].

To use the BO method, we first consider the quark  $Q$  and antiquark  $\bar{Q}$  as the spatially fixed color field sources and use lattice methods to determine the energy levels of the gluons as a function of the  $Q\bar{Q}$  separation  $R$ . Each of these energy levels defines a static potential  $V_{Q\bar{Q}}(R)$  [5]. At the second step in BO method, the heavy quark motion is then reproduced by solving the Schrödinger equation in each of these static potentials [5]. Conventional quarkonia are based on the static potential ( $\Sigma_g^+$ ), and the hybrid quarkonium states should come from the excited potentials (i.e.,  $\Pi_u$ , etc).

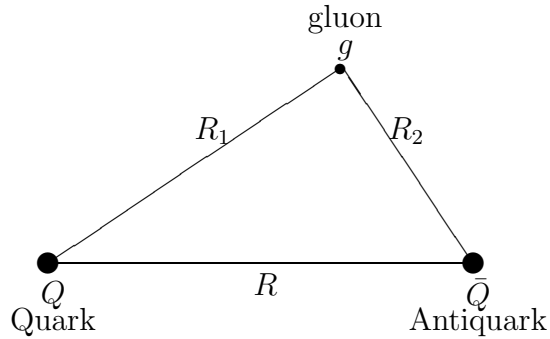


**Figure 4.2.** The hybrid meson,  $Qg\bar{Q}$

In this chapter, we present the results for the spectrum [5] of the gluonic excitations in the presence of a static quark-antiquark pair. Using our potentials, we also determine the hybrid quarkonium spectrum. For comparison with experiments, we also present the conventional quarkonium spectrum, which comes from  $\Sigma_g^+$  potential. Before we evaluate the static potentials, we fattened [9] the spatial gauge links by “APE smearing” [40][41]. Hence, we first discuss the APE smearing.

### 4.3 APE smearing

To reduce the mixings of our operators with its excited states the gluonic lattice operators are constructed from the iteratively-smearred spatial links (i.e., the fat link). We used the APE smearing algorithm described in Refs. [40, 41] to fatten the spatial gauge link matrix  $U_\mu(x)$ ,  $\mu = 1, 2, 3$ . The APE smearing averages a link matrix  $U_\mu(x)$  on the lattice with its nearest neighbors. This means that the smearing procedure is to replace the ordinary link matrix  $U_\mu(x)$  with the weighted sum of the link and  $\alpha$  times its four staples (i.e., three link paths), that is,

$$U_\mu(x) \rightarrow U'_\mu(x) = (1 - \alpha)U_\mu(x) + \frac{\alpha}{4} \sum_{\substack{\nu=1 \\ \nu \neq \mu}}^3 \left\{ U_\nu(x)U_\mu(x + \hat{\nu}a)U_\nu^\dagger(x + \hat{\mu}a) \right. \\ \left. + U_\nu^\dagger(x - \hat{\nu}a)U_\mu(x - \hat{\nu}a)U_\nu^\dagger(x + \hat{\mu}a) \right\}, \quad (4.2)$$

where  $\alpha$  is the smearing fraction. In our dissertation, we choose smearing fraction  $\alpha = \frac{8}{13}$  in order to get a satisfactory ground state enhancement [42, 43, 44, 45].

We construct the new gauge link  $U'_\mu(x)$  as follows: Step 1: Calculate the new gauge link  $U'_\mu(x)$  by Eq. (4.2) and project back to  $SU(3)$ . Step 2: After we do the step 1 for every link, we replace the old gauge link  $U_\mu(x)$  by the new gauge link  $U'_\mu(x)$ . Step 1 and Step 2 define a single smearing sweep. One such a smearing iteration step is shown in Fig. 4.3. By convention, the new gauge link  $U'_\mu(x)$  is called a “fat link” [46]. In this dissertation, before we evaluate the correlators, we take 20 smearing sweeps.



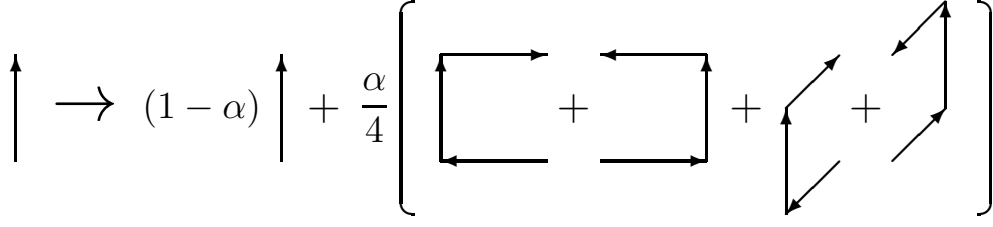


**Figure 4.3.** Visualization of a smearing iteration.

#### 4.4 Computation of the static potentials

The first step in the LBO approximation is to determine the energy levels of the gluons as a function of  $R$ , where heavy quark ( $Q$ ) and antiquark ( $\bar{Q}$ ) are fixed at lattice sites with separation distance  $R$  apart. At this point in the LBO approximation, the quark  $Q$  and antiquark  $\bar{Q}$  which provide the color field are considered to be approximately static [5].

It is possible to describe the spatial distribution of the color field between the static quarks  $Q\bar{Q}$ . There are many papers [3] that study the physical properties of the color flux between static quarks. We are very interested in the transverse extent of the color flux tube (see Fig. 4.4) and the physical properties of the color fields (i.e., electric field or magnetic field). The ground state energy of the color electric field between static quark sources can be interpreted as the origin of the confining interquark potential of the heavy  $Q\bar{Q}$  pairs. The hybrid  $Q\bar{Q}$  potentials which bind quark-antiquark ( $Q\bar{Q}$ ) pairs into the heavy hybrid  $Q\bar{Q}g$  molecules are defined by the excitation content of the confining color flux tube [5].

In this section, we first explain Monte Carlo estimates of the correlators, which

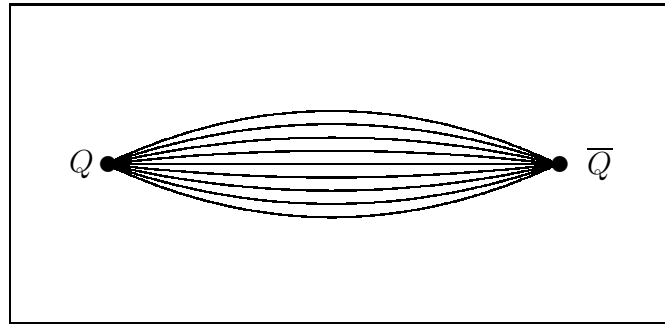


**Figure 4.4.** The distribution of color electric field between static color charges.

are used to calculate the static potential of the  $\Sigma_g^+$  and  $\Pi_u$  respectively. Then we discuss the procedure to fit these correlators. The fitting method we use is the standard Levenberg-Marquardt [47] fitting procedure.

#### 4.4.1 $C_{AA}$ Correlator

To determine the potential energy of the  $Q\bar{Q}$  system we first need the correlator from the  $\Sigma_g^+$  (A) state to the  $\Sigma_g^+$  (A) state. On a starting time slice  $t$ , the quark  $Q$  and antiquark  $\bar{Q}$  are fixed at lattice sites with separation distance of  $R$  whose midpoint is at space point  $\mathbf{r}$  (see Fig. 4.5). The gluonic operator at time slice  $t$  is the ground state, which is the parallel transporter for a straight link path along the quark and antiquark ( $\Sigma_g^+$ ). Before we evaluate the  $C_{AA}$  correlator, we use the APE smearing method to “fatten” spatial links, which means, in effect, that the parallel transporter here is not the conventional parallel transporter using the link matrix, and it is replaced by an weighted average over the link paths connecting the points [9] (see details in Ref. [46]). The gluonic operator at the source is

$$\mathcal{O}_{Source}(\mathbf{r}, \mathbf{R}, t) \equiv \Sigma_g^+(\mathbf{r}, \mathbf{R}, t) \equiv U(\mathbf{r} - \frac{\mathbf{R}}{2} + t\hat{\mathbf{4}}, \mathbf{r} + \frac{\mathbf{R}}{2} + t\hat{\mathbf{4}}), \quad (4.3)$$

where  $\hat{\mathbf{4}}$  is the unit vector in the time direction.

At the final time slice  $t_f$  (i.e.,  $t_f \equiv t + T$ ), the gluonic operator at time slice  $t_f$  is the parallel transporter, which is a straight link path along the quark  $Q$  and

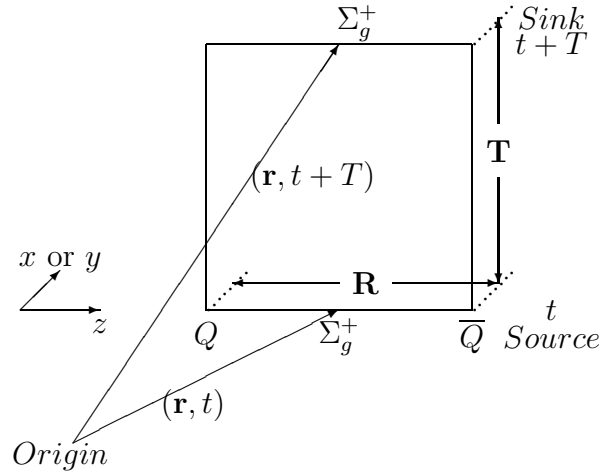


**Figure 4.5.** An illustration of the correlator from A to A.

antiquark  $\bar{Q}$ . The gluonic lattice operator at the sink can be written similarly as

$$\mathcal{O}_{Sink}(\mathbf{r}, \mathbf{R}, t+T) \equiv \Sigma_g^+(\mathbf{r}, \mathbf{R}, t+T) \equiv U(\mathbf{r} - \frac{\mathbf{R}}{2} + t_f \hat{\mathbf{4}}, \mathbf{r} + \frac{\mathbf{R}}{2} + t_f \hat{\mathbf{4}}). \quad (4.4)$$

Therefore, the timeslice correlator  $C_{AA}(T, \mathbf{R})$  from the  $\Sigma_g^+$  state to the  $\Sigma_g^+$  state can be written as

$$\begin{aligned} C_{AA}(T, \mathbf{R}) &= \frac{1}{\Omega} \sum_{\mathbf{r}, t} \left\langle \text{Tr} \left[ \mathcal{O}_{Sink}^\dagger(\mathbf{r}, \mathbf{R}, t+T) \mathcal{O}_{Source}(\mathbf{r}, \mathbf{R}, t) \right] \right\rangle \\ &= \frac{1}{\Omega} \sum_{\mathbf{r}, t} \left\langle \text{Tr} \left[ U(\mathbf{r} - \frac{\mathbf{R}}{2} + t_f \hat{\mathbf{4}}, \mathbf{r} + \frac{\mathbf{R}}{2} + t_f \hat{\mathbf{4}})^\dagger U(\mathbf{r} - \frac{\mathbf{R}}{2} + t_f \hat{\mathbf{4}}, \mathbf{r} + \frac{\mathbf{R}}{2} + t_f \hat{\mathbf{4}}) \right] \right\rangle \\ &= \frac{1}{\Omega} \sum_{\mathbf{r}, t} \left\langle \text{Tr} \left[ \Sigma_g^+(\mathbf{r}, \mathbf{R}, t+T)^\dagger \Sigma_g^+(\mathbf{r}, \mathbf{R}, t) \right] \right\rangle, \end{aligned} \quad (4.5)$$

where  $\Omega = N_x N_y N_z N_t$  is the total lattice volume,  $N_x, N_y, N_z$  are space dimensions, and  $N_t$  is time dimension.

A few algebraic steps relates the correlator to the energy  $V_{\Sigma_g^+}(R)$  of the lowest state excited by the operator.

$$\begin{aligned} C_{AA}(T, \mathbf{R}) &= \frac{1}{\Omega} \sum_{\mathbf{r}, t} \text{Tr} \left\langle 0 \left| \Sigma_g^+(\mathbf{r}, t+T) \Sigma_g^{+\dagger}(\mathbf{r}, t) \right| 0 \right\rangle \\ &= \frac{1}{\Omega} \sum_{\mathbf{r}, t} \left\langle 0 \left| \Sigma_g^+(\mathbf{r}, \mathbf{R}, t+T) \right| A \right\rangle \left\langle A \left| \Sigma_g^{+\dagger}(\mathbf{r}, \mathbf{R}, t) \right| 0 \right\rangle \\ &= \frac{1}{\Omega} \sum_{\mathbf{r}, t} e^{-V_{\Sigma_g^+}(R)T} \left\langle 0 \left| \Sigma_g^+(\mathbf{r}, \mathbf{R}, 0) \right| A \right\rangle \left\langle A \left| \Sigma_g^{+\dagger}(\mathbf{r}, \mathbf{R}, 0) \right| 0 \right\rangle \\ &= Z_a^2 e^{-V_{\Sigma_g^+}(R)T}, \end{aligned} \quad (4.6)$$

where  $|A\rangle$  is the eigenstate of the operator  $\Sigma_g^+$ , and

$$Z_a \equiv \left\langle 0 \left| \Sigma_g^+(\mathbf{r}, \mathbf{R}, 0) \right| A \right\rangle. \quad (4.7)$$

We have assumed that the contributions of higher excited states are negligible. This approximation is valid for large time  $T$ .

Since the gauge configurations are gauge fixed to the temporal gauge ( $A_4(x) = 0$ ) before we estimate the correlator  $C_{AA}$ , the time-link link variables are unit matrices. Therefore, the product of parallel transporters in Eq. (4.5) is equal to the parallel transporter  $U(\mathcal{C}_{R,T})$  along the closed rectangular loop  $\mathcal{C}_{R,T}$  of the side-lengths  $R$  and  $T$  (see Fig. 4.5), that is,  $C_{AA}(T, R) = W(\mathcal{C}_{R,T})$ , the standard Wilson loop.

#### 4.4.2 $C_{HH}$ Correlator

In this section, we calculate the correlator from the  $\Pi_u$  state to the  $\Pi_u$  states (i.e.,  $H$  state to  $H$  state). As before, on a starting time slice  $t$ , the quark  $Q$  and antiquark  $\bar{Q}$  are fixed at lattice sites with separation distance of  $R$  whose midpoint is at space point  $\mathbf{r}$  (see Fig. 4.6). The gluonic operator at time slice  $t$  is the  $\Pi_u$  lattice operator, which traditionally is the parallel transporter along a U-shaped path  $\sqcap$  minus the parallel transporter along the same U-shaped path  $\sqcup$  (i.e.,  $U(\mathcal{C}_{\sqcap}) - U(\mathcal{C}_{\sqcup})$ ) in the opposite transverse direction (see Fig. 4.7). The symbol  $\sqcap$  denotes the U-shaped path from the quark  $Q$  to the antiquark  $\bar{Q}$  whose transverse extent can be in the positive  $x$  or  $y$  direction, and  $\sqcup$  denotes the U-shaped path from the quark  $Q$  to the antiquark  $\bar{Q}$  whose transverse extent can be in the negative  $x$  or  $y$  direction. The gluonic lattice operator at the source can be written as

$$\mathcal{O}_{Source}(\mathbf{r}, \mathbf{R}, t) \equiv \Pi_u(\mathbf{r}, \mathbf{R}, t) \equiv \text{[Diagram of a lens-shaped loop]} . \quad (4.8)$$

For notational simplicity, we define a symbol

$$\text{[Diagram of a lens-shaped loop]} \equiv \text{[Diagram of a U-shaped path with a minus sign]} . \quad (4.9)$$

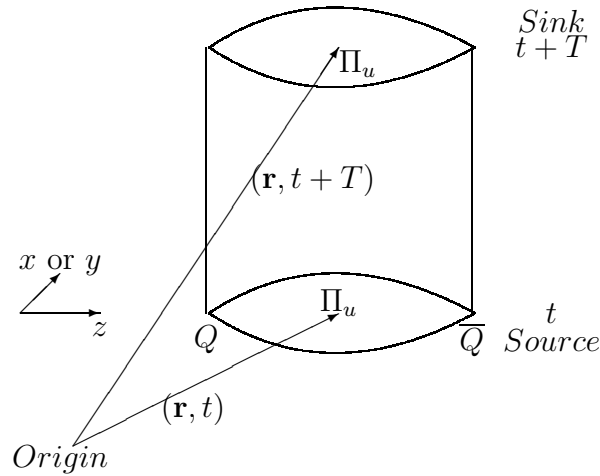


**Figure 4.6.** An illustration of the correlator from  $H$  to  $H$ .

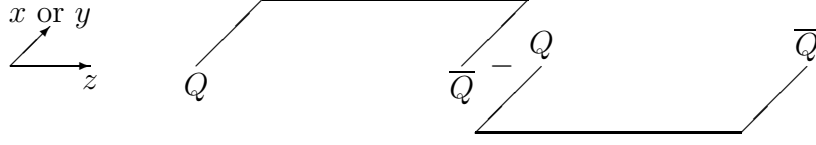


**Figure 4.7.** The creation operator for the  $\Pi_u$  state.

At the final time slice  $t_f$  (i.e.,  $t_f \equiv t + T$ ), the gluonic operator at time slice  $t_f$  can be written as

$$\mathcal{O}_{Sink}(\mathbf{r}, \mathbf{R}, t+T) \equiv \Pi_u(\mathbf{r}, \mathbf{R}, t+T). \quad (4.10)$$

Hence, the timeslice correlator can be written as

$$\begin{aligned} C_{HH}(T, \mathbf{R}) &= \frac{1}{\Omega} \sum_{\mathbf{r}, t} \langle \text{Tr} [\mathcal{O}_{Sink}^\dagger(\mathbf{r}, \mathbf{R}, t+T) \mathcal{O}_{Source}(\mathbf{r}, \mathbf{R}, t)] \rangle \\ &= \frac{1}{\Omega} \sum_{\mathbf{r}, t} \langle \text{Tr} [\Pi_u(\mathbf{r}, \mathbf{R}, t+T) \Pi_u(\mathbf{r}, \mathbf{R}, t)] \rangle \end{aligned} \quad (4.11)$$

Following steps similar to Eq. (4.6), we calculate the energy of the lowest  $\Pi_u$  state  $V_{\Pi_u}(R)$  through

$$\begin{aligned} C_{HH}(T, \mathbf{R}) &= \frac{1}{\Omega} \sum_{\mathbf{r}, t} \text{Tr} \langle 0 | \Pi_u(\mathbf{r}, t+T) \Pi_u^\dagger(\mathbf{r}, t) | 0 \rangle \\ &= \frac{1}{\Omega} \sum_{\mathbf{r}, t} \langle 0 | \Pi_u(\mathbf{r}, \mathbf{R}, t+T) | H \rangle \langle H | \Pi_u^\dagger(\mathbf{r}, \mathbf{R}, t) | 0 \rangle \\ &= \frac{1}{\Omega} \sum_{\mathbf{r}, t} e^{-V_{\Pi_u}(R)T} \langle 0 | \Pi_u(\mathbf{r}, \mathbf{R}, 0) | H \rangle \langle H | \Pi_u^\dagger(\mathbf{r}, \mathbf{R}, 0) | 0 \rangle \\ &= Z_h^2 e^{-V_{\Pi_u}(R)T}, \end{aligned} \quad (4.12)$$

where  $|H\rangle$  is the eigenstate of the operator  $\Pi_u$ , and

$$Z_h \equiv \langle 0 | \Pi_u(\mathbf{r}, \mathbf{R}, 0) | H \rangle. \quad (4.13)$$

We have assumed that the contributions of higher excited states are negligible. This approximation is valid for large time  $T$ .

Since the gauge configurations are gauge fixed to the temporal gauge ( $A_4(x) = 0$ ) before we estimate the correlator  $C_{HH}$ , the time-link link variables are unit matrices. Hence, in our simulation, we actually measure four bent Wilson loops (see Fig. 4.8).

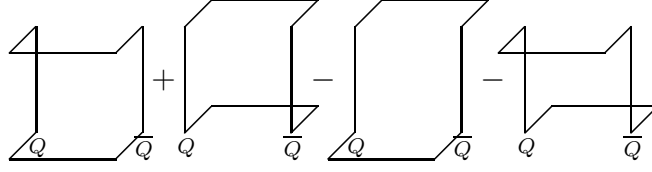


**Figure 4.8.** The bent loop for  $\Pi_u$  states.

#### 4.4.3 The results for the static potentials

In this dissertation, we want to reduce the mixings of our operators with their higher lying excited states. According we take 20 APE smearing sweeps. The correlators of  $C_{AA}(t, R)$  and  $C_{HH}(t, R)$  are then fitted by using a single exponential term. Our best fit values are obtained by using the correlated  $\chi^2$  method. For the correlator of  $C_{AA}(t, R)$ , our fitting range of minimum distance  $t_{\min}$  to  $t_{\max}$  of the source-sink separation is listed in Table 4.1, where the  $a$  is the lattice spacing. And the average least  $\chi^2$  per number of degrees of freedom for different  $R$  is approximately close to one. We list some of the fitting information in Table 4.1.

For the correlator of  $C_{HH}(t, R)$ , our fitting range of minimum distance  $t_{\min}$  to  $t_{\max}$  of the source-sink separation is listed in Table 4.2. And the average  $\chi^2$  per

**Table 4.1.** Fitting information for static potential  $V_{\Sigma_g^+}$ . The first column is the separation distance, the second column, static potential, the third column, the statistical error of the corresponding static potential, and the remaining columns are  $\chi^2$  per number of degrees of freedom, and the time range for the chosen fit.

$R/a$	$aV_{\Sigma_g^+}$	Error for $aV_{\Sigma_g^+}$	$\chi^2/D$	Fitting range
1	0.5396	7.999040e-04	0.2/3	8-12
2	0.8340	5.111520e-03	5.3/3	7-11
3	0.9927	7.192000e-03	1.0/3	6-10
4	1.0996	1.826420e-02	0.7/3	6-10
5	1.2234	1.291270e-02	0.9/3	5-9
6	1.3007	2.307760e-02	2.2/3	5-9
7	1.3912	4.568450e-02	0.2/3	5-9
8	1.5070	7.961440e-02	3.8/3	5-9
9	1.6254	3.601540e-02	3.5/3	4-8
10	1.7338	5.708190e-02	6.6/3	4-8
11	1.8307	1.003580e-01	2.3/3	4-8
12	1.8838	2.552650e-02	2.5/3	3-7

**Table 4.2.** Fitting information for static potential  $V_{\Pi_u}$ . The first column is the separation distance, the second column, static potential, the third column, the statistical error of the corresponding static potential, and the remaining columns are  $\chi^2$  per number of degrees of freedom, and the time range for the chosen fit.

$R/a$	$aV_{\Pi_u}$	Error for $aV_{\Pi_u}$	$\chi^2/D$	Fitting range
1	1.6602	6.8816e-03	1.0/3	3-7
2	1.6430	6.1839e-03	0.7/3	3-7
3	1.6442	6.0712e-03	3.3/3	3-7
4	1.6586	6.5216e-03	4.3/3	3-7
5	1.6996	7.6446e-03	2.0/3	3-7
6	1.7279	9.1389e-03	5.0/3	3-7
7	1.7976	1.1532e-02	4.9/3	3-7
8	1.8317	1.5096e-02	0.9/3	3-7
9	1.9373	2.1053e-02	1.2/3	3-7
10	1.9626	3.0135e-02	2.1/3	3-7
11	2.0732	4.1658e-02	3.3/3	3-7
12	2.1580	6.1574e-02	3.4/3	3-7

number of degrees of freedom for different  $R$  is approximately close to one. We list some of the fitting information in Table 4.2.

#### 4.4.4 Setting the scale

This scale parameter  $r_1$  depends only weakly on the valence quark mass and can be calculated accurately [48][38]. Hence, we prefer to use it to rescale our data. The definition of this parameter and computation of this quantity are shown in Ref. [48][38]. The scale parameter  $r_1$  is determined through

$$R^2 \left. \frac{dV_{\Sigma_g^+}(R)}{dR} \right|_{R=r_1} = 1.0. \quad (4.14)$$

From Ref. [10], we obtain the following value for  $r_1$ :

$$r_1 = 0.317(7) \text{ fm} \quad \text{or} \quad (4.15)$$

$$r_1^{-1} = 621(14) \text{ MeV}. \quad (4.16)$$

From Table II in Ref. [10], we get

$$\frac{r_1}{a} = 2.632(13). \quad (4.17)$$

Therefore, we obtain [10]

$$a^{-1} = 1.634(45)\text{GeV}. \quad (4.18)$$

Our fitting results for the static ground potential  $V_{\Sigma_g^+}(R)$  and first gluonic excitations potential  $V_{\Pi_u}(R)$  are shown in Fig. 4.9. The results are expressed in terms of the scale parameter  $r_1$ .

#### 4.4.5 Fitting procedure

The static ground potential  $V_{\Sigma_g^+}(R)$  is shown as the low part (the octagon one) in Fig. 4.9, the solid curve for  $V_{\Sigma_g^+}(R)$  potential in Fig. 4.9 is a fit to the data by using a Coulombic plus linear form and lattice Coulombic potential [49], that is,

$$V_0 + e_c \left[ \frac{1}{R} \right] + \sigma R, \quad (4.19)$$

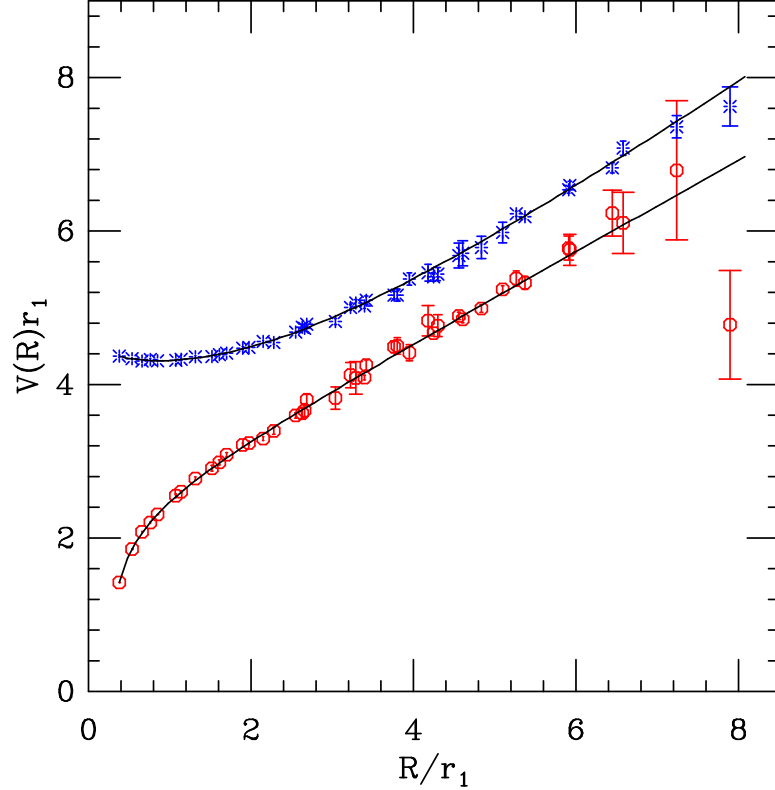


**Figure 4.9.** The static ground potential  $V_{\Sigma_g^+}(R)$  and first gluonic excitations potential  $V_{\Pi_u}(R)$  in terms of the scale parameter  $r_1$  with respect to the quark-antiquark separation  $R$ .



where  $V_0$ ,  $e_c$ , and  $\sigma$  are three fitting parameters, and  $\left[\frac{1}{R}\right]$  is the lattice Coulombic potential, which is calculated in free field theory for the Symanzik improved gauge action [50][51][49] as

$$\left[\frac{1}{R}\right] = \int_{-\pi}^{\pi} \frac{d^3k}{8\pi^2} \frac{e^{i\mathbf{k}\cdot\mathbf{R}}}{\sum_{i=1}^3 \sin^2(\frac{k_i}{2}) + \frac{1}{3} \sum_{i=1}^3 \sin^4(\frac{k_i}{2})}. \quad (4.20)$$

This lattice correction term is used to correct the rotational symmetry of the lattice [49]. In practice we employ it at distances less than  $3a$ . The  $V_0$  can be interpreted as a self-energy. Since only the tree-level coefficients are needed, we use Heller's data for the lattice correction term  $\left[\frac{1}{R}\right]$ . In Table 4.3, we list some of them.

Our fitting gives an acceptable result with a  $\chi^2$  of 46.9 for 39 degrees of freedom, with

$$\begin{aligned} r_1 V_0 &= 2.2731(80) \\ e_c &= -0.3927(27) \\ \sigma r_1^2 &= 0.5870(39), \end{aligned}$$

where we choose all the data within the fitting range of  $r$  from  $\frac{R_{min}}{r_1} = 0.0$  to  $\frac{R_{max}}{r_1} = 7.89688$ . Since  $r_1 V_0 = 2.2731(80)$ , we obtain the self energy  $V_0$ , that is,

$$V_0 = 1.4116(45) \text{ GeV}. \quad (4.21)$$

**Table 4.3.**  $\left[\frac{1}{R}\right]$  for separate distance  $R$ . The first column is the separation distance, the second column is  $\left[\frac{1}{R}\right]$ , and the remaining column is  $\frac{1}{R}$ .

$R$	$\left[\frac{1}{R}\right]$	$\frac{1}{R}$
1.000000000	1.038940053	1.000000000
2.000000000	0.512582839	0.500000000
3.000000000	0.332863472	0.333333333
4.000000000	0.247627405	0.250000000
5.000000000	0.197306796	0.200000000
6.000000000	0.163888673	0.166666667
7.000000000	0.140048006	0.142857143
8.000000000	0.122177437	0.125000000

The first gluonic excitations potential  $V_{\Pi_u}(R)$  is illustrated as the upper part in Fig. 4.9. From Fig. 4.9 we note that at the short distance  $R$  the force between  $Q\bar{Q}$  is repulsive for the  $\Pi_u$  potential, but the force between  $Q\bar{Q}$  is attractive for the  $V_{\Sigma_g^+}$  potential. This can be explained by the color factor [13]. The  $\Sigma_g^+$  potential ( $V_{\Sigma_g^+}$ ) is the singlet static potential in which the quarks  $Q\bar{Q}$  state is in the color singlet representation. The  $\Sigma_g^+$  potential behaves like Eq. (4.19). On the other hand the  $\Pi_u$  potential is a hybrid static potential in which the  $Q\bar{Q}$  state is in the color octet representation. We know that the color factor  $f_c = -\frac{1}{6}$  [13] for color octet configuration of  $Q\bar{Q}$ , and  $f_c = \frac{4}{3}$  [13] for color singlet configuration of  $Q\bar{Q}$ . At short distance  $R$ , the  $\Pi_u$  potential  $V_{\Pi_u}$  should behave like  $\frac{\alpha_s}{6R}$  [52]. That is,

$$V_{\Pi_u} = \frac{\alpha_s}{6R}, \quad R \rightarrow 0, \quad (4.22)$$

where  $\alpha_s$  is strong coupling constant. Eq. (4.19) and Eq. (4.22) can help explain why at short distance  $R$ , the force between  $Q\bar{Q}$  is weakly repulsive for the  $V_{\Pi_u}$  potential, but the force between  $Q\bar{Q}$  is attractive for the  $V_{\Sigma_g^+}$  potential.

The solid curve for the  $V_{\Pi_u}(R)$  potential in Fig. 4.9 is a fit to the data by using the equation

$$e_\pi \left[ \frac{1}{R} \right] + c_0 + \sqrt{b_0 + b_1 R + b_2 R^2}, \quad (4.23)$$

where  $e_\pi$ ,  $c_0$ ,  $b_0$ ,  $b_1$ , and  $b_2$  are five fitting parameters. It gives an acceptable fit with a  $\chi^2$  of 44 with 37 degrees of freedom, with

$$\begin{aligned} c_0 r_1 &= 2.018 \pm 0.211 \\ b_0 r_1^2 &= 5.313 \pm 0.866 \\ b_1 r_1^3 &= -0.761 \pm 0.101 \\ b_2 r_1^4 &= 0.561 \pm 0.028 \\ e_\pi &= 0.036 \pm 0.017. \end{aligned} \quad (4.24)$$

For all  $R$ , in Ref. [5], the authors confirmed that the first-excited potential of the color flux tube is the  $\Pi_u$  potential. Hence, we expect that the lowest lying hybrid mesons should come from the  $V_{\Pi_u}(R)$  potential.

## 4.5 Hybrid quarkonium

The second step in the LBO approximation is to reproduce the heavy quark motion by solving the Schrödinger equation with the potentials of  $V_{\Sigma_g^+}(R)$  or  $V_{\Pi_u}(R)$ . For notational simplicity, we adopt the spherical coordinates. The reduced mass  $\mu$  of the two-body system is

$$\mu = \frac{M_Q M_{\overline{Q}}}{M_Q + M_{\overline{Q}}} = \frac{M_Q}{2}, \quad (4.25)$$

where  $M_Q$  is the mass of the heavy quark  $Q$ ,  $M_{\overline{Q}}$  is the mass of the heavy antiquark  $\overline{Q}$ , and we consider  $M_Q = M_{\overline{Q}}$ . The reduced radial Schrödinger equation of this system is given by [5, 53]

$$\frac{d^2 u(R)}{dR^2} + 2\mu [E - V_{\text{eff}}(R)] u(R) = 0, \quad (4.26)$$

where  $V_{\text{eff}}(R) = V_{Q\overline{Q}}(R) + \frac{\langle \mathbf{L}_{Q\overline{Q}}^2 \rangle}{2\mu R^2}$  is the effective potential [5],  $\mathbf{L}_{Q\overline{Q}}$  is the orbital angular momentum of the quark  $Q$  and antiquark  $\overline{Q}$  (discussed below in detail) [5], and

$$u(R) = \rho(R) R, \quad (4.27)$$

where  $\rho(R)$  is the radial wave function, and  $V_{Q\overline{Q}}(R)$  is either  $V_{\Sigma_g^+}(R)$  or  $V_{\Pi_u}(R)$  [5].

The total angular momentum of the hybrid meson ( $Q\overline{Q}g$ ) is denoted by [5]

$$\mathbf{J} = \mathbf{L} + \mathbf{S}, \quad (4.28)$$

where  $\mathbf{S}$  is the sum of the spins of the quark  $Q$  and antiquark  $\overline{Q}$ , and  $\mathbf{L}$  is the total orbital angular momentum of the hybrid meson. The orbital factor  $\mathbf{L}$  is given by [5]

$$\mathbf{L} = \mathbf{L}_{Q\overline{Q}} + \mathbf{J}_g, \quad (4.29)$$

where  $\mathbf{J}_g$  is the total angular momentum of the gluons. We choose the vector  $\mathbf{n}$  to be unit vector along the axis of the quark  $Q$  and antiquark  $\overline{Q}$  (or  $z$  axis). For the gluon state with  $\Lambda$ , we write the mean value of  $\mathbf{J}_g$  as [53]

$$\langle \mathbf{J}_g \rangle = \mathbf{n} \Lambda. \quad (4.30)$$

Since classically,  $\mathbf{L}_{Q\bar{Q}} = \mathbf{R} \times \mathbf{P}_{Q\bar{Q}}$ , it should be perpendicular to the  $\mathbf{n} = \mathbf{R}/R$  on average (i.e.,  $\langle \mathbf{L}_{Q\bar{Q}} \cdot \mathbf{n} \rangle = 0$ ). Hence, we deduce that [53]  $\langle (\mathbf{L} - \mathbf{J}_g) \cdot \mathbf{n} \rangle = 0$ , or,

$$\langle \mathbf{L} \cdot \mathbf{n} \rangle = \langle \mathbf{J}_g \cdot \mathbf{n} \rangle = \Lambda. \quad (4.31)$$

In the LBO approximation, the eigenvalue  $L(L+1)$  of  $\mathbf{L}^2$  and the eigenvalue  $S(S+1)$  of  $\mathbf{S}^2$  are also good quantum numbers. Hence, the total orbital angular momentum of the quark  $Q$  and antiquark  $\bar{Q}$  is written as [5]

$$\langle \mathbf{L}_{Q\bar{Q}}^2 \rangle = \langle \mathbf{L}^2 \rangle + \langle \mathbf{J}_g^2 \rangle - 2\langle \mathbf{L} \cdot \mathbf{J}_g \rangle \quad (4.32)$$

$$= L(L+1) + \langle \mathbf{J}_g^2 \rangle - 2\Lambda^2. \quad (4.33)$$

For the potential of  $V_{\Sigma_g^+}$ , there are no gluon excitations, so  $\langle \mathbf{J}_g^2 \rangle = 0$ . For the  $V_{\Pi_u}$  potential, we have  $\Lambda = 1$ , so  $\langle \mathbf{J}_g \cdot \mathbf{n} \rangle = 1$  [5]. Hence,  $J_g$  can choose any integer number which is larger than 1 (namely,  $J_g = 1, 2, 3, \dots$ ). From Eq. (4.33), we note that if the system of the hybrid meson have more than one gluon, the energy level will be higher than that of the system with just one gluon [5]. However, here we focus on the decay of the lightest exotic hybrid state. Therefore, we consider the system with just one gluon state [5] (namely,  $\langle \mathbf{J}_g^2 \rangle = 2$ ).

We know that  $\Lambda$  is the  $z$ -component of the angular momentum of the gluon. By convention if  $\Lambda$  is positive, we call it a left-handed gluon state ( $|\text{left}\rangle$ ) which is not an eigenstate of a  $PC$ . If  $\Lambda$  is negative, we call it a right-handed gluon state ( $|\text{right}\rangle$ ) which is also not a  $PC$  eigenstate. However, if as we discuss in more detail in Appendix B, the linear combinations of left-handed and right-handed gluons states are  $|\text{left}\rangle + \epsilon |\text{right}\rangle$  [5], where  $\epsilon = \pm 1$ , are  $PC$  eigenstates. For  $\Sigma_g^+$ , since  $\Lambda = 0$ , we have  $\epsilon = 1$ . Let  $\eta = \pm 1$  be the  $PC$  quantum number of the gluons, which correspond to the subscripts  $g(u)$ . In Appendix A, we prove that the parity and charge conjugation of the hybrid meson are given in the form [5]

$$P = \epsilon (-1)^{L+1} \quad (4.34)$$

$$C = \epsilon \eta (-1)^{L+S}. \quad (4.35)$$

In general the potentials evaluated from Wilson loops in lattice simulations are built up by the same diagrams as the self-energy for the Green's function [54]. The

self energy  $V_0$  renormalizes the quark mass so we absorb it into the definition of  $M_Q$ . The difference between  $V_0$  and  $c_0$  is physically significant, however we should remove the unwanted self-energy contributions. In practice we fit our data for the  $\Sigma_g^+$  potential to the form in Eq. (4.19). The constant  $V_0$  is our approximate estimate of the self-energy contributions.

For the  $\Pi_u$  state, we have  $\Lambda = 1$ , from Eq. (4.31), we obtain that  $L \geq 1$ . The spectra of the heavy hybrid meson ( $b\bar{b}g$ ) built on the potentials of the  $V_{\Sigma_g^+}$  and  $V_{\Pi_u}$  are shown in Fig. 4.10. The energy levels for each state are listed in Table 4.4.

From Ref. [55], we know that in the heavy quark limit, the Hamiltonian operators for  $\Sigma_g^+$ ,  $\Pi_u$  in our LBO approximation is

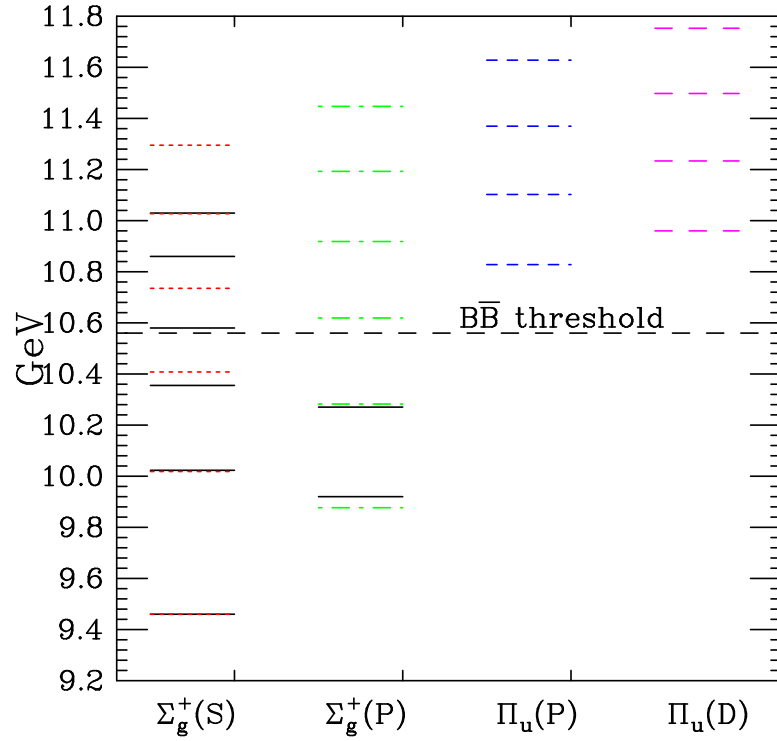


**Figure 4.10.** Spin-averaged  $b\bar{b}$  spectrum in the  $LBO$  approximations. Solid lines specify the experimental measurements. Short dotted, short dashed lines indicate the  $S$  and  $P$  state masses obtained by solving the Schrödinger equation with  $V_{\Sigma_g^+}$  by using  $r_1^{-1} = 0.621$  GeV and  $M_{b1} = 3.88$  GeV for the  $b$  quark mass, respectively. Long dashed, dot-dashed lines indicate the hybrid quarkonium states obtained from the  $V_{\Pi_u}$  ( $L = 1, 2$ ) potentials respectively.

**Table 4.4.** Quarkonium and hybrid quarkonium as computed. The first column gives the first six energy levels for  $\Sigma_g^+(S)$ , the second column, the first six energy levels for  $\Sigma_g^+(P)$ , the third column, the first four energy levels for  $\Pi_u(P)$ , the fourth column, the first four energy levels for  $\Pi_u(D)$ .

$\Sigma_g^+(S)$ GeV	$\Sigma_g^+(P)$ GeV	$\Pi_u(P)$ GeV	$\Pi_u(D)$ GeV
9.4603	9.87656	10.8283	10.96
10.0183	10.2821	11.1025	11.2332
10.4076	10.6194	11.3694	11.4972
10.7349	10.9186	11.628	11.7525
11.0269	11.1924		
11.2951	11.4475		

$$H_{\Sigma_g^+} = 2M_{b0} + \frac{p^2}{2M_{b1}} + V_{\Sigma_g^+}(R) \quad (4.36)$$

$$H_{\Pi_u} = 2M_{b0} + \frac{p^2}{2M_{b1}} + V_{\Pi_u}(R), \quad (4.37)$$

where  $M_{b0}$  is called the rest mass, and  $M_{b1}$  is referred as the kinetic mass [55]. The heavy quark rest mass  $M_{b0}$  was determined by matching the known mass of the  $\Upsilon(1S)$ .

$$M_{\Upsilon(1S)} = 2M_{b0} + E_0, \quad (4.38)$$

where the  $E_0$  is the energy of the ground state in the potential of  $\Sigma_g^+$ . From our LBO approximation, we obtain  $E_0 = 0.1711$  GeV. We know  $M_{\Upsilon(1S)} = 9.4603$  GeV. Hence, we estimate

$$M_{b0} = 4.64 \text{ GeV}. \quad (4.39)$$

The heavy quark mass  $M_b$  is tuned by using a directly measurable physical quantity. A conventional choice is to use the experimentally known  $\Upsilon$  spectrum, namely, the splitting of 2S-1S ( $m_E(2S-1S)$ ) and the splitting of 1P-1S ( $m_E(1P-1S)$ ). From the LBO approximation, we obtain the calculated splitting of 2S-1S ( $m_C(2S-1S)$ ) and the splitting of 1P-1S ( $m_C(1P-1S)$ ). By adjusting the kinetic mass of the  $b$  quark ( $M_b$ ), we make both the difference of splitting of 2S-1S (namely,  $m_C(2S-1S) - m_E(2S-1S)$ ) and the difference of splitting of 1P-1S (namely,  $m_C(1P-1S) -$

$m_E(1P-1S)$ ) as small as possible. Then we obtain the kinetic mass  $M_b$ . In practice we minimize this formula

$$f(M_b) = \sqrt{[m_C(2S-1S) - m_E(2S-1S)]^2 + [m_C(1P-1S) - m_E(1P-1S)]^2} \quad (4.40)$$

to obtain the mass of the  $b$  quark ( $M_b$ ). In our simulation we estimate

$$M_{b1} = 3.88 \text{ GeV}. \quad (4.41)$$

From Fig. 4.10, we note that below the  $B\bar{B}$  threshold, our LBO results are consistent with the spin-averaged experimental measurements, and above the  $B\bar{B}$  threshold, our LBO results are not in good agreement with the spin-averaged experimental measurements. This disagreement probably comes from the fact that above the  $B\bar{B}$  threshold, the  $\Upsilon(4S)$  and  $\Upsilon(5S)$ , etc, can decay to  $B\bar{B}$  [12] and our model does not take those decays into accounts. However due to their exotic properties and heavy quark kinematics, our hybrid states decay only weakly to  $B\bar{B}$  (discussed in Chapter 5). Therefore, our hybrid energy levels are presumably insensitive to this effect. This disagreement also comes from the fact that in our LBO approximation we ignore the high order terms.

From Fig. 4.10, we note that the mass of the lowest-lying hybrid from the  $V_{\Pi_u}$  is approximate 10.83 GeV. In fact we can obtain the precise value of lowest-lying hybrid  $m_H$  from the LBO approximation based on the potential of  $V_{\Pi_u}$ , namely,

$$m_H = 10.8283 \text{ GeV}. \quad (4.42)$$

Above 11 GeV, the LBO approximation based on  $V_{\Pi_u}$  predicts several hybrid states with approximately uniform energy level separations about 200 – 300 MeV. This is a distinct feature of the hybrid quarkonium spectrum.

The reduced radial wave functions for the  $1S$  and  $1P$  conventional quarkonium and that of the lowest-lying  $\Pi_u$  hybrid quarkonium state are shown in Fig. 4.11. For notational convenience, we call the reduced radial wave function for the  $1S$  conventional quarkonium state  $u_{\eta_b}(R)$ , the reduced radial wave function for the  $1P$  conventional quarkonium state  $u_{\chi_b}(R)$ , and the reduced radial wave function for the lowest-lying  $\Pi_u$  hybrid quarkonium state  $u_H(R)$ .

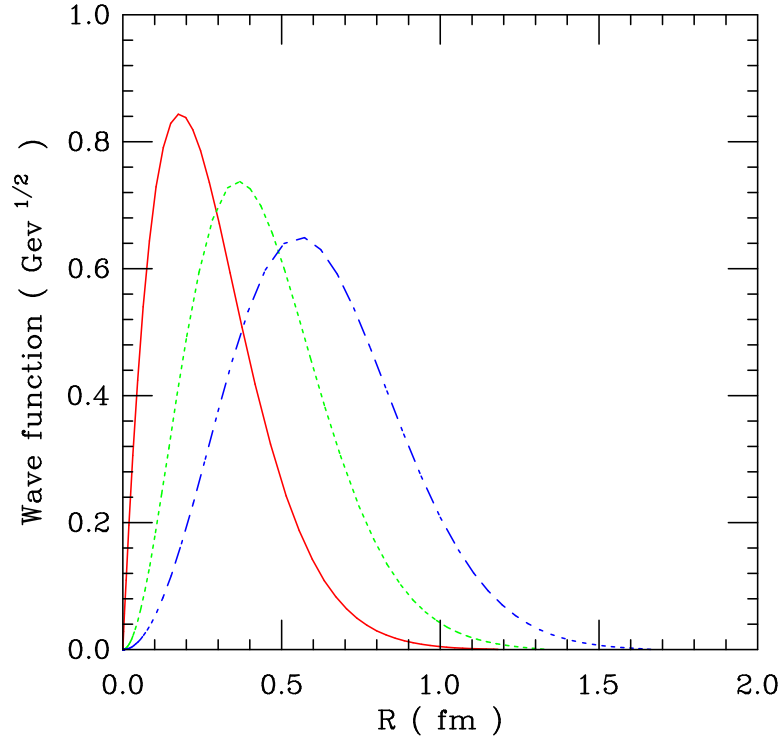


**Figure 4.11.** Reduced radial wave functions versus quark-antiquark separation  $R$ . The solid and dotted curves specify the reduced radial wave functions for the  $1S$  and  $1P$  states of  $\Sigma_g^+$ , respectively, and the short dashed curve specifies the reduced radial wave function of  $\Pi_u$  hybrid state, where all the wave function are normalized.

From Fig. 4.11 we note another distinct feature of the heavy hybrid states. It is the shape of the reduced radial wave function. The hybrid reduced radial wave functions all vanish at the origin ( $R = 0$ ). This can be explained by the repulsive Coulombic term in the potential  $V_{Q\bar{Q}}(R)$  and the special centrifugal term  $V_{\text{eff}}(R)$  in the LBO Schrödinger equation [7]. As depicted in Fig. 4.11, we also note that the hybrid Schrödinger state have a broader reduced radial wave function than those of the conventional quark-antiquark states. In Chapter 5, we use these LBO results to develop the decay model for the hybrid state. In Chapter 8, we use these results to calculate the decay rate.



## CHAPTER 5

### HYBRID MESON DECAY CHANNEL

Most hadronic states are unstable under strong interactions. A comprehensive understanding of the hadronic decay from QCD involves developing the physical models to deal with the unstable hadrons and to extract their hadronic transition matrix elements. The physical models for studying the strong decays of the hadrons have been studied for a long time [56][57]. Here we concentrate on the hadronic decay in the static limit, and employ lattice methods to calculate its transition matrix elements.

For the decays of the hybrid mesons, we study the creation of a light quark-antiquark state from the gluonic field of the hybrid meson, then in the heavy quark limit we discuss its open decay channels with the emphasis on the  $\chi_b S$  channel, where  $S$  is a scalar meson. This scalar channel ( $1^{-+}$ ) leads to  $\pi^+\pi^-$ ,  $\pi^0\pi^0$ , or  $K^+K^-$ ,  $K^+K^-$ .

#### 5.1 Hybrid states on the lattice

In Chapter 4, we studied the properties of the physical hybrid states by solving the Schrödinger equation with these static potentials in the LBO approximation. From Fig. 4.10, we can see that the ground state of the color flux is in the state of  $\Sigma_g^+$ . The first excited state is confirmed to be in the state of  $\Pi_u$  in Ref. [5], and we show this result in Fig. 4.10. We found that the mass of a lightest hybrid spin exotic with  $J^{PC} = 1^{-+}$  is at  $m_H = 10.83$  GeV, about 1.37 GeV heavier than the mass of the  $\Upsilon(1S)$ . Above this energy level there are many hybrid states, including the spin exotic states.

## 5.2 Hybrid meson decay model

In this section, we give a brief review of the possible decay channels of a hybrid meson through the creation of a light quark-antiquark pair ( $q\bar{q}$ ) in the heavy quark limit. The jointed symmetry of the  $q\bar{q}$  and the final gluonic field is identical with the symmetry of the initial representation of the gluonic field [4].

For a spin-exotic hybrid meson which contains an excited gluonic field  $\Pi_u$  with  $\Lambda = 1$  about the separation axis between  $Q\bar{Q}$ , we obtain, from Eq. (4.31), that the orbital angular momentum of the  $Q\bar{Q}$  pair should be greater than or equal to one ( $L \geq 1$ ) [4]. To make the problem simple, we assume that the orbital angular momentum of the  $Q\bar{Q}$  is in the  $P$ -wave (namely,  $L = 1$ ).

In practice, the  $\Pi_u$  state corresponds to an excited gluonic field with  $L^{PC} = 1^{+-}$  or  $L^{PC} = 1^{+-}$  [58]. With the consideration of the spin of the heavy quark  $Q\bar{Q}$ , we obtain a set of eight degenerate states [4]. From the discussion in Chapter 2, we noted that,  $J^{PC} = 1^{-+}$ ,  $0^{+-}$  and  $2^{+-}$  are the spin-exotic hybrid state [58]. Therefore, the spin-exotic hybrid meson has the heavy quark-antiquark pair in a spin triplet ( $S = 1$ ). In any strong decay this is also conserved.

In Chapter 4, we estimated the energy of the low hybrid state, namely,  $E_H = 10.83$  GeV. Therefore, if only considering the energy conservation, The spin-exotic hybrid meson with quantum number  $J^{PC} = 1^{-+}$  have open decay channels:  $B\bar{B}$ ,  $B\bar{B}^*$ ,  $B^*\bar{B}^*$ ,  $\eta_b\eta$ ,  $\eta_b\eta'$ ,  $\chi_b\eta$ ,  $\chi_bS$ ,  $\Upsilon(1s)\omega$  and  $\Upsilon(1s)\phi$  [4].

Page proposed one non-relativistic symmetrization selection rule [59], namely that the hybrid decay does not lead to two identical states:

$$H \not\rightarrow X + Y. \quad (5.1)$$

That is, the decay is suppressed if  $X$  and  $Y$  have an identical internal structure in all respects, as well as an identical radial and gluonic excitation (namely, each meson has orbital angular momentum  $L = 0$  (S-wave)). From this rule we can first exclude the decays to  $B\bar{B}$ ,  $B\bar{B}^*$  and  $B^*\bar{B}^*$ .

For the hybrid meson with  $J^{PC} = 1^{-+}$ , we consider its decay to a  $(Q\bar{q})(\bar{Q}q)$ . If each heavy-light meson  $Q\bar{q}$  has  $L = 0$ , it is impossible, because the spin triplet

state has even  $CP$ , and the spin singlet state has  $\Lambda = 0$  [4]. If one or two heavy-light mesons have a nonzero orbital excitation ( $L \geq 1$ ), it is permitted from the consideration of the symmetry. but not permitted energetically. From Ref. [12], we note that experimental observation mass of the excited ( $L=1$ )  $B$  meson is 5.732 GeV, and the mass of nonexcited ( $L=0$ )  $B$  meson is 5.279 GeV. Therefore, the hybrid exotic meson with mass  $E_H = 10.83$  cannot decay to these two  $B$  mesons if one or two  $B$  mesons have a nonzero orbital excitation ( $L \geq 1$ ).

On the other hand, the decays of a hybrid meson with  $J^{PC} = 1^{-+}$  to  $(Q\bar{Q})(q\bar{q})$  are allowed energetically [4], because the excitation energy in the gluonic field is enough to produce a light quark-antiquark  $q\bar{q}$  pair in a flavor singlet state [4], for example,  $\eta$ ,  $\omega$  and scalar ( $S$ ) channels. However, as we have discussed, its orbital angular momentum is conserved. Hence, the decays to the quarkonia of  $Q\bar{Q}$  are only into a  $\chi_b$  state (P-wave state) in the static limit.

For the decays from a hybrid meson with the  $\Pi_u$  representation to a gluonic field with the  $\Sigma_g^+$  representation, the  $q\bar{q}$  should have a  $\Pi_u$  representation with  $\Lambda = 1$  and  $CP = -1$ . Keep in mind that this orbital wave function of the  $q\bar{q}$  of separation axis between  $Q\bar{Q}$  has no spin component. Therefore, if the  $q\bar{q}$  is the scalar meson with  $J^{PC} = 0^{++}$ , its orbital wave function should have odd  $CP$  [4].

# CHAPTER 6

## OUR CALCULATIONAL METHOD

In Chapter 5 we discussed the possible decay channels of a hybrid meson in the heavy quark limit. The goal of this dissertation is to study these hadronic decays.

In this dissertation, we consider the decay,

$$H \longrightarrow A + B, \tag{6.1}$$

where  $H$  is unstable spin-exotic hybrid state of the static heavy quark. The hybrid meson  $H$  is in the  $\Pi_u$  representation. The  $A$  and  $B$  stand for two decay products. The  $A$  is a conventional quarkonium state  $\chi_b$  in the  $\Sigma_g^+$  representation. The  $B$  is a  $0^{++}\pi\pi$  state [4].

In Chapter 4, we explained in detail the correlators  $C_{AA}$  and  $C_{HH}$ , which we used for calculating the static potential  $V_{\Sigma_g^+}(R)$ ,  $V_{\Pi_u}(R)$  respectively. In this chapter, we discuss in detail the correlators  $C_{BB}$  and  $C_{HAB}$ , which are used to calculate the transition amplitude  $x$  and the decay rate  $\Gamma$  in Chapters 7 and 8.

### 6.1 $C_{BB}$ correlator

In this section we calculate the correlator from B state ( $0^{++}\pi\pi$  state) to B state. We first give the definition of the  $C_{BB}$  correlator. Then we introduce two methods to calculate it. Because we use replica trick in our calculation for the  $C_{BB}$  correlator, we first briefly introduce the replica trick.

#### 6.1.1 Replica trick in lattice

As we discussed in Chapter 3, for the KS staggered fermion, we reduce the number of the tastes per flavor from 16 to 4. To further reduce from 4 to 1, we used the fourth root trick. At the quark level, the fourth root trick can be achieved

by multiplying each dynamical sea quark loop by a factor of  $\frac{1}{4}$  [60]. In Ref. [60], the authors apply this method to staggered chiral perturbation theory (S $\chi$ PT). However in practice, when we use this method to work at all orders in S $\chi$ PT, we cannot make sure that every time we do it correctly at higher order in S $\chi$ PT. A solution for this is to use the replica trick.<sup>1</sup> We can state this trick as [60] follows:

1) Generalize the number of each quark flavor to contain  $n_i$  quarks ( $i=u, d, s$ ) (i.e.,  $n_u$  for up quark,  $n_d$  for down quark,  $n_s$  for strange quark). Therefore, we have

$$n = \sum_{i=u,d,s} n_i \text{ total quark for all flavors } u, d, s.$$

2) Calculate physical quantities in which we are interested (e.g., correlation function) as analytic functions of the  $n_i$ .

3) In the end, set each  $n_i = \frac{1}{4}$ ,  $i = u, d, s$ .

This trick automatically performs the transition from four tastes to one taste per flavor for staggered fermion at all orders. We use this method extensively.

### 6.1.2 The operator for the $C_{BB}$ correlator

On a starting time slice  $t$ , the quark  $Q$  and antiquark  $\bar{Q}$  are fixed at lattice sites with separation distance of  $R$ , whose midpoint is at space point  $\mathbf{r}$ . Let  $\mathbf{s}$  be the spatial point of the  $\pi\pi$  states at the source time, and  $\mathbf{s}'$  corresponding position at the sink time (see Fig. 6.1). In order to make our  $\pi\pi$  state to be  $0^{++}$  flavor singlet, the fermionic lattice operator at the source can be written as

$$\mathcal{O}_{Source}(\mathbf{s}, t) \equiv \sum_{a,g} \frac{\bar{u}_g^a(\mathbf{s}, t) u_g^a(\mathbf{s}, t) + \bar{d}_g^a(\mathbf{s}, t) d_g^a(\mathbf{s}, t)}{\sqrt{2n_r}}, \quad (6.2)$$

where  $g$  is the index of the taste replica,  $n_r$  is the number of the taste replicas, and  $a$  is the color index. At the final time slice  $t_f$  ( $t_f \equiv t + T$ ), the fermionic lattice operator at the sink can be written similarly as

$$\mathcal{O}_{Sink}(\mathbf{s}', t_f) \equiv \sum_{b,g'} \frac{\bar{u}_{g'}^b(\mathbf{s}', t_f) u_{g'}^b(\mathbf{s}', t_f) + \bar{d}_{g'}^b(\mathbf{s}', t_f) d_{g'}^b(\mathbf{s}', t_f)}{\sqrt{2n_r}}, \quad (6.3)$$

where  $g'$  is the index of the taste replica and  $b$  is the color index.

---

<sup>1</sup>The replica trick is originally proposed in Refs. [61] to study the spin glass. Now it has been widely used in the theory of the disordered systems such as QCD [62].

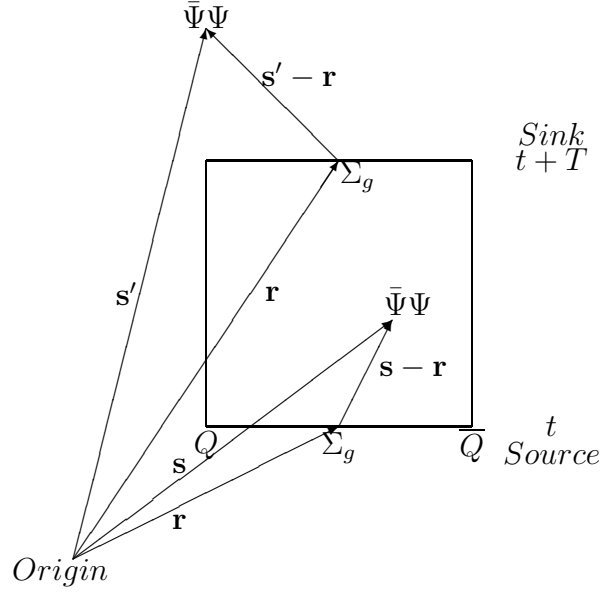


**Figure 6.1.** An illustration of the correlator from  $B$  to  $B$ .

Therefore, the time slice correlator  $C_{BB}$  from  $B$  (namely,  $0^{++} \pi\pi$ ) to  $B$  for a chosen momentum  $\mathbf{k}$  can be evaluated by the formula

$$\begin{aligned}
 C_{BB}(T, \mathbf{k}) &= \frac{1}{\Omega} \sum_{\mathbf{s}, \mathbf{s}', t} \left\langle \text{Tr} [\mathcal{O}_{\text{Sink}}^\dagger(\mathbf{s}', t+T) \mathcal{O}_{\text{Source}}(\mathbf{s}, t)] \right\rangle e^{i\mathbf{k} \cdot (\mathbf{s} - \mathbf{s}')} \\
 &= \frac{1}{\Omega} \frac{1}{n_r} \sum_t \sum_{\mathbf{s}', \mathbf{s}} \sum_{a,b} \sum_{g,g'} \left\{ \left\langle \bar{u}_{g'}^b(\mathbf{s}', t+T) u_{g'}^b(\mathbf{s}', t+T) \bar{u}_g^a(\mathbf{s}, t) u_g^a(\mathbf{s}, t) \right\rangle + \right. \\
 &\quad \left. \left\langle \bar{u}_{g'}^b(\mathbf{s}', t+T) u_{g'}^b(\mathbf{s}', t+T) \bar{d}_g^a(\mathbf{s}, t) d_g^a(\mathbf{s}, t) \right\rangle \right\} e^{i\mathbf{k} \cdot (\mathbf{s} - \mathbf{s}')}, \quad (6.4)
 \end{aligned}$$

where  $\Omega$  is the total lattice volume. Here we consider that the  $u, d$  quarks are degenerate in mass. We can simplify the correlator of  $C_{BB}$  in Eq. (6.4) as

$$\begin{aligned}
 C_{BB}(T, \mathbf{k}) &= \frac{1}{\Omega} \frac{1}{n_r} \sum_t \sum_{\mathbf{s}', \mathbf{s}} \sum_{a,b} \sum_{g,g'} \left\{ \left\langle \bar{u}_{g'}^b(\mathbf{s}', t+T) u_{g'}^b(\mathbf{s}', t+T) \bar{u}_g^a(\mathbf{s}, t) u_g^a(\mathbf{s}, t) \right\rangle + \right. \\
 &\quad \left. \left\langle \bar{u}_{g'}^b(\mathbf{s}', t+T) u_{g'}^b(\mathbf{s}', t+T) \bar{d}_g^a(\mathbf{s}, t) d_g^a(\mathbf{s}, t) \right\rangle \right\} e^{i\mathbf{k} \cdot (\mathbf{s} - \mathbf{s}')}, \quad (6.5)
 \end{aligned}$$

After we perform the Wick contractions of the fermion fields, and sum over the index of the taste replica [15], we obtain

$$C_{BB}(T, \mathbf{k}) = \frac{1}{\Omega} \sum_t \sum_{\mathbf{s}', \mathbf{s}} \left\{ \sum_{a,b} \left\langle M_{bb}^{-1}(\mathbf{s}', t+T; \mathbf{s}', t+T) M_{aa}^{-1}(\mathbf{s}, t; \mathbf{s}, t) \right\rangle e^{i\mathbf{k} \cdot (\mathbf{s} - \mathbf{s}')} \right\} \quad (6.6)$$

$$-\frac{2n_r}{\Omega} \sum_t \sum_{\mathbf{s}', \mathbf{s}} \left\{ \sum_{a,b} \left\langle M_{ba}^{-1}(\mathbf{s}', t+T; \mathbf{s}, t) M_{ab}^{-1}(\mathbf{s}, t; \mathbf{s}', t+T) \right\rangle e^{i\mathbf{k} \cdot (\mathbf{s} - \mathbf{s}')} \right\},$$

where  $M$  is the fermion matrix. Therefore, the correlator  $C_{BB}(T, \mathbf{k})$  contains two parts. The first term in Eq. (6.6) is the disconnected contribution part (i.e., DC part). We label this term  $C_{BB}^{DC}$ .

$$C_{BB}^{DC}(T, \mathbf{k}) = \frac{1}{\Omega} \sum_t \sum_{\mathbf{s}', \mathbf{s}} \left\{ \sum_{a,b} \left\langle M_{aa}^{-1}(\mathbf{s}, t; \mathbf{s}, t) M_{bb}^{-1}(\mathbf{s}', t+T; \mathbf{s}', t+T) \right\rangle e^{i\mathbf{k} \cdot (\mathbf{s} - \mathbf{s}')} \right\}. \quad (6.7)$$

The second term in Eq. (6.6) is the connected contribution for correlator  $C_{BB}$ . We label this term  $C_{BB}^{CC}$ .

$$C_{BB}^{CC}(T, \mathbf{k}) = \frac{1}{\Omega} \sum_t \sum_{\mathbf{s}', \mathbf{s}} \left\{ \sum_{a,b} \left\langle M_{ab}^{-1}(\mathbf{s}, t; \mathbf{s}', t+T) M_{ba}^{-1}(\mathbf{s}', t+T; \mathbf{s}, t) \right\rangle e^{i\mathbf{k} \cdot (\mathbf{s} - \mathbf{s}')} \right\}. \quad (6.8)$$

### 6.1.3 Direct method

In our lattice simulation, we use the direct method to calculate the connected part  $C_{BB}^{CC}(T, \mathbf{k})$ . Eq. (6.7) can be changed into

$$C_{BB}^{CC}(T, \mathbf{k}) = \frac{1}{\Omega} \sum_t \sum_{\mathbf{s}', \mathbf{s}} \left\{ \text{Tr}_c \left[ M^{-1}(\mathbf{s}, t; \mathbf{s}', t+T) M^{-1}(\mathbf{s}', t+T; \mathbf{s}, t) \right] e^{i\mathbf{k} \cdot (\mathbf{s} - \mathbf{s}')} \right\}, \quad (6.9)$$

where  $\text{Tr}_c$  is trace over the color index. We know that

$$M^{-1}(\mathbf{s}, t; \mathbf{s}', t+T) \equiv [M^{-1}(\mathbf{s}', t+T; \mathbf{s}, t)]^\dagger (-1)^{s' - s}, \quad (6.10)$$

where  $s \equiv (\mathbf{s}, t)$ ,  $s' \equiv (\mathbf{s}', t+T)$ ,  $M^{-1}(s; s')$  is  $3 \times 3$  color matrix, and  $(-1)^{s' - s} \equiv (-1)^{s'_1 + s'_2 + s'_3 - s_1 - s_2 - s_3 + T}$ . Finally, we can rewrite our connected part as

$$C_{BB}^{CC}(T, \mathbf{k}) = \frac{1}{\Omega} \sum_t \sum_{\mathbf{s}', \mathbf{s}} \left\{ (-1)^{s' - s} e^{i\mathbf{k} \cdot (\mathbf{s} - \mathbf{s}')} \times \text{Tr}_c \left[ M^{-1}(\mathbf{s}, t; \mathbf{s}', t+T) M^{-1}(\mathbf{s}, t; \mathbf{s}', t+T)^\dagger \right] \right\}. \quad (6.11)$$

We use the conjugate gradient method (CG) to obtain the required matrix element of the inverse fermion matrix  $M(\mathbf{s}, t; \mathbf{s}', t+T)$  by solving the linear system

$$\sum_b M_{a,b}(\mathbf{s}'', t''; \mathbf{s}', t+T) M_{b,c}^{-1}(\mathbf{s}', t+T; \mathbf{s}, t) = \delta_{a,c} \delta_{t'', t} \delta_{\mathbf{s}'', \mathbf{s}} \quad (6.12)$$

for  $M_{b,c}^{-1}(\mathbf{s}', t+T; \mathbf{s}, t)$ , where the  $a, b, c$  are color indices. Since we obtain the matrix element of  $M^{-1}(\mathbf{s}', t+T; \mathbf{s}, t)$ , we can easily calculate  $C_{BB}^{CC}(T, \mathbf{k})$  by Eq. (6.11).

### 6.1.4 Random source method

With the random source we compute both the  $DC$  part and  $CC$  part for the correlator  $C_{BB}$ . This method involves relating the desired correlator to a correlator involving random color fields  $\xi$ :

$$\begin{aligned}
C_{BB}^{RND}(T, \mathbf{k}) &= \frac{1}{\Omega} \sum_t \sum_{\mathbf{s}', \mathbf{s}} \left\{ e^{i\mathbf{k} \cdot (\mathbf{s} - \mathbf{s}')} \times \right. \\
&\quad \frac{1}{N_r} \sum_{\eta} \sum_{a, a'} \sum_{\mathbf{r}'_0, t'_0} \left[ \xi_a^{\eta*}(\mathbf{s}, t) M_{aa'}^{-1}(\mathbf{s}, t; \mathbf{r}'_0, t'_0) \xi_{a'}^{\eta}(\mathbf{r}'_0, t'_0) \right] \times \\
&\quad \left. \frac{1}{N_r} \sum_{\eta'} \sum_{b, b'} \sum_{\mathbf{r}', t'} \left[ \xi_b^{\eta'*}(\mathbf{s}', t+T) M_{bb'}^{-1}(\mathbf{s}', t+T; \mathbf{r}', t') \xi_{b'}^{\eta'}(\mathbf{r}', t') \right] \right\} \\
&= \frac{1}{\Omega} \sum_t \sum_{\mathbf{s}', \mathbf{s}} \left\{ e^{i\mathbf{k} \cdot (\mathbf{s} - \mathbf{s}')} \times \right. \\
&\quad \sum_{\mathbf{r}', t'} \sum_{\mathbf{r}'_0, t'_0} \left[ \sum_{a, a'} \sum_{b, b'} \left( M_{aa'}^{-1}(\mathbf{s}, t; \mathbf{r}'_0, t'_0) M_{bb'}^{-1}(\mathbf{s}', t+T; \mathbf{r}', t') \right) \times \right. \\
&\quad \left. \left. \frac{1}{N_r^2} \sum_{\eta} \sum_{\eta'} \left( \xi_a^{\eta*}(\mathbf{s}, t) \xi_{a'}^{\eta}(\mathbf{r}'_0, t'_0) \xi_b^{\eta'*}(\mathbf{s}', t+T) \xi_{b'}^{\eta'}(\mathbf{r}', t') \right) \right] \right\}, \quad (6.13)
\end{aligned}$$

where  $N_r$  is the total number of random sources,  $\xi$  is the complex vector of the gaussian random numbers,  $a, a', b, b'$  are color indices, and  $\eta, \eta'$  are the indices of the random sources. In the MILC code, we simulate the  $\xi$  to satisfy

$$\begin{aligned}
\langle \text{Re} \xi_x \rangle &= \frac{1}{N_r} \sum_r \text{Re} \xi_x^r = 0 & \langle \text{Im} \xi_x \rangle &= \frac{1}{N_r} \sum_r \text{Im} \xi_x^r = 0 \\
\langle (\text{Re} \xi_x)^2 \rangle &= \frac{1}{N_r} \sum_r (\text{Re} \xi_x^r)^2 = \frac{1}{2} & \langle (\text{Im} \xi_x)^2 \rangle &= \frac{1}{N_r} \sum_r (\text{Im} \xi_x^r)^2 = \frac{1}{2}, \quad (6.14)
\end{aligned}$$

where  $\text{Re} \xi$  is the real part of  $\xi$ , and  $\text{Im} \xi$  is the imagery part of  $\xi$ . We can prove

$$\frac{1}{N_r} \sum_{\eta} \xi_a^{\eta*}(x) \xi_b^{\eta}(y) = \delta_{xy} \delta_{ab} \quad (6.15)$$

$$\frac{1}{N_r} \sum_{\eta} \xi_a^{\eta*}(x) \xi_b^{\eta}(y) \xi_{a'}^{\eta*}(x') \xi_{b'}^{\eta}(y') = \delta_{xy} \delta_{ab} \delta_{a'b'} \delta_{x'y'} + \delta_{ab'} \delta_{xy'} \delta_{ba'} \delta_{yx'}, \quad (6.16)$$

where  $a$  is color index, and  $\eta$  is the index of random source.

For  $\eta \neq \eta'$ , the correlator in Eq. (6.13) gives the disconnected part, that is,

$$C_{BB}^{RND}(T, \mathbf{k})_{\eta \neq \eta'} = C_{BB}^{DC}(T, \mathbf{k}) \times \left( 1 - \frac{1}{N_r} \right). \quad (6.17)$$



For  $\eta = \eta'$ , it gives both the disconnected part and connected part, that is,

$$C_{BB}^{RND}(T, \mathbf{k})_{\eta=\eta'} = \frac{1}{N_r} \left( C_{BB}^{DC}(T, \mathbf{k}) + C_{BB}^{CC}(T, \mathbf{k}) \right). \quad (6.18)$$

Therefore, we obtain both the disconnected part and the connected part of the correlator  $C_{BB}$  from this method. In practice, we compare the result of the connected part from this method with the result of the connected part from the direct method to justify our results from this method. From our calculation we find that if we choose the  $N_r$  large enough, the numbers from two methods agree.

Let

$$\sigma^\eta(\mathbf{s}, t) \equiv \sum_{a,a'} \sum_{\mathbf{r}_0', t'_0} \xi_a^{\eta*}(\mathbf{s}, t) M_{aa'}^{-1}(\mathbf{s}, t; \mathbf{r}_0', t'_0) \xi_{a'}^\eta(\mathbf{r}_0', t'_0) \quad (6.19)$$

$$\sigma^{\eta'}(\mathbf{s}', t+T) \equiv \sum_{b,b'} \sum_{\mathbf{r}', t'} \xi_b^{\eta'*}(\mathbf{s}', t+T) M_{bb'}^{-1}(\mathbf{s}', t+T; \mathbf{r}', t') \xi_{b'}^{\eta'}(\mathbf{r}', t'). \quad (6.20)$$

Then Eq. (6.13) can be rewritten as

$$C_{BB}^{RND}(T, \mathbf{k}) = \frac{1}{\Omega} \frac{1}{N_r^2} \sum_{\eta, \eta'} \sum_t \sum_{\mathbf{s}', \mathbf{s}} \left\{ \sigma^\eta(\mathbf{s}, t) \sigma^{\eta'}(\mathbf{s}', t+T) e^{i\mathbf{k} \cdot (\mathbf{s} - \mathbf{s}')} \right\}. \quad (6.21)$$

If we define the Fourier transform:  $\sigma^\eta(\mathbf{k}, t) = \sum_{\mathbf{s}} \sigma^\eta(\mathbf{s}, t) e^{-i\mathbf{k} \cdot \mathbf{s}}$ , then Eq. (6.13) can be rewritten as

$$C_{BB}^{RND}(T, \mathbf{k}) = \frac{1}{\Omega} \frac{1}{N_r^2} \sum_t \sum_{\eta, \eta'} \sigma^\eta(-\mathbf{k}, t) \sigma^{\eta'}(\mathbf{k}, t+T). \quad (6.22)$$

From the above discussion, we know that, for  $\eta \neq \eta'$ , the above correlator gives the disconnected part and for  $\eta = \eta'$ , it gives both disconnected and connected parts.

## 6.2 $C_{HAB}$ correlator

In this section we show how to calculate the correlator from the  $\Pi_u$  state or  $H$  to our two final states  $A$  and  $B$  state. On a starting time slice  $t$ , the quark  $Q$  and antiquark  $\bar{Q}$  are fixed on lattice sites with a separation distance  $R$  whose midpoint is at space point  $\mathbf{r}$  (see Fig. 6.2). The gluonic operator at time slice  $t$  is the  $\Pi_u$  lattice operator as we described in Sec. 4.4.2.

At the final time slice  $t+T$ , the gluonic lattice operator can be written as

$$\mathcal{O}_{Sink}(\mathbf{r}, \mathbf{R}, t+T) \equiv \sum_{\mathbf{s}} \Sigma_g^+(\mathbf{r}, \mathbf{R}, t+T) w(\mathbf{s} - \mathbf{r}) \times$$

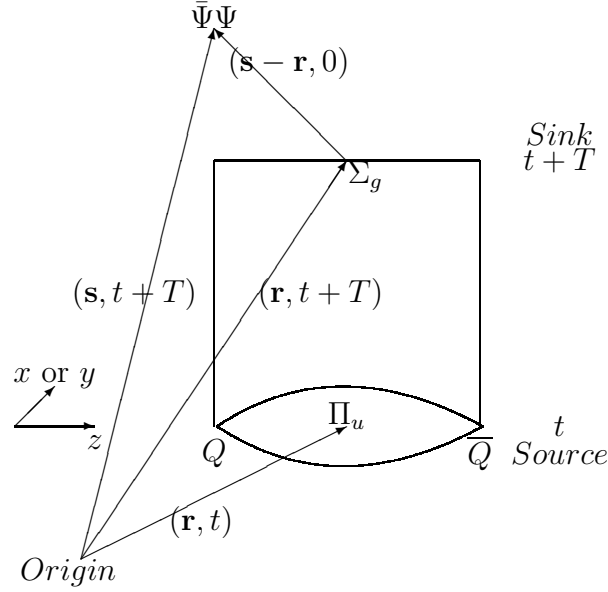


**Figure 6.2.** An illustration of the correlator from  $H$  to  $AB$ .

$$\begin{aligned} & \sum_a \frac{\bar{u}^a(\mathbf{s}, t+T)u^a(\mathbf{s}, t+T) + \bar{d}^a(\mathbf{s}, t+T)d^a(\mathbf{s}, t+T)}{\sqrt{2}} \\ &= \sqrt{2} \sum_{\mathbf{s}, a} \Sigma_g^+(\mathbf{r}, \mathbf{R}, t+T) w(\mathbf{s}-\mathbf{r}) \bar{u}^a(\mathbf{s}, t+T) u^a(\mathbf{s}, t+T), \quad (6.23) \end{aligned}$$

where we consider that the  $u, d$  quarks are degenerate in mass and their production amplitude are identical. The  $w(\mathbf{s}-\mathbf{r})$ <sup>2</sup> is the wave function of  $\bar{u}^a(\mathbf{s}, t+T)u^a(\mathbf{s}, t+T)$ . Here we should note that wave function  $w(\mathbf{s}-\mathbf{r})$  is just our choice for the final state. We assume it is a real function (i.e.,  $w^* = w$ ). We should choose a suitable wave function  $w(\mathbf{s}-\mathbf{r})$  to make sure that the initial and final states are in same symmetries. With these definitions the time slice correlator can be written as

$$\begin{aligned} C_{HAB}(T, \mathbf{R}) &= \frac{1}{\Omega} \sum_{\mathbf{r}, t} \left\langle \text{Tr} \left[ \mathcal{O}_{Sink}^\dagger(\mathbf{r}, \mathbf{R}, t+T) \mathcal{O}_{Source}(\mathbf{r}, \mathbf{R}, t) \right] \right\rangle \\ &= \frac{\sqrt{2}}{\Omega} \sum_{\mathbf{r}, t} \sum_{\mathbf{s}} \left\langle \sum_a \bar{u}^a(\mathbf{s}, t+T) u^a(\mathbf{s}, t+T) \right\rangle w(\mathbf{s}-\mathbf{r}) \times \\ &\quad \text{Tr} \left[ \Sigma_g^+(\mathbf{r}, \mathbf{R}, t+T) \Pi_u(\mathbf{r}, \mathbf{R}, t) \right] \\ &= \frac{\sqrt{2}}{\Omega} \sum_{\mathbf{r}, t} \sum_{\mathbf{s}} \sum_a M_{aa}^{-1}(\mathbf{s}, t+T; \mathbf{s}, t+T) w(\mathbf{s}-\mathbf{r}) \times \end{aligned}$$

---

<sup>2</sup>In Chapter 5, we discussed the  $CP$  symmetry of the wave function  $w(\mathbf{s}-\mathbf{r})$ .

$$\text{Tr} \left[ \Sigma_g^+(\mathbf{r}, \mathbf{R}, t+T) \Pi_u(\mathbf{r}, \mathbf{R}, t) \right]. \quad (6.24)$$

From the random source method, we can evaluate  $\sum_a \bar{u}^a(\mathbf{s}, t+T) u^a(\mathbf{s}, t+T)$  from

$$\begin{aligned} \left\langle \sum_a \bar{u}^a(\mathbf{s}, t+T) u^a(\mathbf{s}, t+T) \right\rangle &= \sum_a M_{aa}^{-1}(\mathbf{s}, t+T; \mathbf{s}, t+T) \\ &= \frac{1}{N_r} \sum_\eta \sigma^\eta(\mathbf{s}, t+T). \end{aligned} \quad (6.25)$$

Since the configurations are gauge fixed to the temporal gauge before we estimate the correlator, the time-link link variables are unit matrices. Hence, we measure the product of the parallel transporters in Eq. (6.24) (i.e.,  $\text{Tr} \left[ \Sigma_g^+(\mathbf{r}, \mathbf{R}, t+T) \Pi_u(\mathbf{r}, \mathbf{R}, t) \right]$ ) by two bent Wilson loops shown in Fig. 6.3. In terms of

$$S(\mathbf{s}, t+T) \equiv \sum_a M_{aa}^{-1}(\mathbf{s}, t+T; \mathbf{s}, t+T) \quad (6.26)$$

$$\mathcal{A}(\mathbf{r}, \mathbf{R}, t, T) \equiv \text{Tr} \left[ \Sigma_g^+(\mathbf{r}, \mathbf{R}, t+T) \Pi_u(\mathbf{r}, \mathbf{R}, t) \right], \quad (6.27)$$

we have

$$C_{HAB}(T, \mathbf{R}) = \frac{\sqrt{2}}{\Omega} \sum_{\mathbf{r}, t} \sum_{\mathbf{s}} S(\mathbf{s}, t+T) w(\mathbf{s}-\mathbf{r}) \mathcal{A}(\mathbf{r}, \mathbf{R}, t, T). \quad (6.28)$$

We can express the wave function of the  $\pi\pi$  state in momentum space,

$$w(\mathbf{s}, \mathbf{r}) \equiv w(\mathbf{s}-\mathbf{r}) = \sum_{\mathbf{p}} e^{i\mathbf{p} \cdot (\mathbf{r}-\mathbf{s})} w(\mathbf{p}). \quad (6.29)$$

Then we can rewrite Eq. (6.28) as

$$C_{HAB}(T, \mathbf{R}) = \frac{\sqrt{2}}{\Omega} \sum_{t, \mathbf{p}} \left\{ w(\mathbf{p}) \sum_{\mathbf{s}} S(\mathbf{s}, t+T) e^{-i\mathbf{p} \cdot \mathbf{s}} \sum_{\mathbf{r}} \mathcal{A}(\mathbf{r}, \mathbf{R}, t, T) e^{i\mathbf{p} \cdot \mathbf{r}} \right\}. \quad (6.30)$$

If we perform the following Fourier transforms,

$$\mathcal{A}(-\mathbf{p}, \mathbf{R}, t, T) = \sum_{\mathbf{r}} \mathcal{A}(\mathbf{r}, \mathbf{R}, t, T) e^{i\mathbf{p} \cdot \mathbf{r}} \quad (6.31)$$

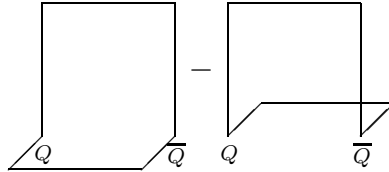


**Figure 6.3.** An illustration of the calculation of  $\mathcal{A}$ .

$$S(\mathbf{p}, t+T) = \sum_{\mathbf{s}} S(\mathbf{s}, t+T) e^{-i\mathbf{p}\cdot\mathbf{s}}, \quad (6.32)$$

we arrive at

$$C_{HAB}(T, \mathbf{R}) = \frac{\sqrt{2}}{\Omega} \sum_t \sum_{\mathbf{p}} w(\mathbf{p}) S(\mathbf{p}, t+T) \mathcal{A}(-\mathbf{p}, \mathbf{R}, t, T). \quad (6.33)$$

Now we discuss the symmetry of the wave function  $w(\mathbf{s} - \mathbf{r})$ . It depends on the meson, which was created in the decay. For scalar meson production (with  $J^{PC} = 0^{++}$ ), the  $w(\mathbf{s} - \mathbf{r})$  must be in a  $\Pi_u$  representation. This can be achieved by making  $w(\mathbf{s} - \mathbf{r})$  odd in the  $x$  direction and even in the  $y$  and  $z$  directions, where  $x$  is the direction of the transverse extent of the  $\Pi_u$  state. Another method to check this symmetry is to consider the parity, since  $P_x$ ,  $P_y$  and  $CP_z$  are conserved in the heavy decay in heavy quark limit. Now we consider our  $\Pi_u$  potential state, which is odd under  $P_x$  and even under  $P_y$  and  $CP_z$ . The  $\Sigma_g^+$  operator is even under all three operations. Therefore, the symmetry requires that the wave function  $w$  be odd under the inversion  $P_x$  and even under  $P_y$  and  $P_z$  (since  $C = +1$  for the scalar meson). So, we choose the wave function as

$$w(\mathbf{k}, \mathbf{r}) = \sin(k_x \cdot x) \cos(k_y \cdot y) \cos(k_z \cdot z), \quad (6.34)$$

where the  $\mathbf{k} = (k_x, k_y, k_z)$  is the chosen momentum. It have the desired symmetry. In terms of plane waves

$$\begin{aligned} w(\mathbf{p}) &= \frac{1}{V} \sum_{\mathbf{r}} e^{i\mathbf{p}\cdot\mathbf{r}} w(\mathbf{r}) \\ &= \frac{1}{8i} \left\{ \delta_{\mathbf{p}, \mathbf{k}} + \delta_{\mathbf{p}, \mathbf{k}_1} + \delta_{\mathbf{p}, \mathbf{k}_2} + \delta_{\mathbf{p}, \mathbf{k}_3} - \delta_{\mathbf{p}, -\mathbf{k}} - \delta_{\mathbf{p}, -\mathbf{k}_1} - \delta_{\mathbf{p}, -\mathbf{k}_2} - \delta_{\mathbf{p}, -\mathbf{k}_3} \right\}, \end{aligned} \quad (6.35)$$

where  $\mathbf{k}_1 \equiv (k_x, k_y, -k_z)$ ,  $\mathbf{k}_2 \equiv (k_x, -k_y, k_z)$ , and  $\mathbf{k}_3 \equiv (k_x, -k_y, -k_z)$ .

We can then rewrite Eq. (6.33) as

$$\begin{aligned} C_{HAB}(T, \mathbf{R})_{\mathbf{k}} &= \frac{\sqrt{2}}{\Omega} \sum_t \frac{1}{8i} \left\{ S(\mathbf{k}, t+T) \mathcal{A}(-\mathbf{k}, \mathbf{R}, t, T) - S(-\mathbf{k}, t+T) \mathcal{A}(\mathbf{k}, \mathbf{R}, t, T) \right. \\ &\quad + S(\mathbf{k}_1, t+T) \mathcal{A}(-\mathbf{k}_1, \mathbf{R}, t, T) - S(-\mathbf{k}_1, t+T) \mathcal{A}(\mathbf{k}_1, \mathbf{R}, t, T) \\ &\quad + S(\mathbf{k}_2, t+T) \mathcal{A}(-\mathbf{k}_2, \mathbf{R}, t, T) - S(-\mathbf{k}_2, t+T) \mathcal{A}(\mathbf{k}_2, \mathbf{R}, t, T) \\ &\quad \left. + S(\mathbf{k}_3, t+T) \mathcal{A}(-\mathbf{k}_3, \mathbf{R}, t, T) - S(-\mathbf{k}_3, t+T) \mathcal{A}(\mathbf{k}_3, \mathbf{R}, t, T) \right\}. \end{aligned} \quad (6.36)$$

We use this formula to calculate the desired correlator  $C_{HAB}$ .

# CHAPTER 7

## HYBRID MESON DECAY FROM THE LATTICE

For notational simplicity and without loss of generality, in this chapter we consider the generic strong decay

$$H \rightarrow A + B, \tag{7.1}$$

where  $A$  and  $B$  are stable particles.

In Chapter 5, we studied the hybrid meson decay channel. It is possible to employ some rather restricted conditions on a lattice to extract the transition matrix elements ( $x$ ) [4]. In this chapter, we first use the time-dependent perturbation theory to study the  $C_{HAB}$  correlator. Then we introduce a method to extract  $x$  directly from lattice [4].

### 7.1 Perturbation expansion for $C_{HAB}$ correlator

In this section we use perturbation theory to study the correlator  $C_{HAB}$  in Sec. 6.3, that is to calculate the correlator from the  $\Pi_u$  state (i.e., H state) to two-body states (namely, AB state). To use this approach, we should discuss whether the perturbation theory here is justified or not. The condition we need is that  $\Gamma \ll \Delta E$ , where  $\Gamma$  is the decay rate, and  $\Delta E = E_H - E_A$ . This is the narrow width approximation. In Chapter 8, we will discuss this question.

For notational simplicity we refer to the lattice operator at the source  $H$  as (Please see details in Chapter 6),

$$\mathcal{O}_H(\mathbf{r}, \mathbf{R}, t), \tag{7.2}$$

and we refer to the lattice operator at the sink  $AB$  as

$$\mathcal{O}_{AB}(\mathbf{r}, \mathbf{R}, t+T) \equiv \sum_{\mathbf{s}} \mathcal{O}_A(\mathbf{r}, \mathbf{R}, t+T) w(\mathbf{s} - \mathbf{r}) \mathcal{O}_B(\mathbf{s}, t+T), \quad (7.3)$$

where  $w(\mathbf{s} - \mathbf{r})$  is the distribution wave function of the meson  $B$ .

In this notation the time slice correlator is given by

$$C_{HAB}(t, \mathbf{R}) = \frac{1}{\Omega} \sum_{\mathbf{r}, t} \left\langle \mathcal{O}_{AB}^\dagger(\mathbf{r}, \mathbf{R}, t+T) \mathcal{O}_H(\mathbf{r}, \mathbf{R}, t) \right\rangle, \quad (7.4)$$

where  $\mathbf{R}$  indicates that the correlator  $C_{HAB}(t)$  is calculated at a fixed orientation of the  $Q\bar{Q}$ , and  $\mathbf{r}$  is the midpoint of the  $Q\bar{Q}$  (see Fig. 6.2). The system can be described by a Hamiltonian  $\hat{H}$ , that is,

$$\hat{H} = \hat{H}_0 + V_I, \quad (7.5)$$

where  $\hat{H}_0$  is the unperturbed Hamiltonian, and  $V_I$  is the transition potential. In perturbation theory we assume that  $V_I$  is numerically small. Hence,

$$e^{-\hat{H}t} \simeq e^{-\hat{H}_0 t} + \sum_{t_1=0}^t e^{-\hat{H}_0(t-t_1)} V_I(t) e^{-\hat{H}_0 t_1} + \dots \quad (7.6)$$

Therefore, we obtain

$$\begin{aligned} C_{HAB}(T, \mathbf{R}) &= \frac{1}{\Omega} \sum_{\mathbf{r}, t} \left\langle 0 \left| e^{\hat{H}(t+T)} \mathcal{O}_{AB}^\dagger(\mathbf{r}, \mathbf{R}, 0) e^{-\hat{H}(t+T)} e^{-\hat{H}t} \mathcal{O}_H(\mathbf{r}, \mathbf{R}, 0) e^{-\hat{H}t} \right| 0 \right\rangle \\ &\approx \frac{1}{\Omega} \sum_{\mathbf{r}, t} \sum_{t_1=0}^{T-1} \left\langle 0 \left| \mathcal{O}_{AB}^\dagger(\mathbf{r}, \mathbf{R}, 0) e^{-\hat{H}_0(T-t_1)} V_I(t_1) e^{-\hat{H}_0 t_1} \mathcal{O}_H(\mathbf{r}, \mathbf{R}, 0) \right| 0 \right\rangle + \\ &\quad \frac{1}{\Omega} \sum_{\mathbf{r}} \left\langle 0 \left| \mathcal{O}_{AB}^\dagger(\mathbf{r}, \mathbf{R}, 0) e^{-\hat{H}_0 T} \mathcal{O}_H(\mathbf{r}, \mathbf{R}, 0) \right| 0 \right\rangle \end{aligned} \quad (7.7)$$

The second term in Eq. (7.7) is zero, because the  $H_0$  does not, by itself, cause the transition. Thus we can rewrite Eq. (7.7) as

$$C_{HAB}(T, \mathbf{R}) = \frac{1}{\Omega} \sum_{\mathbf{r}, t} \sum_{t_1=0}^{T-1} \left\langle 0 \left| \mathcal{O}_{AB}^\dagger(\mathbf{r}, \mathbf{R}, 0) e^{-\hat{H}_0(T-t_1)} V_I(t_1) e^{-\hat{H}_0 t_1} \mathcal{O}_H(\mathbf{r}, \mathbf{R}, 0) \right| 0 \right\rangle. \quad (7.8)$$

In this dissertation, we model the transition potential as

$$V_I(t') \equiv \sum_{\mathbf{R}'} \sum_{\mathbf{r}'} \sum_{\mathbf{s}'} \bar{x}(\mathbf{R}') \mathcal{C}_{\Sigma_g^+}^\dagger(\mathbf{R}', \mathbf{r}', t') \mathcal{C}_{\Pi_u}(\mathbf{R}', \mathbf{r}', t') a^3 \bar{\psi} \psi(\mathbf{s}', t') w_I(\mathbf{s}' - \mathbf{r}'), \quad (7.9)$$

where  $\bar{x}(\mathbf{R}')$  is the overall normalization factor that controls the transition amplitude,  $\mathcal{C}_{\Sigma_g^+}^\dagger$  is a creation operator for the  $\Sigma_g^+$  state,  $\mathcal{C}_{\Pi_u}$  is an annihilation operator

for  $\Pi_u$  state, and  $w_I(\mathbf{s}' - \mathbf{r}')$  is the distribution wave function of the  $\bar{\psi}\psi(\mathbf{s}', t')$ , which is dictated by the decay.

$$C_{HAB}(T, \mathbf{R}) = \bar{x}(\mathbf{R}) \frac{1}{\Omega} \sum_{\mathbf{r}, t} \sum_{t'=0}^{T-1} \sum_{\mathbf{R}'} \sum_{\mathbf{r}'} \sum_{\mathbf{s}'} \left\langle 0 \left| \mathcal{O}_{AB}^\dagger(\mathbf{r}, \mathbf{R}, t') e^{-\hat{H}_0(T-t')} \mathcal{C}_{\Sigma_g^+}^\dagger(\mathbf{R}', \mathbf{r}', t') \right. \right. \\ \left. \left. \mathcal{C}_{\Pi_u}(\mathbf{R}', \mathbf{r}', 0) \bar{\psi}\psi(\mathbf{s}', t') w_I(\mathbf{s}' - \mathbf{r}') e^{-\hat{H}_0 t'} \mathcal{O}_H(\mathbf{r}, \mathbf{R}, 0) \right| 0 \right\rangle. \quad (7.10)$$

If we plug into the operator  $\mathcal{O}_{AB}^\dagger(\mathbf{r}, \mathbf{R}, 0)$ , we obtain

$$C_{HAB}(T, \mathbf{R}) = \bar{x}(\mathbf{R}) \frac{1}{\Omega} \sum_{\mathbf{r}, t} \sum_{t'=0}^{T-1} \sum_{\mathbf{R}', \mathbf{r}'} \sum_{\mathbf{s}, \mathbf{s}'} \left\langle 0 \left| \mathcal{O}_{\Sigma_g^+}^\dagger(\mathbf{r}, \mathbf{R}, 0) \bar{\psi}\psi(\mathbf{s}, t+T) w^*(\mathbf{s} - \mathbf{r}) e^{-\hat{H}_0(T-t')} \right. \right. \\ \left. \left. \mathcal{C}_{\Sigma_g^+}^\dagger(\mathbf{R}', \mathbf{r}', 0) \mathcal{C}_{\Pi_u}(\mathbf{R}', \mathbf{r}', 0) \bar{\psi}\psi(\mathbf{s}', t') w_I(\mathbf{s}' - \mathbf{r}') e^{-\hat{H}_0 t'} \mathcal{O}_{\Pi_u}(\mathbf{r}, \mathbf{R}, 0) \right| 0 \right\rangle \\ = \bar{x}(\mathbf{R}) \frac{1}{\Omega} \sum_{\mathbf{r}, t} \sum_{t'=0}^{T-1} \sum_{\mathbf{s}, \mathbf{s}'} \sum_{\mathbf{p}, \mathbf{q}} Z_a e^{-E_{\Sigma_g^+}(T-t')} Z_h e^{-E_{\Pi_u} t'} e^{-i\mathbf{q} \cdot (\mathbf{s} - \mathbf{r})} e^{i\mathbf{p} \cdot (\mathbf{s}' - \mathbf{r})} \\ w^*(\mathbf{q}) w_I(\mathbf{p}) \left\langle 0 \left| \bar{\psi}\psi(\mathbf{s}, t+T) \bar{\psi}\psi(\mathbf{s}', t' + t) \right| 0 \right\rangle \\ = \bar{x}(\mathbf{R}) \frac{1}{N_t} \sum_{\mathbf{q}} \sum_t \sum_{t'=0}^{T-1} \sum_{\mathbf{s}, \mathbf{s}'} Z_a e^{-E_{\Sigma_g^+}(T-t')} Z_h e^{-E_{\Pi_u} t'} e^{i\mathbf{q} \cdot (\mathbf{s} - \mathbf{s}')} w^*(\mathbf{q}) w_I(\mathbf{q}) \\ \left\langle 0 \left| \bar{\psi}\psi(\mathbf{s}, t+T) \bar{\psi}\psi(\mathbf{s}', t' + t) \right| 0 \right\rangle, \quad (7.11)$$

where  $Z_a$  is defined in Eq. (4.6),  $Z_h$  is defined in Eq. (4.12), and we express the wave function of the  $\pi\pi$  state in momentum space,

$$w(\mathbf{s} - \mathbf{r}) = \sum_{\mathbf{p}} e^{i\mathbf{p} \cdot (\mathbf{r} - \mathbf{s})} w(\mathbf{p}). \quad (7.12)$$

We can rewrite Eq. (7.11) as

$$C_{HAB}(T, \mathbf{R}) = \bar{x}(\mathbf{R}) V \sum_{\mathbf{q}} w^*(\mathbf{q}) w_I(\mathbf{q}) \sum_{t'=0}^{T-1} Z_a e^{-E_{\Sigma_g^+}(T-t')} Z_h e^{-E_{\Pi_u} t'} \times \\ \frac{1}{\Omega} \sum_t \sum_{\mathbf{s}, \mathbf{s}'} e^{i\mathbf{q} \cdot (\mathbf{s} - \mathbf{s}')} \left\langle 0 \left| \bar{\psi}\psi(\mathbf{s}, t+T) \bar{\psi}\psi(\mathbf{s}', t' + t) \right| 0 \right\rangle, \quad (7.13)$$

where  $V = N_x N_y N_z$ . In Chapter 6, we calculate  $C_{BB}(T, \mathbf{k})$  through

$$C_{BB}(T, \mathbf{k}) = \frac{1}{\Omega} \sum_t \sum_{\mathbf{s}, \mathbf{s}'} e^{i\mathbf{k} \cdot (\mathbf{s} - \mathbf{s}')} \left\langle 0 \left| \bar{\psi}\psi(\mathbf{s}, t+T) \bar{\psi}\psi(\mathbf{s}', t) \right| 0 \right\rangle. \quad (7.14)$$

Therefore, we obtain

$$C_{HAB}(T, \mathbf{R}) = \bar{x}(\mathbf{R}) V \sum_{\mathbf{q}} w^*(\mathbf{q}) w_I(\mathbf{q}) \sum_{t'=0}^{T-1} Z_a e^{-E_{\Sigma_g^+}(T-t')} Z_h e^{-E_{\Pi_u} t'} C_{BB}(T-t', \mathbf{q}), \quad (7.15)$$

From Eq. (4.6) and Eq. (4.12), we have

$$C_{AA}(R, T-t') = Z_a^2 e^{-E_{\Sigma_g^+}(R) \times (T-t')} \quad (7.16)$$

$$C_{HH}(R, t') = Z_h^2 e^{-E_{\Pi_u}(R) \times t'}. \quad (7.17)$$

So we can rewrite this result in terms of all the correlators as

$$C_{HAB}(T, \mathbf{R}) = \sum_{\mathbf{q}} w^*(\mathbf{q}) w_I(\mathbf{q}) \frac{V}{Z_a Z_h} \sum_{t'=0}^{T-1} C_{AA}(\mathbf{R}, T-t') \bar{x}(\mathbf{R}) C_{HH}(\mathbf{R}, t') C_{BB}(\mathbf{q}, T-t'). \quad (7.18)$$

In Chapter 6, we discussed the symmetry of the wave function  $w$ , and we chose the wave function  $w$  as Eq. (6.34). Then we obtain

$$C_{HAB}(T, \mathbf{R}, \mathbf{k}) = \frac{w_I(\mathbf{k}) V}{Z_a Z_h} \sum_{t'=0}^{T-1} C_{AA}(\mathbf{R}, T-t') \bar{x}(\mathbf{R}) C_{HH}(\mathbf{R}, t') C_{BB}(T-t', \mathbf{k}), \quad (7.19)$$

where we consider the cubic symmetry (namely,  $C_{BB}(T-t', \mathbf{R}, -\mathbf{k}) = C_{BB}(T-t', \mathbf{R}, \mathbf{k})$ , etc). Here we absorb the  $i$  into  $w_I(\mathbf{k})$  (i.e.,  $i w_I(\mathbf{k}) \rightarrow w_I(\mathbf{k})$ ). Note that the wave function  $w_I$  must have the same symmetry as the wave function  $w$ .

## 7.2 Decays from the lattice

In practice it is possible to extract the transition amplitude  $x$  directly from the lattice [4]. Here we describe this approach in principle. Using a suitable lattice operator to create the hybrid state  $H$  at  $t = 0$  and annihilate a two-body state with relative momenta  $\mathbf{k}$  and  $-\mathbf{k}$  at time  $t$ . In Sec. 7.1, we used perturbation theory to obtain the correlator  $C_{H-AB}(t)$  from an  $H$  state with mass  $E_H$  and a two-body state  $(A, B)$  with energy  $E_A, E_B$ , that is, <sup>1</sup>

$$C_{HAB}(t, \mathbf{R}, \mathbf{k}) = \frac{w_I(\mathbf{k}) V}{Z_a Z_h} \sum_{t'=0}^{t-1} C_{AA}(\mathbf{R}, t-t') \bar{x}(\mathbf{k}) C_{HH}(\mathbf{R}, t') C_{BB}(T-t', \mathbf{k}), \quad (7.20)$$

where the summation is over the intermediate  $t$ -value  $t'$ , and  $t'$  is an integer. By obtaining  $Z_h$  from the correlator  $C_{H-H}(t)$  from  $H \rightarrow H$ , and  $Z_a$  from the correlator  $C_{A-A}(t)$  from  $A \rightarrow A$ , also measuring the correlator  $C_{B-B}(t)$  from  $B \rightarrow B$ , and the

---

<sup>1</sup>This equation is same as Eq. (7.19), just change  $T$  into  $t$ .



correlator  $C_{H-AB}(t)$  from  $H \rightarrow AB$ , we can extract the transition amplitude  $\bar{x}(\mathbf{R})$  in principle, that is,

$$\bar{x}(\mathbf{R})w_I(\mathbf{k}) = \frac{Z_a Z_h}{V} \frac{C_{HAB}(t, \mathbf{R}, \mathbf{k})}{\sum_{t'=0}^{t-1} C_{AA}(\mathbf{R}, t-t') C_{HH}(\mathbf{R}, t') C_{BB}(t-t', \mathbf{k})}. \quad (7.21)$$

If we define

$$x(\mathbf{k}, \mathbf{R}) \equiv \bar{x}(\mathbf{R}) w_I(\mathbf{k}) V, \quad (7.22)$$

we obtain

$$x(\mathbf{k}, \mathbf{R}) = \frac{C_{HAB}(t, \mathbf{R}, \mathbf{k}) Z_a Z_h}{\sum_{t'=0}^{t-1} C_{AA}(\mathbf{R}, t-t') C_{HH}(\mathbf{R}, t') C_{BB}(t-t', \mathbf{k})}. \quad (7.23)$$

Therefore, from Eq. (7.23), we can extract the transition amplitude  $x(\mathbf{k}, \mathbf{R})$  from the lattice.

In this dissertation we focus on the decay channel to  $\pi\pi$  branch, that is,

$$H \rightarrow \chi_b + \pi + \pi, \quad (7.24)$$

where  $\pi\pi$  is in scalar channel. In the lattice simulation, due to the taste symmetry breaking, there exist the splittings between pions ( $\pi$ ) of various tastes [60][10][63]. We classify the pions into five types, namely,  $\pi_5$ ,  $\pi_A$ ,  $\pi_V$ ,  $\pi_I$ , and  $\pi_T$  which correspond the pions with taste pseudoscalar, axial, vector, singlet, and tensor respectively. In order to calculate the decay channel to  $\pi\pi$  branch correctly, we should count these five channels correctly. In Ref. [64], the authors predict the weights for each taste of the  $\pi\pi$  intermediate state in bubble contribution channel. We list them in Table 7.1.

In our model, the transition amplitude of the Goldstone  $\pi_5\pi_5$  can be calculated in lab frame (see details in Appendix D) by the formula

$$x_{PP}(\mathbf{p}) = \langle \pi_5(\mathbf{p}_1) \pi_5(\mathbf{p}_2), A | V_I^{\text{lab}} | H \rangle, \quad (7.25)$$

where  $V_I^{\text{lab}}$  is the interaction potential in lab frame, which is denoted in Eq. (D.6), and the subscript  $PP$  specifies the Goldstone  $\pi_5\pi_5$  channel, that is,

$$x_{PP}(\mathbf{p}_1, \mathbf{p}_2) = \langle \pi_5(\mathbf{p}_1) \pi_5(\mathbf{p}_2) | \bar{\psi}\psi(\mathbf{p}) | 0 \rangle x(p) \delta^{(3)}(\mathbf{P}_H - \mathbf{P}_A - \mathbf{p})$$

**Table 7.1.** The weights for different tastes of the  $\pi\pi$  intermediate states. The first column is the taste, the second column is its weight.

Taste	Weight
I (singlet)	$-3/4$
V (vector)	$4/4$
T (tensor)	$6/4$
A (axial)	$4/4$
P (pseudoscalar)	$1/4$

$$= b_{PP}(\mathbf{p}_1, \mathbf{p}_2) x(p) \delta^{(3)}(\mathbf{P}_H - \mathbf{P}_A - \mathbf{p}), \quad (7.26)$$

where  $x(p)$  is calculated by Eq. (D.27) (see details in Appendix D),  $\mathbf{p} = \mathbf{p}_1 + \mathbf{p}_2$ , and  $b_{PP}(\mathbf{p}_1, \mathbf{p}_2) \equiv \langle \pi_5(\mathbf{p}_1) \pi_5(\mathbf{p}_2) | \bar{\psi} \psi(\mathbf{p}) | 0 \rangle$  is a constant, which does not depend on  $\mathbf{R}$ , calculated to be [64]

$$b_{PP}(\mathbf{p}_1, \mathbf{p}_2) = \frac{1}{a^3} \sqrt{\frac{B_0^2}{4L^3}} \frac{1}{\sqrt{2E_{\pi_P}(\mathbf{p}_1)}} \frac{1}{\sqrt{2E_{\pi_P}(\mathbf{p}_2)}}, \quad (7.27)$$

where  $B_0$  is the coupling constant,  $E_{\pi_P}(\mathbf{p}) = \sqrt{\mathbf{p}^2 + M_{U_5}^2}$  and  $M_{U_5}$  is the mass of Goldstone pion. Please see details in Ref. [64] or Appendix D.

Similarly, another channels can be also measured. That is,

$$x_{AA}(\mathbf{p}_1, \mathbf{p}_2) = b_{AA}(\mathbf{p}_1, \mathbf{p}_2) x(p) \delta^{(3)}(\mathbf{P}_H - \mathbf{P}_A - \mathbf{p}) \quad (7.28)$$

$$x_{VV}(\mathbf{p}_1, \mathbf{p}_2) = b_{VV}(\mathbf{p}_1, \mathbf{p}_2) x(p) \delta^{(3)}(\mathbf{P}_H - \mathbf{P}_A - \mathbf{p}) \quad (7.29)$$

$$x_{II}(\mathbf{p}_1, \mathbf{p}_2) = b_{II}(\mathbf{p}_1, \mathbf{p}_2) x(p) \delta^{(3)}(\mathbf{P}_H - \mathbf{P}_A - \mathbf{p}) \quad (7.30)$$

$$x_{TT}(\mathbf{p}_1, \mathbf{p}_2) = b_{TT}(\mathbf{p}_1, \mathbf{p}_2) x(p) \delta^{(3)}(\mathbf{P}_H - \mathbf{P}_A - \mathbf{p}), \quad (7.31)$$

where the subscripts AA, VV, II, and TT stand for the axial, vector, singlet, tensor channels respectively.

$$b_{AA}(\mathbf{p}_1, \mathbf{p}_2) = \frac{1}{a^3} \sqrt{\frac{B_0^2}{4L^3}} \frac{1}{\sqrt{2E_{\pi_A}(\mathbf{p}_1)}} \frac{1}{\sqrt{2E_{\pi_A}(\mathbf{p}_2)}} \quad (7.32)$$

$$b_{VV}(\mathbf{p}_1, \mathbf{p}_2) = \frac{1}{a^3} \sqrt{\frac{B_0^2}{4L^3}} \frac{1}{\sqrt{2E_{\pi_V}(\mathbf{p}_1)}} \frac{1}{\sqrt{2E_{\pi_V}(\mathbf{p}_2)}} \quad (7.33)$$

$$b_{II}(\mathbf{p}_1, \mathbf{p}_2) = \frac{1}{a^3} \sqrt{\frac{B_0^2}{4L^3}} \frac{1}{\sqrt{2E_{\pi_I}(\mathbf{p}_1)}} \frac{1}{\sqrt{2E_{\pi_I}(\mathbf{p}_2)}} \quad (7.34)$$

$$b_{TT}(\mathbf{p}_1, \mathbf{p}_2) = \frac{1}{a^3} \sqrt{\frac{B_0^2}{4L^3}} \frac{1}{\sqrt{2E_{\pi_T}(\mathbf{p}_1)}} \frac{1}{\sqrt{2E_{\pi_T}(\mathbf{p}_2)}}, \quad (7.35)$$

where  $E_{\pi_V}(\mathbf{p})$ ,  $E_{\pi_A}(\mathbf{p})$ ,  $E_{\pi_I}(\mathbf{p})$ , and  $E_{\pi_T}(\mathbf{p})$  are denoted like  $E_{\pi_p}(\mathbf{P})$ .

The transition amplitude of the  $\pi\pi$  channel can be calculated by the formula

$$\langle \pi\pi, A | V_I^{\text{lab}} | H \rangle = x_{\pi\pi}(p) \delta^{(3)}(\mathbf{P}_H - \mathbf{P}_A - \mathbf{p}) \quad (7.36)$$

where  $V_I^{\text{lab}}$  is denoted by Eq. (D.6), and the subscript  $\pi\pi$  specifies the  $\pi\pi$  channel.

After some algebra, we obtain

$$x_{\pi\pi}(p_1, p_2) = b_{\pi\pi}(\mathbf{p}_1, \mathbf{p}_2) x(p), \quad (7.37)$$

where  $b_{\pi\pi}(\mathbf{p}_1, \mathbf{p}_2) \equiv \langle \pi\pi(\mathbf{p}) | \bar{\psi}\psi(\mathbf{p}) | 0 \rangle$  is a constant, which does not depend on  $\mathbf{R}$ .

If we consider Table. 7.1, we obtain

$$b_{\pi\pi}^2(\mathbf{p}_1, \mathbf{p}_2) = \frac{1}{4} b_{PP}^2(\mathbf{p}_1, \mathbf{p}_2) + b_{AA}^2(\mathbf{p}_1, \mathbf{p}_2) + b_{VV}^2(\mathbf{p}_1, \mathbf{p}_2) - \frac{3}{4} b_{II}^2(\mathbf{p}_1, \mathbf{p}_2) + \frac{6}{4} b_{TT}^2(\mathbf{p}_1, \mathbf{p}_2). \quad (7.38)$$

In continuum limit, we can estimate

$$b_{\pi\pi}(\mathbf{p}_1, \mathbf{p}_2) = \frac{1}{a^3} \sqrt{\frac{3B_0^2}{4L^3}} \frac{1}{\sqrt{2E_{\pi}(\mathbf{p}_1)}} \frac{1}{\sqrt{2E_{\pi}(\mathbf{p}_2)}}, \quad (7.39)$$

where  $E_{\pi}(\mathbf{p})$  is the energy of pion with momentum  $\mathbf{p}$ . In practice, we can rewrite Eq. (7.37) as

$$x_{\pi\pi}(p_1, p_2) = \hat{x}_{\pi\pi}(p) \frac{1}{\sqrt{2E_{\pi}(\mathbf{p}_1)} \sqrt{2E_{\pi}(\mathbf{p}_2)}}, \quad (7.40)$$

where

$$\hat{x}_{\pi\pi}(p) = \frac{1}{a^3} \sqrt{\frac{3B_0^2}{4L^3}} x(p). \quad (7.41)$$

We can also define a constant, that is.

$$\hat{b}_{\pi\pi} = \frac{1}{a^3} \sqrt{\frac{3B_0^2}{4L^3}}. \quad (7.42)$$

In Chapter 8, we show how to calculate the decay rate from  $x_{\pi\pi}(p)$ .

## CHAPTER 8

### OUR NUMERICAL RESULTS

In this chapter we give our lattice numerical simulation results. First we present the calculation of the mass of the  $f_0$  meson. Then we show the detailed procedure to obtain the lattice transition matrix element  $x$ , and calculate the decay rate.

In this dissertation, we use 520 dynamical MILC fermion configurations with  $N_f = 2 + 1$  flavors of sea quarks (namely,  $am_{u,d} = 0.005$ , and  $am_s = 0.05$ ). The coupling constant is  $\beta = 6.76$ . The lattice dimension is  $24^3 64$ , with the lattice spacing  $a$  of around 0.12 fm. All the results we show in this chapter come from this ensemble of gauge configurations.

#### 8.1 $f_0$ meson

Recently there exists a growing interest in the  $f_0$  meson. The analyzes of the  $\pi\pi$  scattering phase shift suggested a brand resonance of the  $f_0$  meson with  $I = 0$  and  $J^{PC} = 0^{++}$  [65]. In this section we first discuss an interpolating operator for the  $f_0$  meson. Then we give the detailed procedures for determining its mass.

##### 8.1.1 Operator for $f_0$ meson

We choose an operator with isospin  $I = 0$  and  $J^{PC} = 0^{++}$  at the sink and source,

$$\hat{f}_0(x) \equiv \sum_{r=1}^{n_r} \frac{\bar{u}_r(x)u_r(x) + \bar{d}_r(x)d_r(x)}{\sqrt{2n_r}}, \quad (8.1)$$

where  $r$  is the index of the taste replica,  $n_r$  is the number of the taste replica, and for notational simplicity we omit the color index and spin index.

The timeslice correlator for the  $f_0$  meson is given by,

$$C(t, \mathbf{k}) = \sum_{\mathbf{x}} \left\{ \langle \hat{f}_0(\mathbf{x}, t) \hat{f}_0(\mathbf{0}, 0) \rangle - \langle \hat{f}_0 \rangle^2 \right\} e^{i\mathbf{k} \cdot \mathbf{x}}, \quad (8.2)$$

where the  $x = (\mathbf{x}, t)$  is lattice position,  $\mathbf{0}$  is zero vector (namely,  $\mathbf{0} = (0, 0, 0)$ ),  $\langle \hat{f}_0 \rangle$  is the vacuum expectation value, and  $\mathbf{k}$  is the chosen momentum.

In Chapter 6, we discussed this correlator in detail. From Ref. [60], we know that  $n_r = 1/4$  for the  $1 + 1 + 1$  theory. Thus, we obtained

$$C(t, \mathbf{k}) = C^{CC}(t, \mathbf{k}) - \frac{1}{2}C^{DC}(t, \mathbf{k}), \quad (8.3)$$

where  $C(t, \mathbf{k})$  is described by Eq. (6.6),  $C^{CC}(t, \mathbf{k})$  is described by Eq. (6.8), and  $C^{DC}(t, \mathbf{k})$  is described by Eq. (6.7). The superscript  $CC$  stands for the connected contribution. The superscript  $DC$  stands for the disconnected contribution.

### 8.1.2 Procedures for determining the $f_0$ mass

As we discussed in Chapter 6 we used the point sources and the point sink operators for the  $f_0$  propagator. For the point source, we just set a 1 on only one point on a chosen time slice, and zero everywhere else. In order to improve the statistics, when we calculate the connected part, we computed correlators from eight source time slices evenly spread through the lattice (i.e., only one source time slice was chosen at a time), and averaged the correlators. Moreover, for the nonzero momentum mesons we used a quark source with 1 and an antiquark source with  $e^{i\mathbf{k} \cdot \mathbf{s}}$  on only one point on the chosen time slices, where the  $\mathbf{k}$  is our chosen momentum, and the  $\mathbf{s}$  is the position of the quark source (see Fig. 6.1).

From Ref. [64], we know, for staggered quarks, that the meson correlators have the generic single-particle contribution [38]

$$\mathcal{C}(t) = \sum_i A_i \left( e^{-m_i t} + e^{-m_i(N_t - t)} \right) + \sum_i A'_i (-1)^t \left( e^{-m'_i t} + e^{-m'_i(N_t - t)} \right), \quad (8.4)$$

where the oscillating terms correspond to a particle with opposite parity. In our case for the  $f_0$  meson correlator, we assume only one mass with each parity in the fits of Eq. (8.4).<sup>1</sup> From the discussion in Appendix B, we must consider the two meson contributions. Therefore, we have

$$\mathcal{C}(t) = A_1 \left( e^{-m_1 t} + e^{-m_1(N_t - t)} \right) + A_2 (-1)^t \left( e^{-m_2 t} + e^{-m_2(N_t - t)} \right) + B_{f_0}^{S\chi PT}(t), \quad (8.5)$$

---

<sup>1</sup>In Ref. [64] we show that, in our concrete calculation, our operator is the state with  $I \otimes I$  and state of  $\gamma_0 \gamma_5 \otimes \gamma_0 \gamma_5$  (its oscillating term).

where  $B_{f_0}^{S\chi PT}(t)$  is denoted in Eq. (D.14). If we rearrange the terms in Eq. (D.14), we obtain

$$B_{f_0}^{S\chi PT}(t) = \frac{B_0^2}{4L^3} \left\{ f_{\text{Bubble}}(t) + \delta_V f_{\text{Vhairpin}}(t) + \delta_A f_{\text{Ahairpin}}(t) \right\}, \quad (8.6)$$

here  $B_0$  is the coupling constant,  $\delta_V = a^2 \delta'_V$  is the hairpin coupling of a pair of taste-vector mesons,  $\delta_A = a^2 \delta'_A$  is the hairpin coupling of a pair of taste-axial mesons, and

$$\begin{aligned} f_{\text{Vhairpin}}(t) \equiv & \frac{1}{\delta_V} \sum_{\mathbf{k}} \left\{ -4 \frac{e^{-\left(\sqrt{(\mathbf{p}+\mathbf{k})^2 + M_{U_V}^2} + \sqrt{\mathbf{k}^2 + M_{U_V}^2}\right)t}}{\sqrt{(\mathbf{p}+\mathbf{k})^2 + M_{U_V}^2} \sqrt{\mathbf{k}^2 + M_{U_V}^2}} \right. \\ & + C_{V_\eta}^2 \frac{e^{-\left(\sqrt{(\mathbf{p}+\mathbf{k})^2 + M_{\eta V}^2} + \sqrt{\mathbf{k}^2 + M_{\eta V}^2}\right)t}}{\sqrt{(\mathbf{p}+\mathbf{k})^2 + M_{\eta V}^2} \sqrt{\mathbf{k}^2 + M_{\eta V}^2}} + C_{V_{\eta'}}^2 \frac{e^{-\left(\sqrt{(\mathbf{p}+\mathbf{k})^2 + M_{\eta' V}^2} + \sqrt{\mathbf{k}^2 + M_{\eta' V}^2}\right)t}}{\sqrt{(\mathbf{p}+\mathbf{k})^2 + M_{\eta' V}^2} \sqrt{\mathbf{k}^2 + M_{\eta' V}^2}} \\ & \left. - C_{V_\eta} C_{V_{\eta'}} \left[ \frac{e^{-\left(\sqrt{(\mathbf{p}+\mathbf{k})^2 + M_{\eta V}^2} + \sqrt{\mathbf{k}^2 + M_{\eta' V}^2}\right)t}}{\sqrt{(\mathbf{p}+\mathbf{k})^2 + M_{\eta V}^2} \sqrt{\mathbf{k}^2 + M_{\eta' V}^2}} + \frac{e^{-\left(\sqrt{(\mathbf{p}+\mathbf{k})^2 + M_{\eta' V}^2} + \sqrt{\mathbf{k}^2 + M_{\eta V}^2}\right)t}}{\sqrt{(\mathbf{p}+\mathbf{k})^2 + M_{\eta' V}^2} \sqrt{\mathbf{k}^2 + M_{\eta V}^2}} \right] \right\} \quad (8.7) \end{aligned}$$

$$\begin{aligned} f_{\text{Bubble}}(t) \equiv & \sum_{\mathbf{k}} \left\{ \frac{1}{9} \frac{e^{-\left(\sqrt{(\mathbf{p}+\mathbf{k})^2 + M_{\eta I}^2} + \sqrt{\mathbf{k}^2 + M_{\eta I}^2}\right)t}}{\sqrt{(\mathbf{p}+\mathbf{k})^2 + M_{\eta I}^2} \sqrt{\mathbf{k}^2 + M_{\eta I}^2}} - \frac{e^{-\left(\sqrt{(\mathbf{p}+\mathbf{k})^2 + M_{U_I}^2} + \sqrt{\mathbf{k}^2 + M_{U_I}^2}\right)t}}{\sqrt{(\mathbf{p}+\mathbf{k})^2 + M_{U_I}^2} \sqrt{\mathbf{k}^2 + M_{U_I}^2}} \right. \\ & \left. + \frac{1}{16} \sum_{b=1}^{16} \left[ 4 \frac{e^{-\left(\sqrt{(\mathbf{p}+\mathbf{k})^2 + M_{U_b}^2} + \sqrt{\mathbf{k}^2 + M_{U_b}^2}\right)t}}{\sqrt{(\mathbf{p}+\mathbf{k})^2 + M_{U_b}^2} \sqrt{\mathbf{k}^2 + M_{U_b}^2}} + \frac{e^{-\left(\sqrt{(\mathbf{p}+\mathbf{k})^2 + M_{K_b}^2} + \sqrt{\mathbf{k}^2 + M_{K_b}^2}\right)t}}{\sqrt{(\mathbf{p}+\mathbf{k})^2 + M_{K_b}^2} \sqrt{\mathbf{k}^2 + M_{K_b}^2}} \right] \right\}, \quad (8.8) \end{aligned}$$

where  $\delta_V$ ,  $\delta_A$ ,  $B_0$ ,  $C_{V_\eta}$ ,  $C_{V_{\eta'}}$ ,  $C_{A_\eta}$ ,  $C_{A_{\eta'}}$  are constants, which are given in Appendix B,  $M_{\eta V}$ ,  $M_{\eta A}$ ,  $M_{\eta' V}$ ,  $M_{\eta' A}$  are given in Appendix B, and for  $f_{\text{Ahairpin}}(t)$ , we just require  $V \rightarrow A$  in  $f_{\text{Vhairpin}}(t)$ .

The tree-level masses of the mesons are [60]

$$M_{ff'_b}^2 = B_0(m_f + m_{f'}) + a^2 \Delta_b, \quad (8.9)$$

where  $\bar{f}f'$  are two flavors which make up,  $b = 1, \dots, 16$  are the taste, and the term of  $a^2 \Delta_b$  comes from taste symmetry breaking. Here for brevity, we denote

$$M_{U_b} \equiv M_{\pi_b} \equiv M_{uu_b} \equiv M_{dd_b} \equiv M_{ud_b}, \quad M_{S_b} \equiv M_{ss_b}, \quad M_{B_b} \equiv M_{us_b}. \quad (8.10)$$

By convention the  $M_{U_P}$  is the mass of the Goldstone pion, and the  $M_{K_P}$  is the mass of the Goldstone kaon.

All the masses needed for Eq. (8.7) are well known. From the mass-squared splittings in Table III of Ref. [66] also the  $aM_{U_P} = 0.1594$ ,  $aM_{K_P} = 0.36523$  in Ref. [10], we obtain

$$\begin{aligned} aM_{U_A} &= 0.2342, & aM_{U_T} &= 0.2694, & aM_{U_V} &= 0.2966, & aM_{U_I} &= 0.3205. \\ aM_{K_A} &= 0.4036, & aM_{K_T} &= 0.4250, & aM_{K_V} &= 0.4428, & aM_{K_I} &= 0.4591. \end{aligned}$$

The  $M_\eta$  is estimated from the Gell-Mann-Okubo formula

$$m_\eta^2 = \frac{m_\pi^2 + 2m_S^2}{3}, \quad (8.11)$$

that is,

$$aM_{\eta_I} = 0.4958. \quad (8.12)$$

The first term ( $J^{PC} = 1^{++}$ ) in Eq. (8.5) gives the mass of the  $f_0$  meson, and the oscillating term ( $J^{PC} = 1^{+-}$ ) in Eq. (8.5) gives the mass of the  $\eta_A$  meson. In Ref. [64], we do a fit to all of the correlator data at once. In this grand fit, the masses of the  $f_0$  meson,  $a_0$  meson,  $\eta_{05}$  meson, and  $\pi_{05}$  meson, the couplings of  $\delta_V$ ,  $\delta_A$ , and  $B_0$  were determined. We choose all the data within the fitting range of  $t$  from 5 to 18 (namely, the minimum distances  $t_{\min} = 5$ ). Our fitting gives an acceptable result with a  $\chi^2$  of 127 with 114 degrees of freedom, with

$$am_{f_0} = 0.47(7) \quad (8.13)$$

From Ref. [10], for our set of configurations, we know

$$a^{-1} = 1.634(45) \text{ GeV}, \quad (8.14)$$

then gets

$$m_{f_0} = (768 \pm 136) \text{ MeV}. \quad (8.15)$$

Also we get

$$aB_0 = 3.12 \pm 0.42. \quad (8.16)$$

In next section we use this number to evaluate the decay rate.

## 8.2 Lattice transition matrix element

From the discussion of the symmetry of the wave function in Sec. 6.3, we know the possible minimum momentum is  $\mathbf{k} = (1, 0, 0)\frac{2\pi}{L}$  for the scalar meson creation [4]. In this section, we will show the detailed procedures to obtain the overall decay rate at this chosen momentum. Then we will consider the momentum of  $\mathbf{k} = (1, 1, 0)\frac{2\pi}{L}$ ,  $\mathbf{k} = (1, 1, 1)\frac{2\pi}{L}$ , and  $\mathbf{k} = (2, 0, 0)\frac{2\pi}{L}$ . From the data of these four chosen momenta, we can obtain a decay rate that has physical meaning.

### 8.2.1 The wave function of the excited gluonic states

In Chapter 4, we used the LBO approximation to solve for the gluonic field around a static quark-antiquark  $Q\bar{Q}$  at separation  $R$  to determine first the static potential. Then we solved the Schrödinger equation with that potential to determine its spectrum and wave function. From Fig. 4.11, we note that the potential ( $\Pi_u$ ) that binds the hybrid meson is comparatively flat. Hence, the hybrid meson has a broad radial wave function, which we denote by  $u_H$  in Chapter 4. This observation allows a quick estimate for the decay rate. For example, in Chapter 5, we justified the decay from the hybrid meson state to the P-wave  $\chi_b$  state (i.e., we refer to the wave function of this state as  $u_{\chi_b}$  in Chapter 4). In order to integrate over  $R$  easily, we rescale Fig. 4.11 in terms of lattice spacing  $a$ , and show it in Fig. 8.1. We see that the lack of the nodes in the relevant wave functions results in a quite large spatial wave function overlap factor. Moreover if we assume the transition rate is independent of  $R$ , we obtain

$$\int u_H u_{\chi_b} dR = 0.8643, \quad (8.17)$$

where  $u_H$ ,  $u_{\chi_b}$  are normalized. From the other side, this big overlap factor justifies the decay from the hybrid meson state to the P-wave  $\chi_b$  state. Later in this chapter, we calculate the decay rate of this channel.

### 8.2.2 Simulation procedure

In Chapter 6 we have already discussed how to create operators for the  $\Pi_u$ ,  $\Sigma_g^+ + S(0^{++})$ , and we use Eq. (6.33) to calculate the correlator  $C_{HAB}$ . We also



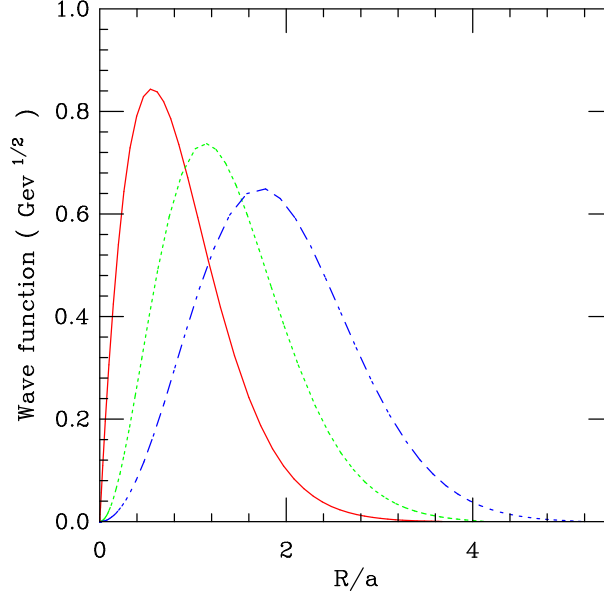


**Figure 8.1.** Reduced radial wave function versus  $R$  in units of  $a$ . The solid curve, dotted curve, and short dash curve specify the reduced radial wave functions for the  $1S$ ,  $1P$  states of  $\Sigma_g^+$ , and  $\Pi_u$  hybrid state, respectively.

discussed the symmetry of the wave function  $w(\mathbf{r})$ .

In practice we evaluate the difference of two Wilson loops. As we discussed in Chapter 6, we call this observable  $\mathcal{A}(\mathbf{r})$  and its spatial Fourier transform  $\mathcal{A}(\mathbf{k})$ . The fermion loop of light quark meson ( $f_0$  meson) is evaluated at each spatial point  $\mathbf{s}$  at time  $t + T$  and its Fourier transform is  $S(\mathbf{k})$ . We actually used 20 iterations of *APE* smearing for both spatial ends of  $\mathcal{A}$ . The transverse extent of the  $\Pi_u$  end is two lattice spacings. We summed over all possible orientation to improve statistics.

### 8.2.3 Our numerical results for decay rate

For notational simplicity, we focus on the chosen momentum  $\mathbf{k} = (1, 0, 0) \frac{2\pi}{L}$ . For scalar decays, we choose the wave function as in Eq. (6.34). According to Eq. (6.36), in terms of these components of the momentum, we estimate the required correlator  $C_{HAB}(t, \mathbf{R}, \mathbf{k})$ . From Eq. (7.23), we evaluate the bare transition amplitude  $x(\mathbf{k}, \mathbf{R}, t)$  at each  $t$  and  $\mathbf{R}$  for fixed momentum  $\mathbf{k}$ , that is,

$$x(\mathbf{k}, \mathbf{R}, t) = \frac{C_{HAB}(t, \mathbf{R}, \mathbf{k}) Z_a Z_h}{\sum_{t'=0}^{t-1} C_{AA}(\mathbf{R}, t-t') C_{HH}(\mathbf{R}, t') C_{BB}(t-t', \mathbf{k})}. \quad (8.18)$$

We measure  $Z_h$  from the correlator  $C_{H-H}(t)$  from  $H \rightarrow H$  as explained in Sec. 4.4.2, and  $Z_a$  from the correlator  $C_{A-A}(t)$  from  $A \rightarrow A$  as explained in Sec. 4.4.1. The  $Z_a$  and  $Z_h$  values for different  $R$  are shown in Fig. 8.2, where the burst one is for  $Z_h$ , and the octagon one is for  $Z_a$ .

When we evaluate the bare transition amplitude  $x(\mathbf{k}, \mathbf{R}, t)$ , we use jackknife method. Here we should point out when we construct the jackknife sample, we just throw out one measurement.

For illustration, the values of  $x(\mathbf{k}, \mathbf{R}, t)$  for  $\frac{R}{a} = 1$  and momentum  $\mathbf{k} = (1, 0, 0)\frac{2\pi}{L}$  at different  $t$  are shown in Fig. 8.3. For the range from  $t = 2$  to  $t = 5$ , there exists a plateau for  $x(\mathbf{k}, \mathbf{R}, t)$ . We fit this plateau to get  $x(\mathbf{k}, \mathbf{R}) = 0.3253 \pm 0.0093$  with a  $\chi^2$  of 0.03 for 3 degrees of freedom.

In our lattice simulation we obtain the  $x(\mathbf{k}, \mathbf{R}, t)$  values shown in Fig. 8.4 and Fig. 8.5. From these data we can extract the values of  $x(\mathbf{k}, \mathbf{R})$  for momentum  $\mathbf{k} = (1, 0, 0)\frac{2\pi}{L}$  at all separations  $R$ . In Table 8.1, for  $\mathbf{k} = (1, 0, 0)\frac{2\pi}{L}$  we list all the values of  $x(\mathbf{k}, \mathbf{R})$  for different  $R$ , fitting range, etc. Also we plot the values of  $x(\mathbf{k}, \mathbf{R})$  in Fig. 8.6. From Fig. 8.6, we note an increase of  $x(\mathbf{k}, R)$  with

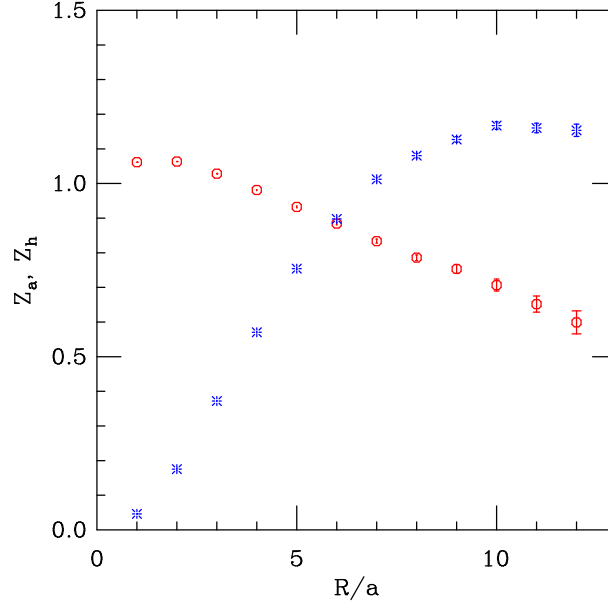


**Figure 8.2.** The overlap amplitudes of  $Z_a$  and  $Z_h$  versus  $R$ , the burst one is for  $Z_h$ , and the octagon one is for  $Z_a$ .

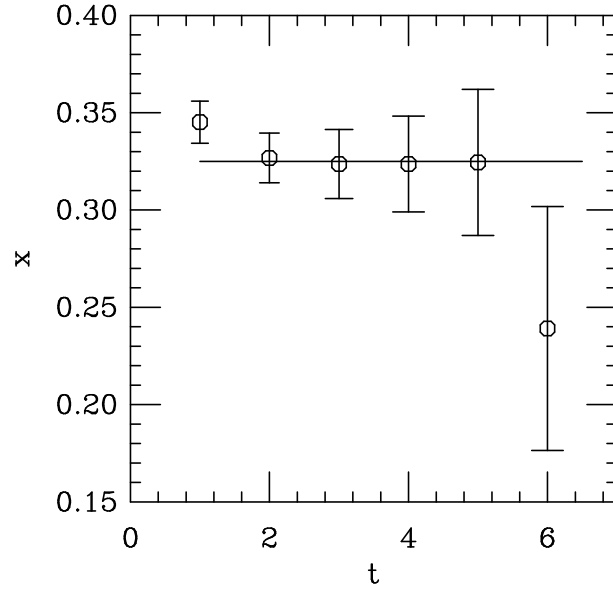


**Figure 8.3.** The  $x(\mathbf{k}, \mathbf{R}, t)$  values for  $\frac{R}{a} = 1$  versus  $t$  with  $\mathbf{k} = (1, 0, 0)\frac{2\pi}{L}$ .

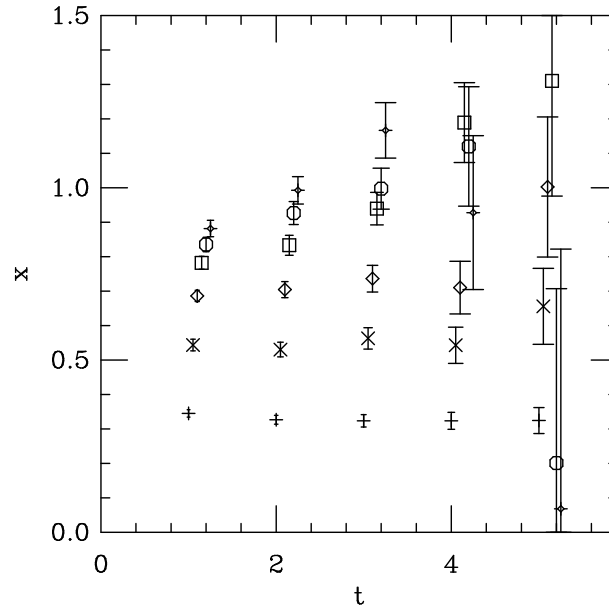


**Figure 8.4.** The  $x(\mathbf{k}, \mathbf{R}, t)$  values with momentum  $\mathbf{k} = (1, 0, 0)\frac{2\pi}{L}$  versus  $t$ . Here values for  $\frac{R}{a} = 1, 2, \dots, 6$  are represented by the plus sign, cross, diamond, square, octagon, and fancy diamond, respectively.

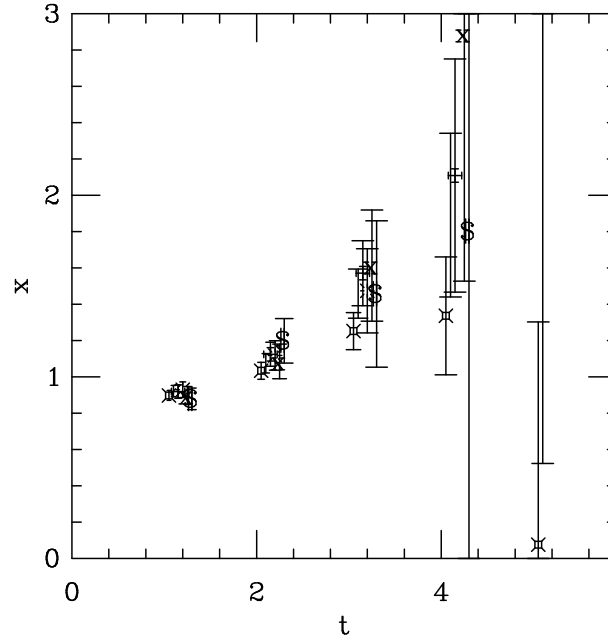


**Figure 8.5.** The  $x(\mathbf{k}, \mathbf{R}, t)$  values with momentum  $\mathbf{k} = (1, 0, 0) \frac{2\pi}{L}$  versus  $t$ . Here values for  $\frac{R}{a} = 7, 8, \dots, 12$  are represented by fancy square, fancy cross, fancy plus, burst, cross, and dollar sign, respectively.

**Table 8.1.** The  $x(\mathbf{k}, \mathbf{R})$  values with momentum  $\mathbf{k} = (1, 0, 0) \frac{2\pi}{L}$ . The first column is the separate distance, and Column two is the transition amplitude. The remaining columns are the time range for the chosen fit,  $\chi^2$  and number of degrees of freedom for the fit.

$R/a$	$ax$	Fitting range	$\chi^2/D$
1	0.3215(105)	2–5	0.0266/3
2	0.5430(196)	2–5	1.81/3
3	0.7170(272)	2–5	2.51/3
4	0.8636(303)	2–3	3.71/1
5	0.9520(382)	2–4	2.02/2
6	1.1328(826)	3–5	3.01/2
7	1.270(119)	3–5	0.987/2
8	1.511(163)	3–5	1.07/2
9	1.615(189))	3–5	1.36/2
10	1.567(240)	3–5	3.54/2
11	1.672(297)	3–5	0.893/2
12	1.465(395)	3–5	0.16/2

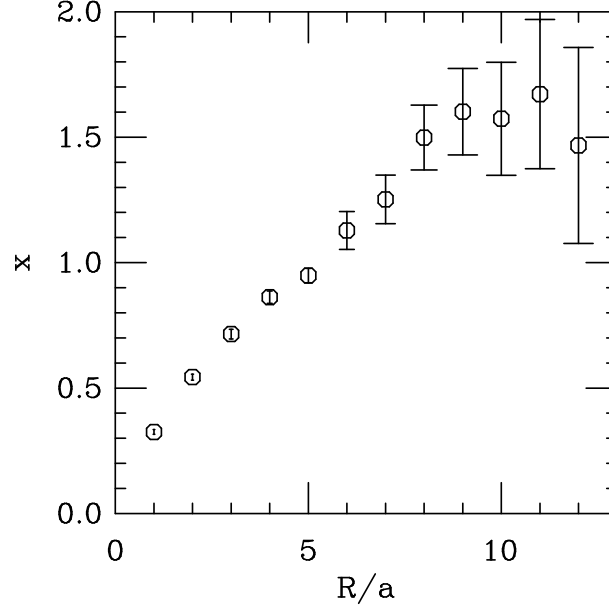


**Figure 8.6.** The  $x(\mathbf{k}, R)$  values with momentum  $\mathbf{k} = (1, 0, 0) \frac{2\pi}{L}$  versus  $R$ .

respect to  $R$ . and a hint of saturation at large  $R$ . One approach to interpret the  $R$ -dependence of  $x(\mathbf{k}, R)$  is by noting that the scalar meson wave function  $w$  has a node at the center of the  $\Pi_u$  state in the transverse direction, since the  $w$  is odd in this direction, and therefore it is sensitive to the transverse width of the excited gluonic flux [67] in the  $\Pi_u$  state. Just as we find, this can explain the increase [67] with longitudinal extent  $R$  leading to a plateau.

Now we have the bare transition amplitude values  $x(\mathbf{k}, R)$ . These values depend on  $R$ . In Appendix D, we develop a formula to integrate out  $R$ . From Eq. (D.35), we obtain the overall transition amplitude for fixed momentum  $\mathbf{k}$  (i.e.,  $\tilde{x}(\mathbf{k})$ ),

$$\tilde{x}(\mathbf{k}) = \frac{1}{2} \int u_H(R) x(R, \mathbf{k}) u_{\chi_b}(R) dR. \quad (8.19)$$

We obtained the values of  $u_H(R)$  and  $u_{\chi_b}(R)$  from the LBO treatment in Chapter 4, and we also plot them in Fig. 8.1. From Fig. 8.1, we note that when  $R > 3a$ , the value of  $u_{\chi_b}(R)$  is approximate close to zero. Hence, only values of  $x(R, \mathbf{k})$  for  $R = 1a, 2a$ , and  $3a$  mainly contribute to the  $\tilde{x}(\mathbf{k})$  value.

**Table 8.2.** The  $x(\mathbf{k}, \mathbf{R})$  values with momentum  $\mathbf{k} = (2, 0, 0)\frac{2\pi}{L}$ . The first column is the separate distance, and Column two is transition amplitude. The remaining columns are the fitting range,  $\chi^2$  and number of degrees of freedom for the fit.

$R/a$	$ax$	Fitting range	$\chi^2/D$
1	0.4007(114)	2-5	0.952/3
2	0.6433(181)	2-5	1.8/3
3	0.8515(221)	2-5	0.658/3
4	1.0001(242)	2-5	3.85/3
5	1.0006(276)	2-4	1.51/2
6	1.2160(310)	2-4	2.52/2

From the values of  $x(R, \mathbf{k})$ ,  $u_H(R)$ ,  $u_{\chi_b}(R)$ , we can get an overall  $x$  value for momentum  $\mathbf{k} = (1, 0, 0)\frac{2\pi}{L}$  by Eq. (8.19), that is,

$$a\tilde{x}(100) = 0.1693(60), \quad (8.20)$$

where the 100 specifies the chosen momentum.

From the same procedure, we can get overall  $x$  value for momentum  $\mathbf{k} = (2, 0, 0)\frac{2\pi}{L}$ , that is,

$$a\tilde{x}(200) = 0.2007(50), \quad (8.21)$$

the overall  $x$  value for momentum  $\mathbf{k} = (1, 1, 0)\frac{2\pi}{L}$ , that is,

$$a\tilde{x}(110) = 0.1482(41), \quad (8.22)$$

and the overall  $x$  value for momentum  $\mathbf{k} = (1, 1, 1)\frac{2\pi}{L}$ , that is,

$$a\tilde{x}(111) = 0.1115(28). \quad (8.23)$$

For concreteness, in Tables 8.2, 8.3, and 8.4, we list the values of  $x(\mathbf{k}, R)$  for different  $R$  with momentum  $\mathbf{k} = (2, 0, 0)\frac{2\pi}{L}$ ,  $\mathbf{k} = (1, 1, 0)\frac{2\pi}{L}$ , and  $\mathbf{k} = (1, 1, 1)\frac{2\pi}{L}$  respectively. Since when  $R > 3a$ , the values of  $u_{\chi_b}(R)$  are negligible, and only  $x(R, \mathbf{k})$  of  $R = 1a, 2a, 3a$  mainly contribute to the  $\tilde{x}(\mathbf{k})$  value. We omitted the results for  $R > 6a$  in the table.

**Table 8.3.** The  $x(\mathbf{k}, \mathbf{R})$  values with momentum  $\mathbf{k} = (1, 1, 0)\frac{2\pi}{L}$ . The first column is the separate distance, and Column two is transition amplitude. The remaining columns are the fitting range,  $\chi^2$  and number of degrees of freedom for the fit.

$R/a$	$ax$	Fitting range	$\chi^2/D$
1	0.2909(85)	2-5	0.344/3
2	0.4695(150)	2-5	0.841/3
3	0.6352(174)	2-5	3.1 /3
4	0.7512(217)	2-4	3.35/2
5	0.9205(483)	3-5	0.0467/2
6	1.0056(620)	3-5	0.0896/2

From our grand fit in Ref. [64], we found

$$aB_0 = 3.12 \pm 0.42. \quad (8.24)$$

Hence, from Eq. (7.38), we have

$$a^4 \hat{b}_{\pi\pi} = 0.0230(31). \quad (8.25)$$

Therefore, from Eq. (D.37), we obtain the transition amplitude of the  $\pi\pi$  channel for momentum  $\mathbf{k} = (1, 0, 0)\frac{2\pi}{L}$ , that is,

$$a^5 \hat{x}(100) = 0.00389(66), \quad (8.26)$$

where the 100 specifies the chosen momentum  $\mathbf{n} = (1, 0, 0)$ . From the same procedure, we can get overall transition amplitude  $x$  for other three momentum. We list all the results of transition amplitude in Table 8.5, where the first column is the chosen momentum, and the second column is overall transition amplitude.

From these  $\hat{x}$ -values, in Appendix D we relate the overall LBO decay amplitude  $x(p)$  to the lattice transition amplitudes  $x_{\pi\pi}(\mathbf{k})$  as Eq. (D.38). That is, we can use the follow formula

$$\hat{x}_{\pi\pi}(p) = \frac{1}{L^3} \sum_{k_x \neq 0, k_y, k_z} \sum_{x, y, z} a^3 N_{sj1}(pr) Y_{11}(\theta, \phi) \hat{x}(\mathbf{k}) \sin(k_x x) \cos(k_y y) \cos(k_z z). \quad (8.27)$$

**Table 8.4.** The  $x(\mathbf{k}, \mathbf{R})$  values with momentum  $\mathbf{k} = (1, 1, 1)\frac{2\pi}{L}$ . The first column is the separate distance, and the second column transition amplitude. The remaining columns are the fitting range,  $\chi^2$  and number of degrees of freedom for the fit.

$R/a$	$ax$	Fitting range	$\chi^2/D$
1	0.2742(65)	2-5	0.0458/3
2	0.3843(105)	2-5	0.672/3
3	0.4493(117)	2-5	1.85/3
4	0.3425(132)	2-4	5.11/2
5	0.3540(308)	3-5	2.41/2
6	-0.00207(436)	3-5	2.79/2

**Table 8.5.** The overall transition amplitude  $x$ , The first column is the chosen momentum, and Column two is overall transition amplitude.

$\mathbf{k}$	$a^3\hat{x}$
$(1, 0, 0)2\pi/L$	0.00389(66)
$(2, 0, 0)2\pi/L$	0.00461(74)
$(1, 1, 0)2\pi/L$	0.00341(55)
$(1, 1, 1)2\pi/L$	0.00256(41)

This result gives the transition amplitude  $x$  at any given momentum  $p$ . Here  $N_s$  is a normalization factor,  $j_1(pr)$  is the spherical Bessel function, and  $Y_{1,m_s}(\theta, \phi)$  is the spherical harmonic function. In terms of our measured values, we have

$$\begin{aligned}
 \hat{x}_{\pi\pi}(p) = & \frac{1}{L^3} \sum_{x,y,z} a^3 N_s j_1(pr) Y_{11}(\theta, \phi) \times \left\{ \hat{x}(100) \sin(x) + \hat{x}(200) \sin(2x) \right. \\
 & \left. + \hat{x}(110) \sin(x) \cos(y) + \hat{x}(111) \sin(x) \cos(y) \cos(z) \right\}, \quad (8.28)
 \end{aligned}$$

where we sum over just a few small values of  $k$ . With these values in Table 8.5, we evaluate  $x_{\pi\pi}(p)$  at any given momentum  $p$ . We show the transition amplitude  $x_{\pi\pi}(p)$  versus momentum  $p$  in Fig. 8.7. Since we just measure a few  $x$ 's with small momentum. As discussed in Appendix D, the values shown in Fig. 8.7 for high momentum are not reliable. We test that it is reliable for the small momentum  $p$ .

For the decay

$$H \rightarrow \chi_b + \pi + \pi, \quad (8.29)$$



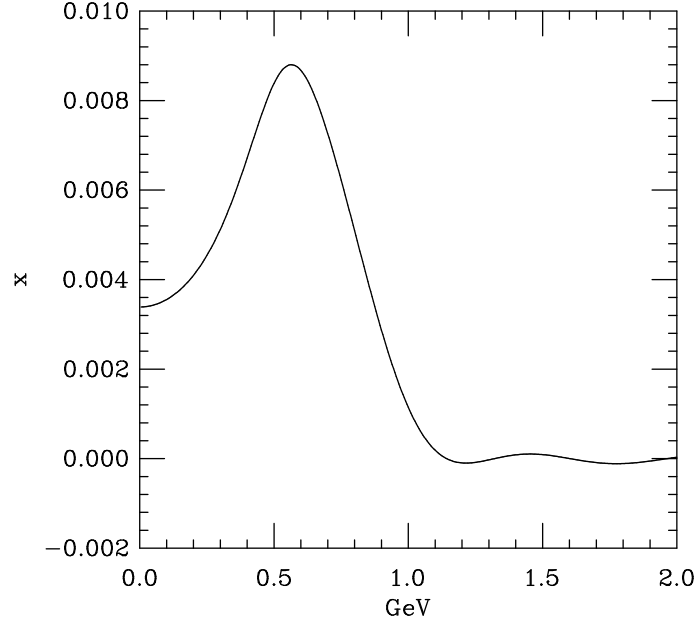


**Figure 8.7.** The transition amplitude  $x(p)$  versus momentum  $p$ .

From Fermi's Golden Rule for the transition rate  $\Gamma$ , we need to calculate the phase factor. Because the calculation of phase factor is tedious. We show the detailed procedure in Appendix E to obtain a formula to evaluate the transition rate  $\Gamma$ ,

$$\Gamma = 8\pi^3 \left(\frac{La}{2\pi}\right)^6 \int_0^{p_{\max}} dp p^2 \hat{x}_{\pi\pi}(p)^2 \sqrt{\frac{1}{4} - \frac{m_\pi^2}{(\Delta M)^2 - p^2}}, \quad (8.30)$$

where  $M_A$  is the mass of the  $\chi_b$  state,  $M_H$  is the mass of the  $H$  state,  $\Delta M = M_H - M_A$ , and

$$p_{\max} = \sqrt{(\Delta M)^2 - 4m_\pi^2}. \quad (8.31)$$

Here  $m_\pi$  is the mass of pion meson.

For our simulation, we have  $M_H = 10.828$  GeV and  $M_A = 9.877$  GeV, hence  $\Delta M = 0.951$  GeV, thus  $p_{\max} = 0.83$  GeV. We can estimate  $x_{\pi\pi}(p)$  by Eq. (8.28). Hence, by integrating Eq. (8.30), we can obtain overall transition rate

$$\Gamma = 3.62(98) \text{ MeV}, \quad (8.32)$$

for the decay  $H \rightarrow \chi_b + \pi + \pi$ . In Chapter 7, we use the perturbation expansion for  $C_{HAB}$  correlator to find a way to extract the transition amplitude  $x$ . To use this

method, we should discuss whether it is justified or not. The condition we need is  $\Gamma \ll \Delta E$ . Since  $\Gamma \ll \Delta E$ , our lattice method for decay rate is justified.

## CHAPTER 9

### CONCLUSION

In this chapter, we first discuss the evidence for the  $f_0$  meson. Then we discuss the evidence for light quark hybrid exotic mesons. Next we discuss hybrid exotic quarkonium decay. Finally, we summarize our results.

#### 9.1 Evidence for $f_0$ meson

For the past 45 years, the question of the existence and nature of the  $f_0$ -meson has attracted the attention of many authors [68]. The subjects of investigation are the internal properties of the  $f_0$ -meson and its role as an intermediate particle in various processes, both in vacuum and in hot and dense matter. It appears as a broad enhancement in the isospin  $I = 0$ ,  $J = 0$   $\pi\pi$  scattering amplitude. The experimental value of the  $f_0$ -meson mass is not accurately determined and lies in a wide interval [12]

$$M_{f_0} = 400 - 1200 \text{ MeV}, \quad (9.1)$$

This uncertainty is explained by large values of the decay width of this meson into two pions [12]

$$\Gamma_{f_0} = 600 - 1000 \text{ MeV}. \quad (9.2)$$

Recently, the Fermilab experiment E791 [69] showed strong evidence for the existence of an  $I = 0$ ,  $J = 0$   $\pi^+\pi^-$  resonance in charmed  $D^+$  meson decay. The  $\pi^+\pi^-$  resonance in E791 is compatible with the scalar meson  $f_0(500)$ . It was also observed in the Cabbibo-suppressed decay  $D^+ \rightarrow \pi^-\pi^+\pi^+$  [69]. The  $D^+ \rightarrow f_0(500)\pi^+$  decay contribution is dominant, being responsible for approximately half of the decays through the particular resonant sequence:  $D^+ \rightarrow \pi + f_0 \rightarrow \pi^-\pi^+\pi^+$  decay [69]. The measured mass and width of the  $f_0$  meson are  $478 \pm 31 \text{ MeV}$  and

$338 \pm 48$  MeV, respectively. Several other experimental results can be explained by the existence of the  $f_0$  meson resonance [70][71][72][73][74].

## 9.2 Evidence for light-quark hybrid exotic mesons

There are two ways to study hybrid exotic mesons. One approach is to use lattice QCD calculation. A summary of current LQCD calculations for the lowest lying light quark ( $u$  or  $d$ )  $J^{PC} = 1^{-+}$  hybrid exotic meson is listed in Table 9.1. These lattice QCD calculations are quenched or partially quenched. All of this numbers indicate that the rough mass of hybrid exotic meson is about 1.8-2.1 GeV.

Another approach is to directly perform experiment [79]. Several high statistics experimental searches for hybrid exotic mesons have been carried out. These experiments show credible evidence for the existence of  $J^{PC} = 1^{-+}$  hybrid exotics  $\pi_1(1400)$ ,  $\pi_1(1600)$ ,  $\pi_1(2000)$ . The  $\pi_1(1400)$  was first reported by the VES Collaboration at IHEP [80] and was confirmed by the E852 Collaboration at BNL in the  $\pi^- p \rightarrow \eta \pi^- p$  reaction [81]. This was followed with additional confirmation by the Crystal Barrel Collaboration at the CERN LEAR facility in antiproton-neutron annihilation [82]. In the Particle Data Group (PDG) listings [83], the mass of the  $\pi_1(1400)$  is  $M = 1376 \pm 17$  MeV and its width  $\Gamma = 300 \pm 40$  MeV with observed decays to  $\pi\eta$ . A second  $J^{PC} = 1^{-+}$  exotic hybrid candidate, the  $\pi_1(1600)$ , was first observed at BNL E852 in  $\pi^- p \rightarrow \rho p \rightarrow \pi^+ \pi^- \pi^- p$  [84]. Since that time further evidence for the  $\pi_1(1600)$  has been provided through its decays into  $\eta' \pi$  [85],  $f_1 \pi$  [86], and  $b_1 \pi$  [87]. The PDG [83] lists the mass and width of this state as  $M = 1596_{-14}^{+25}$  MeV and  $\Gamma = 312_{-24}^{+64}$  MeV.

**Table 9.1.** Quenched lattice QCD calculations for the mass of  $u\bar{u}g$  hybrid exotic meson ( $J^{PC} = 1^{-+}$ ).

Collaboration(Year)	Computed Mass(GeV)	Reference
UKQCD (1997)	$1.87 \pm 0.2$	[75]
SESAM (1998)	$1.90 \pm 0.2$	[76]
Mei and Luo(2003)	$2.013 \pm 0.026$	[77]
MILC(2004)	$1.792 \pm 0.139$	[78]

Another candidate  $J^{PC} = 1^{-+}$  meson is  $\pi_1(2000)$ , which has been seen through its decays into  $b_1\pi$  [87] and  $f_1\pi$  [86] at BNL E852. The  $J^{PC}$  for  $b_1$  is  $1^{+-}$ , and the  $J^{PC}$  for  $f_1$  is  $1^{++}$ . This state is the least controversial of the announced exotics, because its mass is consistent with theoretical expectations and its decay modes are consistent with expectations for hybrid mesons. However the statistical accuracy of the existing data still needs improvement.

Because the lattice simulation of the heavy quark hybrid exotics (namely,  $b\bar{b}g$ ) is difficult, and searching them from experiment need pretty high energy, hence there are no papers about this kind of heavy quark hybrid exotics. The result of this dissertation will bring a little contribution in this field.

### 9.3 Hybrid exotic quarkonium decay

Recent observations of charmonium states in  $B$ -meson decays suggest that charmonium hybrid mesons ( $h_c$ )<sup>1</sup> can be produced in  $B$  meson decay [89, 90, 88]. Some of these states are likely to be narrow with subsequent decays to  $J/\psi \pi^+\pi^-$ , etc.

Recent developments in both theory and experiment lead us to expect that charmonium hybrids will be produced in  $B$  decays. The partial widths for  $B \rightarrow c\bar{c} + X$ , with  $c\bar{c}$  representing specific final states such as  $J/\psi$ ,  $\chi_{c0}$ ,  $\chi_{c1}$ ,  $\chi_{c2}$ , etc. Possible decay schemes are [88]:  $h_c(0^{+-}, 2^{+-}) \rightarrow J/\psi + (\pi^+\pi^-, \eta, \eta')$ ,  $h_c(1^{-+}) \rightarrow \eta_c + (\pi^+\pi^-, \eta, \eta')$ . These decay modes can give distinctive signals. Both  $0^{+-}$  and  $2^{+-}$  should decay via the  $J/\psi \pi\pi$  cascade [88]. The  $h_c(1^{-+})$  state is expected to be the lightest exotic  $c\bar{c}$  hybrid, and therefore in this case the cascade goes to  $\eta_c\pi\pi$ .

The  $X(3872)$  is a narrow state decaying into  $\pi^+\pi^-J/\psi$ , with a mass  $M_X \sim 3872 \text{ MeV}$ . Given the observed mass, in the charmonium region, it is natural to assert that the  $X(3872)$  is itself a charmonium state. However it is difficult to identify the  $X(3872)$  with any of the expected narrow  $c\bar{c}$  mesons, leading to suggestions that it is a more exotic particle [91][92][93].

---

<sup>1</sup>The notation  $h_c$  is introduced in Ref. [88]. I use his notation in the discussion of this section.

## 9.4 Summary

We reviewed arguments that, in the heavy quark limit, the decay channel of a  $J^{PC} = 1^{-+}$  spin-exotic hybrid meson will be dominated by the creation of a flavor singlet light quark-antiquark. In this dissertation, we explored this decay in lattice QCD with  $N_f = 3$  flavors of dynamical sea quark with masses close to the physical values. We studied the transition between an excited hybrid gluonic state (i.e.,  $\Pi_u$  state) and a ground state gluonic state (i.e.,  $\chi_b$  state) with the production of a flavor-singlet light quark-antiquark pair. The dominant decay channel should be the  $\pi\pi$  channel. We introduced a phenomenological model for the decay and directly studied the transition to two pions on the lattice. We obtained a little bit smaller transition amplitude for this decay channel.

Our numerical result for the scalar  $f_0$  meson is  $am = 0.47(7)$  (or  $m_{f_0} = (768 \pm 136)$  MeV for this lattice spacing  $a = 0.12$  fm, the mass of up quark ( $am_u = 0.005$ ), and the mass of strange quark ( $am_s = 0.05$ ). The energy release from the hybrid meson at 10.833 GeV to the  $\chi_b$  state at 9.893 GeV is 0.940 GeV. Therefore, it is impossible to decay to a scalar meson heavier than 940 MeV. For  $b$  quarks the relevant transitions is  $H \rightarrow \chi_b \pi\pi$ . Our raw lattice result is an overall decay rate of 3.62(98) MeV for the scalar meson.

The evaluation of this transitions amplitude in this dissertation is a fascinating step for the phenomenological study of hybrid decays. Our results are consistent with our expectation that the spin-exotic hybrid meson states are relatively narrow. We hope our results will be able to guide the experimental search for a  $\bar{b}bg$  and  $f_0$  meson, etc.

In this dissertation, we performed our research on one ensemble of lattice gauge configuration. That means our results are at a single lattice spacing and light quark mass. As we discussed in Chapter 3. The physical one should be in continuum limit (lattice spacing  $a \rightarrow 0$ ). Hence, we still work on other different configurations. In the continuum limit, we get the decay rates that have physical means.

## APPENDIX A

### THE $PC$ OF THE HYBRID MESON

In this appendix, we want to prove Eq. (4.34), and Eq. (4.35), which we use in Chapter 4 to evaluate the  $PC$  of the hybrid meson.

Here we first introduce the azimuthal angle  $\theta$ , the zenith angle  $\psi$  of the axis of the  $Q\bar{Q}$  and  $R$ , the distance (radius) between  $Q$  and  $\bar{Q}$  with respect to a fixed system of coordinates  $\xi, \eta, \zeta$ . Besides the fixed system of the coordinates  $\xi, \eta, \zeta$ , we also introduce a moving system of the coordinates  $x, y, z$ . And the two system have the same origin. The  $z$ -axis is in the direction of the axis of  $Q\bar{Q}$ , and the  $x$ -axis is lying in the  $\xi - \eta$  plane. In bpdy-fixed system of the coordinates  $x, y, z$ , we also introduce the cylinder coordinates: radial  $\rho$ , angle  $\alpha$ , and  $z$ . The angle  $\alpha$  is measured in xy-plane from the x-axis with  $0 \leq \alpha < 2\pi$ .

The coordinates  $\xi_g, \eta_g, \zeta_g$  of the gluon and the coordinates  $x_g, y_g, z_g$  of the gluon have following relationship

$$x_g = -\xi_g \sin \psi + \eta_g \cos \psi \quad (\text{A.1})$$

$$y_g = -\xi_g \cos \theta \cos \psi + \eta_g \cos \theta \sin \psi + \zeta_g \sin \theta \quad (\text{A.2})$$

$$z_g = -\xi_g \sin \theta \cos \psi + \eta_g \sin \theta \sin \psi + \zeta_g \cos \theta. \quad (\text{A.3})$$

We know, under the operation of parity, that the  $\theta, \psi$  change according to

$$\theta \rightarrow \pi - \theta \quad (\text{A.4})$$

$$\psi \rightarrow \pi + \psi. \quad (\text{A.5})$$

Also the  $\xi, \eta, \zeta$  change sign. From Eqs. (B.1,B.2,B.3), we obtain that, under the operation of parity, the  $x$  and  $z$  do not change sign, and  $y$  change sign. This means that, under the operation of parity,

$$\alpha \rightarrow -\alpha. \quad (\text{A.6})$$

The wave function of the hybrid meson is, then,

$$\chi_{n,\Lambda,L,M_L} = \phi_{n,\Lambda,L}(\rho, \alpha, z) \Xi_{n,\Lambda,L,M_L}(r) \Theta_{L,M_L,\Lambda}(\theta) \Phi_{M_L}(\psi), \quad (\text{A.7})$$

where  $L$  is the total angular momentum of the hybrid meson,  $M_L$  is the  $\zeta$ -component of  $L$ ,  $\Lambda$  is the  $z$ -component of the angular momentum of the gluon, and  $n$  stands for the others quantum numbers, which specify the state of the hybrid meson,  $\phi_{n,\Lambda,L}(\rho, \alpha, z)$  is the gluon wave function, and  $\Xi_{n,\Lambda,L,M_L}(r)$  is the “radial part” of  $Q\bar{Q}$  wave function. The  $\theta$  dependence is given by  $\Theta_{L,M_L,\Lambda}(\theta)$ . Finally,  $\Phi_{M_L}(\psi)$  gives the “ $\psi$ ” dependence.

According to the solution in Page 299 of Ref. [53], we obtain

$$\begin{aligned} \Theta_{L,M_L,\Lambda}(\theta) = & (-i)^L \sqrt{\frac{(2L+1)!(L+M_L)!}{(L-\Lambda)!(L+\Lambda)!(L-M_L)!}} \times \frac{(1-\cos \theta)^{\frac{\Lambda-M_L}{2}}}{(1+\cos \theta)^{\frac{\Lambda+M_L}{2}}} \times \\ & \left\{ \left( \frac{\partial}{\partial \cos \theta} \right)^{L-M_L} (1-\cos \theta)^{L-\Lambda} (1+\cos \theta)^{L+\Lambda} \right\}, \end{aligned} \quad (\text{A.8})$$

which we are called the left-handed gluon state, and

$$\begin{aligned} \Theta_{L,M_L,-\Lambda}(\theta) = & (-i)^L \sqrt{\frac{(2L+1)!(L+M_L)!}{(L-\Lambda)!(L+\Lambda)!(L-M_L)!}} \times \frac{(1-\cos \theta)^{\frac{-\Lambda-M_L}{2}}}{(1+\cos \theta)^{\frac{-\Lambda+M_L}{2}}} \times \\ & \left\{ \left( \frac{\partial}{\partial \cos \theta} \right)^{L-M_L} (1-\cos \theta)^{L+\Lambda} (1+\cos \theta)^{L-\Lambda} \right\}, \end{aligned} \quad (\text{A.9})$$

which we are called the right-handed gluon state. It is obvious that the left-handed gluon state and the right-handed state are not eigenstates of parity. Now if we combine them, we can construct eigenstates of parity.

$$\begin{aligned} \Theta_{L,M_L,\Lambda}(\theta) + \epsilon \Theta_{L,M_L,-\Lambda}(\theta) = & (-i)^L \sqrt{\frac{(2L+1)!(L+M_L)!}{(L-\Lambda)!(L+\Lambda)!(L-M_L)!}} \times \left\{ \right. \\ & \frac{(1-\cos \theta)^{\frac{\Lambda-M_L}{2}}}{(1+\cos \theta)^{\frac{\Lambda+M_L}{2}}} \left( \frac{\partial}{\partial \cos \theta} \right)^{L-M_L} (1-\cos \theta)^{L-\Lambda} (1+\cos \theta)^{L+\Lambda} + \\ & \left. \epsilon \frac{(1-\cos \theta)^{\frac{-\Lambda-M_L}{2}}}{(1+\cos \theta)^{\frac{-\Lambda+M_L}{2}}} \left( \frac{\partial}{\partial \cos \theta} \right)^{L-M_L} (1-\cos \theta)^{L+\Lambda} (1+\cos \theta)^{L-\Lambda} \right\}, \end{aligned} \quad (\text{A.10})$$

where  $\epsilon = \pm 1$ .



Hence, we obtain

$$P \{ \Theta_{L,M_L,\Lambda}(\theta) + \epsilon \Theta_{L,M_L,-\Lambda}(\theta) \} = \Theta_{L,M_L,\Lambda}(\pi - \theta) + \epsilon \Theta_{L,M_L,-\Lambda}(\pi - \theta). \quad (\text{A.11})$$

Now if we consider the identity  $\cos(\pi - \theta) = -\cos \theta$ , we obtain

$$\begin{aligned} P \{ \Theta_{L,M_L,\Lambda}(\theta) + \epsilon \Theta_{L,M_L,-\Lambda}(\theta) \} &= (-i)^L \sqrt{\frac{(2L+1)!(L+M_L)!}{(L-\Lambda)!(L+\Lambda)!(L-M_L)!}} \times \epsilon (-1)^{L-M_L} \\ &\left\{ \epsilon \frac{(1+\cos \theta)^{\frac{\Lambda-M_L}{2}}}{(1-\cos \theta)^{\frac{\Lambda+M_L}{2}}} \left( \frac{\partial}{\partial \cos \theta} \right)^{L-M_L} (1+\cos \theta)^{L-\Lambda} (1-\cos \theta)^{L+\Lambda} + \right. \\ &\left. \frac{(1-\cos \theta)^{\frac{\Lambda-M_L}{2}}}{(1+\cos \theta)^{\frac{\Lambda+M_L}{2}}} \left( \frac{\partial}{\partial \cos \theta} \right)^{L-M_L} (1+\cos \theta)^{L-\Lambda} (1-\cos \theta)^{L+\Lambda} \right\}. \end{aligned} \quad (\text{A.12})$$

Hence, we obtain

$$P \{ \Theta_{L,M_L,\Lambda}(\theta) + \epsilon \Theta_{L,M_L,-\Lambda}(\theta) \} = \epsilon (-1)^{L-M_L} \{ \Theta_{L,M_L,\Lambda}(\theta) + \epsilon \Theta_{L,M_L,-\Lambda}(\theta) \}. \quad (\text{A.13})$$

The “ $\psi$ ” part of the gluon wave function (namely,  $\Phi(\psi)$ ) is

$$\Phi_{M_L}(\psi) = \frac{1}{\sqrt{2\pi}} e^{iM_L\psi}. \quad (\text{A.14})$$

It is obvious that

$$P \Phi_{M_L}(\psi) = (-1)^{M_L} \Phi_{M_L}(\psi). \quad (\text{A.15})$$

And the “ $\alpha$ ” part of the gluon wave function in  $\phi_{n,\Lambda,L}(\rho, \alpha, z)$  is

$$\phi_{\Lambda}(\alpha) = \frac{1}{\sqrt{2\pi}} e^{i\Lambda\alpha}. \quad (\text{A.16})$$

It is obvious that

$$P \phi_{\Lambda}(\alpha) = \phi_{-\Lambda}(\alpha). \quad (\text{A.17})$$

If we consider the intrinsic parity of the meson is -1 [14], the total parity of the hybrid meson is given by  $P = \epsilon (-1)^{L-M_L} \times (-1)^{M_L} \times (-1)^1$ , that is,

$$P = \epsilon (-1)^{L+1}. \quad (\text{A.18})$$

Let us define the  $PC$  quantum number of the gluon to be  $\eta$ , if we also consider that the symmetry of the spin wave function under charge-conjugation is  $(-1)^{S+1}$  [14], we obtain the charge-conjugation of the hybrid meson, namely

$$C = \epsilon \eta (-1)^{L+S}. \quad (\text{A.19})$$

## APPENDIX B

### BUBBLE CONTRIBUTION FOR $a_0$ CORRELATOR

The mass of the  $a_0$  meson can be reliably determined on the lattice. In order to determine the mass of the  $a_0$  meson, we evaluate the  $a_0$  correlator

$$C(t) = \sum_{\mathbf{x}} \langle \bar{d}(\mathbf{x}, t) u(\mathbf{x}, t) \bar{u}(\mathbf{0}, 0) d(\mathbf{0}, 0) \rangle. \quad (\text{B.1})$$

The extraction of the mass of the  $a_0$  meson ( $J^P = 0^+$  and  $I = 1$ ) is straightforward. However there exist many multihadron states with  $J^P = 0^+$  and  $I = 1$  which can propagate between the source and the sink. Of special interest in multihadron states is *the intermediate state with two pseudoscalars*  $P_1 P_2$  which we refer to as *the bubble contribution* ( $B$ ) [63]. If the masses of  $P_1$  and  $P_2$  are small, the bubble contribution  $B$  gives a considerable contribution to the  $a_0$  correlator, and it should be included in the fit of the lattice correlator in Eq. (B.1), that is,

$$C(t) = A e^{-m_{\sigma} t} + B(t), \quad (\text{B.2})$$

where we omit the unimportant contributions from the excited  $a_0$  meson and other high order multihadron intermediate states.

#### B.1 Coupling of a scalar current to pseudoscalar

Before we embark on the calculation of the bubble contribution, in this section we first derive the coupling of a point scalar current  $\bar{d}_r(x) u_r(x)$  to a pair of the pseudoscalar fields at the lowest energy order of the staggered chiral perturbation theory (S $\chi$ PT), where the subscript  $r$  in the expression  $u_r(x)$  is the index of the taste replica for a given quark flavor  $u$ . The effective scalar current can be determined from the dependence of the lattice  $QCD$  Lagrangian and the staggered

chiral Lagrangian on the spurion field  $\mathcal{M}$ , where  $\mathcal{M}$  is the staggered quark mass matrix. For  $n$  Kogut-Susskind (KS) flavors,  $\mathcal{M}$  is a  $4nn_r \times 4nn_r$  matrix.

$$\mathcal{M} = \begin{pmatrix} m_{uu}I \otimes I_R & m_{ud}I \otimes I_R & m_{us}I \otimes I_R & \cdots \\ m_{du}I \otimes I_R & m_{dd}I \otimes I_R & m_{ds}I \otimes I_R & \cdots \\ m_{su}I \otimes I_R & m_{sd}I \otimes I_R & m_{ss}I \otimes I_R & \cdots \\ \vdots & \vdots & \vdots & \ddots \end{pmatrix}, \quad (\text{B.3})$$

where  $I$  is a  $4 \times 4$  unit matrix, and  $I_R$  is  $n_r \times n_r$  unit replica matrix. In short,  $\mathcal{M} = \mathbf{m} \otimes I \otimes I_R$ , where

$$\mathbf{m} = \begin{pmatrix} m_{uu} & m_{ud} & m_{us} & \cdots \\ m_{du} & m_{dd} & m_{ds} & \cdots \\ m_{su} & m_{sd} & m_{ss} & \cdots \\ \vdots & \vdots & \vdots & \ddots \end{pmatrix} \quad (\text{B.4})$$

is the  $n \times n$  quark mass matrix. We know from  $QCD$  that the quark current  $\bar{d}_r(x)u_r(x)$  is given by

$$\bar{d}_r(x)u_r(x) = -\frac{\partial \mathcal{L}_{QCD}}{\partial m_{d_r u_r}(x)}, \quad (\text{B.5})$$

where  $\mathcal{L}_{QCD}$  is the  $QCD$  Lagrangian.

Since staggered chiral lagrangian ( $\mathcal{L}_{S\chi PT}$ ) is an effective equivalent Lagrangian for  $\mathcal{L}_{QCD}$  in low energy limit, the effective current  $\bar{u}_r(x)u_r(x)$  is obtained from

$$\bar{d}_r(x)u_r(x) = -\frac{\partial \mathcal{L}_{S\chi PT}}{\partial \mathcal{M}_{d_r u_r}(x)}, \quad (\text{B.6})$$

where

$$\mathcal{L}_{S\chi PT} = \frac{1}{8}f_\pi^2 \text{Tr}[\partial^\mu \Sigma \partial_\mu \Sigma^\dagger] - \frac{1}{4}B_0 f_\pi^2 \text{Tr}[\mathcal{M}^\dagger \Sigma + \Sigma^\dagger \mathcal{M}] \quad (\text{B.7})$$

is the staggered chiral Lagrangian [60]. We omit the high order terms and the terms that are independent of  $\mathcal{M}$ ,  $f_\pi$  is the tree-level pion decay constant ( $f_\pi = 131$  MeV [60]),  $B_0$  is the constant with the dimension of the mass [94], and  $\Sigma = \exp\left(\frac{2i\Phi}{f_\pi}\right)$  [60]. The field  $\Phi = \sum_{b=1}^{16} \frac{1}{2} T^b \otimes \phi^b$  is described in terms of the mass eigenstate field  $\phi^b$  [60], where  $\phi^b$  is a  $3 \times 3$  pseudoscalar matrix with flavor components  $\phi_{f_r f'_r}^b$  with flavor  $f, f'$ , the index of the taste replica  $r, r'$ , and taste  $b$  which is given by generators  $T^b = \{\xi_5, i\xi_5 \xi_\mu, i\xi_\mu \xi_\nu, \xi_\mu, \xi_I\}$  [60]. Hence,  $\Phi$  is  $4nn_r \times 4nn_r$  pseudoscalar matrix in  $S\chi PT$  [60], and the subscripts  $u, d$  denote its valance flavor

component. Therefore,  $\Sigma$  is also a  $4nn_r \times 4nn_r$  matrix. The  $\text{Tr}$  is the full  $4nn_r \times 4nn_r$  trace. Therefore, the effective current is [94]

$$\bar{d}_r(x)u_r(x) = B_0 \text{Tr}_t[\Phi(x)^2]_{d_ru_r}, \quad (\text{B.8})$$

where the notation  $\text{Tr}_t$  stands for the trace over taste.

## B.2 Bubble Contribution

In this section we compute the bubble contribution from two intermediate states to the  $a_0$  correlator in Eq. (B.1). From the discussion in Sec. B.1, the point scalar current can be described in terms of the pseudoscalar field  $\Phi$  by using  $S\chi\text{PT}$  [94][63],

$$\bar{d}_r(x)u_r(x) = B_0 \text{Tr}_t[\Phi(x)^2]_{d_ru_r} \quad (\text{B.9})$$

$$\bar{u}_r(x)d_r(x) = B_0 \text{Tr}_t[\Phi(x)^2]_{u_rd_r}, \quad (\text{B.10})$$

where  $B_0 = \frac{M_\pi^2}{2m_q}$  is the coupling of the point scalar current to the pseudoscalar field  $\Phi(x)$ , which can be numerically determined from the lattice simulation.

Now we consider the lattice simulations with staggered KS valence quarks and three flavors of staggered KS dynamical sea quarks with  $m_u = m_d \neq m_s$ . We only consider the correlators where the valence-quark mass is equal to the  $u$  or  $d$  dynamical sea-quark mass. We know that our  $a_0$  correlator is estimated by using the taste-singlet source and taste-singlet sink. This  $a_0$  correlator takes contribution from the  $a_0$  meson and the bubble contribution. For concreteness, the bubble contribution to the  $a_0$  correlator in a theory with  $n_r$  tastes per flavor and three flavors (namely,  $N_f = 2 + 1$ ) of KS dynamical sea quarks is [60]

$$\begin{aligned} B_{a_0}^{S\chi PT}(x) &= \frac{B_0^2}{n_r} \sum_{r,r'=1}^{n_r} \left\{ \left\langle \bar{d}_r(x)u_r(x) \bar{u}_{r'}(0)d_{r'}(0) \right\rangle_{\text{Bubble}} \right\} \\ &= \frac{B_0^2}{n_r} \sum_{r,r'=1}^{n_r} \left\{ \left\langle \text{Tr}_t[\Phi^2]_{d_ru_r} \text{Tr}_t[\Phi^2]_{u_rd_{r'}} \right\rangle \right\}, \end{aligned} \quad (\text{B.11})$$

where the subscript  $a_0$  specifies the bubble contribution for  $a_0$  meson. If we consider this identity  $\text{Tr}_t(T^a T^b) = 4\delta_{ab}$ , we arrive at

$$B_{a_0}^{S\chi PT}(x) = \frac{B_0^2}{n_r} \sum_{\substack{a=1 \\ b=1}}^{16} \sum_{\substack{i=1 \\ j=1}}^{N_f} \sum_{\substack{r,r'=1 \\ t,t'=1}}^{n_r} \langle \phi_{d_r i_t}^a(x) \phi_{i_t u_r}^a(x) \phi_{u_{r'} j_{t'}}^b(0) \phi_{j_{t'} d_{r'}}^b(0) \rangle. \quad (\text{B.12})$$

where  $a, b, a', b'$  are taste indices,  $i, j$  are flavor indices, and  $r, t, r', t'$  are the indices of the taste replica. The Wick contractions result in the products of two propagators for the pseudoscalar fields. Therefore, the bubble contribution can be expressed in terms of the pseudoscalar propagators  $\langle \phi^b \phi^b \rangle$ .

$$B_{a_0}^{S\chi PT}(x) = \frac{B_0^2}{n_r} \sum_{b=1}^{16} \sum_{r,r'=1}^{n_r} \sum_{t,t'=1}^{n_r} \left\{ 2\langle \phi_{u_r d_t}^b(x) \phi_{d_{t'} u_{r'}}^b(0) \rangle \langle \phi_{u_t u_r}^b(x) \phi_{d_{r'} d_{t'}}^b(0) \rangle + \right. \\ \left. 2\langle \phi_{u_r d_t}^b(x) \phi_{d_{t'} u_{r'}}^b(0) \rangle \langle \phi_{u_t u_r}^b(x) \phi_{u_{r'} u_{t'}}^b(0) \rangle + \right. \\ \left. \langle \phi_{u_r s_t}^b(x) \phi_{s_{t'} u_{r'}}^b(0) \rangle \langle \phi_{s_t u_r}^b(x) \phi_{u_{r'} s_{t'}}^b(0) \rangle \right\}, \quad (\text{B.13})$$

where we use charge symmetry to equate correlators with  $u \leftrightarrow d$ .

First of all, we sum over the indices of the taste replica in Eq. (B.13). For illustration, we consider the second term in Eq. (B.13) for taste  $b = I, V, A$ .

$$\begin{aligned} & \sum_{r,r'} \sum_{t,t'} \left\{ \langle \phi_{u_r u_t}^b(x) \phi_{u_{r'} u_{t'}}^b(0) \rangle \langle \phi_{u_t d_r}^b(x) \phi_{d_{t'} u_{r'}}^b(0) \rangle \right\} \\ = & \sum_{r,r'} \left\{ \langle \phi_{u_r u_r}^b(x) \phi_{u_{r'} u_{r'}}^b(0) \rangle \langle \phi_{u_r d_r}^b(x) \phi_{d_{r'} u_{r'}}^b(0) \rangle \right\}_{r \neq r'} + \\ & \sum_{r,t} \left\{ \langle \phi_{u_r u_t}^b(x) \phi_{u_r u_t}^b(0) \rangle \langle \phi_{u_t d_r}^b(x) \phi_{d_t u_r}^b(0) \rangle \right\}_{r \neq t} + \\ & \sum_{r,t} \left\{ \langle \phi_{u_r u_t}^b(x) \phi_{u_t u_r}^b(0) \rangle \langle \phi_{u_t d_r}^b(x) \phi_{d_r u_t}^b(0) \rangle \right\}_{r \neq t} + \\ & \sum_r \left\{ \langle \phi_{u_r u_r}^b(x) \phi_{u_r u_r}^b(0) \rangle \langle \phi_{u_t d_r}^b(x) \phi_{d_r u_r}^b(0) \rangle \right\}. \end{aligned} \quad (\text{B.14})$$

The first term and the second term in Eq. (B.14) should be zero, and the third term in Eq. (B.14) should be

$$n_r(n_r - 1) \langle \phi_{u_r u_r}^b \phi_{u_r u_r}^b \rangle_{\text{CC}} \langle \phi_{u_r d_r}^b \phi_{d_r u_r}^b \rangle_{\text{CC}}, \quad (\text{B.15})$$

where the notation CC stands for the connected contribution. The fourth term in Eq. (B.14) should be

$$n_r \left\{ \langle \phi_{u_r u_r}^b(x) \phi_{u_r u_r}^b(0) \rangle_{\text{CC}} \langle \phi_{u_r d_r}^b(x) \phi_{d_r u_r}^b(0) \rangle_{\text{CC}} + \right.$$

$$\langle \phi_{u_r u_r}^b(x) \phi_{u_r u_r}^b(0) \rangle_{\text{DC}} \langle \phi_{u_r d_r}^b(x) \phi_{d_r u_r}^b(0) \rangle_{\text{CC}} \Big\}, \quad (\text{B.16})$$

where the notation DC stands for the disconnected contribution. Hence, the second term in Eq. (B.14) can be changed into

$$\begin{aligned} \sum_{r,r'} \sum_{t,t'} \Big\{ \langle \phi_{u_r u_t}^b(x) \phi_{u_r u_t}^b(0) \rangle \langle \phi_{u_t d_r}^b(x) \phi_{d_t u_r}^b(0) \rangle \Big\} = \\ n_r^2 \langle \phi_{u_r u_r}^b(x) \phi_{u_r u_r}^b(0) \rangle_{\text{CC}} \langle \phi_{u_r d_r}^b(x) \phi_{d_r u_r}^b(0) \rangle_{\text{CC}} + \\ n_r \langle \phi_{u_r u_r}^b(x) \phi_{u_r u_r}^b(0) \rangle_{\text{DC}} \langle \phi_{u_r d_r}^b(x) \phi_{d_r u_r}^b(0) \rangle_{\text{CC}}. \end{aligned} \quad (\text{B.17})$$

Because there is no disconnected contribution for taste  $b \neq I, V, A$ , therefore Eq. (B.14) can be written as

$$\begin{aligned} \sum_{r,r'} \sum_{t,t'} \Big\{ \langle \phi_{u_r u_t}^b(x) \phi_{u_r u_t}^b(0) \rangle \langle \phi_{u_t u_r}^b(x) \phi_{u_t u_r}^b(0) \rangle \Big\} \\ = n_r^2 \langle \phi_{u_r u_r}^b(x) \phi_{u_r u_r}^b(0) \rangle_{\text{CC}} \langle \phi_{u_r d_r}^b(x) \phi_{d_r u_r}^b(0) \rangle_{\text{CC}}. \end{aligned} \quad (\text{B.18})$$

From the similar procedure, for taste  $b = I, V, A$ , we obtain

$$\begin{aligned} \sum_{r,r'} \sum_{t,t'} \Big\{ \langle \phi_{u_r d_t}^b(x) \phi_{d_r u_t}^b(0) \rangle \langle \phi_{u_t u_r}^b(x) \phi_{d_t d_r}^b(0) \rangle \Big\} \\ = n_r \langle \phi_{u_r d_r}^b(x) \phi_{d_r u_r}^b(0) \rangle_{\text{CC}} \langle \phi_{u_r u_r}^b(x) \phi_{d_r d_r}^b(0) \rangle_{\text{DC}}, \end{aligned} \quad (\text{B.19})$$

where we consider the  $\langle \phi_{uu}^b \phi_{dd}^b \rangle$  does not include the connected contribution. For taste  $b \neq I, V, A$ , this term should be zero. For any taste  $b$ , we obtain

$$\begin{aligned} \sum_{r,r'} \sum_{t,t'} \Big\{ \langle \phi_{u_r s_t}^b(x) \phi_{s_r u_t}^b(0) \rangle \langle \phi_{s_t u_r}^b(x) \phi_{u_t s_r}^b(0) \rangle \Big\} \\ = n_r^2 \langle \phi_{u_r s_r}^b(x) \phi_{s_r u_r}^b(0) \rangle_{\text{CC}} \langle \phi_{s_r u_r}^b(x) \phi_{u_r s_r}^b(0) \rangle_{\text{CC}}. \end{aligned} \quad (\text{B.20})$$

From now on, since there is no summation over the index of the taste replica. We suppress it. Thus we can rewrite Eq. (B.13) as

$$\begin{aligned} B_{a_0}^{S\chi PT}(x) = n_r B_0^2 \sum_{b=1}^{16} \Big\{ 2 \langle \phi_{ud}^b(x) \phi_{du}^b(0) \rangle_{\text{CC}} \langle \phi_{uu}^b(x) \phi_{uu}^b(0) \rangle_{\text{CC}} + \\ \langle \phi_{us}^b(x) \phi_{su}^b(0) \rangle_{\text{CC}} \langle \phi_{su}^b(x) \phi_{us}^b(0) \rangle_{\text{CC}} \Big\} \\ + 4 B_0^2 \sum_{b=I,V,A} \Big\{ \langle \phi_{uu}^b(x) \phi_{uu}^b(0) \rangle_{\text{DC}} \langle \phi_{ud}^b(x) \phi_{du}^b(0) \rangle_{\text{CC}} \Big\}, \end{aligned} \quad (\text{B.21})$$

The propagators  $\langle \phi^b \phi^b \rangle$  for the pseudoscalar field  $\phi^b$  for various tastes  $b$  are studied in Ref. [60]. Propagators for all tastes ( $I, V, A, T, P$ ) have connected contributions,

while only tastes  $I$ ,  $V$  and  $A$  have disconnected contributions. Hence, Eq. (B.21) can be rewritten by plugging in the mesonic propagators, that is,

$$B_{a_0}^{S\chi PT}(t) = F.T.[ B_{a_0}^{S\chi PT}(p) ]_{\mathbf{p}=0} \quad \text{with} \quad (\text{B.22})$$

$$\begin{aligned} B_{a_0}^{S\chi PT}(p) = & \frac{B_0^2}{n_r} \sum_k \left\{ -4 \frac{1}{(k+p)^2 + M_{U_V}^2} \delta_V \frac{k^2 + M_{S_V}^2}{(k^2 + M_{U_V}^2)(k^2 + M_{\eta_V}^2)(k^2 + M_{\eta'V}^2)} \right. \\ & -4 \frac{1}{(k+p)^2 + M_{U_A}^2} \delta_A \frac{k^2 + M_{S_A}^2}{(k^2 + M_{U_A}^2)(k^2 + M_{\eta_A}^2)(k^2 + M_{\eta'A}^2)} \\ & -n_r^2 \sum_{b=1}^{16} \left[ 2 \frac{1}{(k+p)^2 + M_{U_b}^2} \frac{1}{k^2 + M_{U_b}^2} + \frac{1}{(k+p)^2 + M_{K_b}^2} \frac{1}{k^2 + M_{K_b}^2} \right] \\ & \left. -2 \frac{1}{(k+p)^2 + M_{U_I}^2} \frac{1}{k^2 + M_{U_I}^2} + \frac{2}{3} \frac{1}{(k+p)^2 + M_{U_I}^2} \frac{1}{k^2 + M_{\eta_I}^2} \right\}, \quad (\text{B.23}) \end{aligned}$$

where  $\delta_V = a^2 \delta'_V$ ,  $\delta_A = a^2 \delta'_A$  and [63][60]

$$M_{\eta_I} = \frac{1}{3} M_{U_I}^2 + \frac{2}{3} M_{S_I}^2 \quad (\text{B.24})$$

$$M_{\eta_V}^2 = \frac{1}{2} (M_{U_V}^2 + M_{S_V}^2 + 3n_r \delta_V - Z_V) \quad (\text{B.25})$$

$$M_{\eta'V}^2 = \frac{1}{2} (M_{U_V}^2 + M_{S_V}^2 + 3n_r \delta_V + Z_V). \quad (\text{B.26})$$

Here

$$Z_V = \sqrt{(M_{S_V}^2 - M_{U_V}^2)^2 - 2n_r \delta_V (M_{S_V}^2 - M_{U_V}^2) + 9(n_r \delta_V)^2}. \quad (\text{B.27})$$

For the axial taste we just requires  $V \rightarrow A$ . The pseudoscalar masses  $M_{U_b} \equiv M_{\pi_b} = 2B_0 m_u + a^2 \Delta_b$ ,  $M_{S_b} \equiv M_{ss_b} = 2B_0 m_s + a^2 \Delta_b$  and  $M_{K_b} \equiv M_{us_b} = B_0(m_u + m_s) + a^2 \Delta_b$  have been determined by MILC simulations [38, 10]. The taste breaking term  $a^2 \Delta_b$  is independent of the flavor [60] and will disappear in the continuum limit (i.e.,  $a \rightarrow 0$ ). We can prove that

$$\frac{k^2 + M_{S_V}^2}{(k^2 + M_{U_V}^2)(k^2 + M_{\eta_V}^2)(k^2 + M_{\eta'V}^2)} = \frac{1}{4n_r \delta_V} \left\{ \frac{2}{k^2 + M_{U_V}^2} - \frac{C_{V_\eta}}{k^2 + M_{\eta_V}^2} + \frac{C_{V_{\eta'}}}{k^2 + M_{\eta'V}^2} \right\}, \quad (\text{B.28})$$

where

$$C_{V_\eta} = \frac{(M_{S_V}^2 - M_{U_V}^2 - n_r \delta_V + Z_V)}{Z_V} \quad (\text{B.29})$$

$$C_{V_{\eta'}} = \frac{(M_{S_V}^2 - M_{U_V}^2 - n_r \delta_V - Z_V)}{Z_V}. \quad (\text{B.30})$$

For the axial taste we just requires  $V \rightarrow A$ . We simplify Eq. (B.23) as

$$\begin{aligned} B_{a_0}^{S\chi PT}(p) = & \frac{B_0^2}{n_r} \sum_{\mathbf{k}} \left\{ -\frac{1}{(k+p)^2 + M_{U_V}^2} \frac{4C_{V_{\eta'}}}{k^2 + M_{\eta'V}^2} - \frac{1}{(k+p)^2 + M_{U_A}^2} \frac{4C_{A_{\eta'}}}{k^2 + M_{\eta'A}^2} \right. \\ & - 8 \frac{1}{(k+p)^2 + M_{U_V}^2} \frac{1}{k^2 + M_{U_V}^2} + \frac{1}{(k+p)^2 + M_{U_V}^2} \frac{4C_{V_{\eta}}}{k^2 + M_{\eta V}^2} \\ & - 8 \frac{1}{(k+p)^2 + M_{U_A}^2} \frac{1}{k^2 + M_{U_A}^2} + \frac{1}{(k+p)^2 + M_{U_A}^2} \frac{4C_{V_{\eta}}}{k^2 + M_{\eta A}^2} \\ & + n_r^2 \sum_{b=1}^{16} \left[ 2 \frac{1}{(k+p)^2 + M_{U_b}^2} \frac{1}{k^2 + M_{U_b}^2} + \frac{1}{(k+p)^2 + M_{K_b}^2} \frac{1}{k^2 + M_{K_b}^2} \right] \\ & \left. - 2 \frac{1}{(k+p)^2 + M_{U_I}^2} \frac{1}{k^2 + M_{U_I}^2} + \frac{2}{3} \frac{1}{(k+p)^2 + M_{U_I}^2} \frac{1}{k^2 + M_{\eta I}^2} \right\}. \quad (\text{B.31}) \end{aligned}$$

For 1 + 1 + 1 theory, we obtain

$$\begin{aligned} B_{a_0}^{S\chi PT}(t) = & \frac{B_0^2}{4n_r L^3} \sum_{\mathbf{k}} \left\{ \frac{2}{3} \frac{e^{-\left(\sqrt{(\mathbf{p}+\mathbf{k})^2 + M_{U_I}^2} + \sqrt{\mathbf{k}^2 + M_{\eta I}^2}\right)t}}{\sqrt{(\mathbf{p}+\mathbf{k})^2 + M_{U_I}^2} \sqrt{\mathbf{k}^2 + M_{\eta I}^2}} - 2 \frac{e^{-\left(\sqrt{(\mathbf{p}+\mathbf{k})^2 + M_{U_I}^2} + \sqrt{\mathbf{k}^2 + M_{U_I}^2}\right)t}}{\sqrt{(\mathbf{p}+\mathbf{k})^2 + M_{U_I}^2} \sqrt{\mathbf{k}^2 + M_{U_I}^2}} \right. \\ & + 4C_{V_{\eta}} \frac{e^{-\left(\sqrt{(\mathbf{p}+\mathbf{k})^2 + M_{U_V}^2} + \sqrt{\mathbf{k}^2 + M_{\eta V}^2}\right)t}}{\sqrt{(\mathbf{p}+\mathbf{k})^2 + M_{U_V}^2} \sqrt{\mathbf{k}^2 + M_{\eta V}^2}} - 4C_{V_{\eta'}} \frac{e^{-\left(\sqrt{(\mathbf{p}+\mathbf{k})^2 + M_{U_V}^2} + \sqrt{\mathbf{k}^2 + M_{\eta'V}^2}\right)t}}{\sqrt{(\mathbf{p}+\mathbf{k})^2 + M_{U_V}^2} \sqrt{\mathbf{k}^2 + M_{\eta'V}^2}} \\ & + 4C_{A_{\eta}} \frac{e^{-\left(\sqrt{(\mathbf{p}+\mathbf{k})^2 + M_{U_A}^2} + \sqrt{\mathbf{k}^2 + M_{\eta A}^2}\right)t}}{\sqrt{(\mathbf{p}+\mathbf{k})^2 + M_{U_A}^2} \sqrt{\mathbf{k}^2 + M_{\eta A}^2}} - 4C_{A_{\eta'}} \frac{e^{-\left(\sqrt{(\mathbf{p}+\mathbf{k})^2 + M_{U_A}^2} + \sqrt{\mathbf{k}^2 + M_{\eta'A}^2}\right)t}}{\sqrt{(\mathbf{p}+\mathbf{k})^2 + M_{U_A}^2} \sqrt{\mathbf{k}^2 + M_{\eta'A}^2}} \\ & - 8 \frac{e^{-\left(\sqrt{(\mathbf{p}+\mathbf{k})^2 + M_{U_V}^2} + \sqrt{\mathbf{k}^2 + M_{U_V}^2}\right)t}}{\sqrt{(\mathbf{p}+\mathbf{k})^2 + M_{U_V}^2} \sqrt{\mathbf{k}^2 + M_{U_V}^2}} - 8 \frac{e^{-\left(\sqrt{(\mathbf{p}+\mathbf{k})^2 + M_{U_A}^2} + \sqrt{\mathbf{k}^2 + M_{U_A}^2}\right)t}}{\sqrt{(\mathbf{p}+\mathbf{k})^2 + M_{U_A}^2} \sqrt{\mathbf{k}^2 + M_{U_A}^2}} \\ & \left. + \frac{1}{8} \sum_{b=1}^{16} \frac{e^{-\left(\sqrt{(\mathbf{p}+\mathbf{k})^2 + M_{U_b}^2} + \sqrt{\mathbf{k}^2 + M_{U_b}^2}\right)t}}{\sqrt{(\mathbf{p}+\mathbf{k})^2 + M_{U_b}^2} \sqrt{\mathbf{k}^2 + M_{U_b}^2}} + \frac{1}{16} \sum_{b=1}^{16} \frac{e^{-\left(\sqrt{(\mathbf{p}+\mathbf{k})^2 + M_{K_b}^2} + \sqrt{\mathbf{k}^2 + M_{K_b}^2}\right)t}}{\sqrt{(\mathbf{p}+\mathbf{k})^2 + M_{K_b}^2} \sqrt{\mathbf{k}^2 + M_{K_b}^2}} \right\}. \quad (\text{B.32}) \end{aligned}$$



## APPENDIX C

### BUBBLE CONTRIBUTION FOR $f_0$ CORRELATOR

The mass of the  $f_0$  meson can be reliably determined on the lattice. In order to determine the mass of the  $f_0$  meson, we use lattice simulations to evaluate the scalar  $f_0$  correlator in Eq. (8.3), that is,

$$C(t) = \sum_{\mathbf{x}} \langle \bar{u}_r(\mathbf{x}, t) u_r(\mathbf{x}, t) \bar{u}_r(\mathbf{0}, 0) u_r(\mathbf{0}, 0) \rangle_{CC} + 2n_r \sum_{\mathbf{x}} \langle \bar{u}_r(\mathbf{x}, t) u_r(\mathbf{x}, t) \bar{u}_r(\mathbf{0}, 0) u_r(\mathbf{0}, 0) \rangle_{DC}, \quad (\text{C.1})$$

where  $r$  and  $r'$  is the indices of the taste replica. The extraction of the mass of the  $f_0$  meson ( $J^P = 0^+$  and  $I = 0$ ) is straightforward. However there are many multihadron states with  $J^P = 0^+$  and  $I = 0$  can propagate between the source and sink of scalar  $f_0$  correlator. Of special interest is the bubble contribution  $B$ , which gives a considerable contribution to the scalar  $f_0$  correlator, and it should be included in the fit of the lattice correlator in Eq. (C.1),

$$C(t) = Ae^{-m_{f_0}t} + B(t), \quad (\text{C.2})$$

where we omit the unimportant contributions from the excited scalar  $f_0$  meson and other high order multihadron intermediate states.

#### C.1 Bubble contribution

In this section we compute the bubble contribution to the scalar  $f_0$  correlator in Eq. (C.1). From the discussion in Sec. B.1, the point scalar current can be described in terms of the pseudoscalar field  $\Phi$  by using S $\chi$ PT [94][63]

$$\bar{u}_r(x) u_r(x) = B_0 \text{Tr}_t[\Phi(x)^2]_{u_r u_r}, \quad \bar{d}_r(x) d_r(x) = B_0 \text{Tr}_t[\Phi(x)^2]_{d_r d_r}, \quad (\text{C.3})$$

where  $B_0$  is the coupling of the point scalar current to the pseudoscalar field  $\Phi(x)$ .

We know that our scalar  $f_0$  correlator is estimated by using the taste-singlet source and taste-singlet sink. It takes contribution from the scalar  $f_0$  meson and the bubble contribution. For concreteness, the bubble contribution in a theory with  $n_r$  tastes per flavor and three flavors of KS dynamical sea quarks is [60]

$$B_{f_0}^{S\chi PT}(x) = \frac{B_0^2}{n_r} \sum_{r,r'=1}^{n_r} \left\{ \left\langle \text{Tr}_t[\Phi^2]_{u_r u_r} \text{Tr}_t[\Phi^2]_{u_{r'} u_{r'}} \right\rangle + \left\langle \text{Tr}_t[\Phi^2]_{u_r u_r} \text{Tr}_t[\Phi^2]_{d_{r'} d_{r'}} \right\rangle \right\}, \quad (\text{C.4})$$

where  $\Phi$  is  $12n_r \times 12n_r$  pseudoscalar matrix in  $S\chi PT$  [60], the subscripts  $u, d$  denote its valance flavor component, and the subscript  $f_0$  specifies the bubble contribution for the  $f_0$  meson. If we consider this identity  $\text{Tr}_t(T^a T^b) = 4\delta_{ab}$ , we obtain

$$B_{f_0}^{S\chi PT}(x) = \frac{B_0^2}{n_r} \sum_{a=1}^{16} \sum_{b=1}^{16} \sum_{i=1}^{N_f} \sum_{j=1}^{N_f} \sum_{r,r'=1}^{n_r} \sum_{t,t'=1}^{n_r} \langle \phi_{u_r i_t}^a(x) \phi_{i_t u_r}^a(x) \phi_{u_{r'} j_{t'}}^b(0) \phi_{j_{t'} u_{r'}}^b(0) \rangle + \frac{B_0^2}{n_r} \sum_{a=1}^{16} \sum_{b=1}^{16} \sum_{i=1}^{N_f} \sum_{j=1}^{N_f} \sum_{r,r'=1}^{n_r} \sum_{t,t'=1}^{n_r} \langle \phi_{u_r i_t}^a(x) \phi_{i_t u_r}^a(x) \phi_{d_{r'} j_{t'}}^b(0) \phi_{j_{t'} d_{r'}}^b(0) \rangle. \quad (\text{C.5})$$

where  $a, b, a', b'$  are taste indices, and  $i, j$  are flavor indices, and  $r, t, r', t'$  are the indices of the taste replica. From similar procedure in Sec. B.2, we obtain

$$B_{f_0}^{S\chi PT}(x) = \frac{1}{n_r} B_0^2 \sum_{b=1}^{16} \left\{ 4n_r^2 \langle \phi_{ud}^b(x) \phi_{du}^b(0) \rangle n_r^2 \langle \phi_{du}^b(x) \phi_{ud}^b(0) \rangle + \langle \phi_{us}^b(x) \phi_{su}^b(0) \rangle \langle \phi_{su}^b(x) \phi_{us}^b(0) \rangle \right\} + \frac{1}{n_r} B_0^2 \sum_{b=I,V,A} \left\{ 4n_r^2 \langle \phi_{uu}^b(x) \phi_{uu}^b(0) \rangle_{\text{DC}} \langle \phi_{uu}^b(x) \phi_{uu}^b(0) \rangle_{\text{DC}} + 4n_r \langle \phi_{uu}^b(x) \phi_{uu}^b(0) \rangle_{\text{DC}} \langle \phi_{uu}^b(x) \phi_{uu}^b(0) \rangle_{\text{CC}} \right\}, \quad (\text{C.6})$$

where we consider the  $u, d$  quarks are degenerate in mass. The bubble contribution in Eq. (C.4) can be rewritten by plugging in the mesonic propagators,

$$B_{f_0}^{S\chi PT}(t) = F.T.[ B_{f_0}^{S\chi PT}(p) ]_{\mathbf{p}=\mathbf{0}} \quad \text{with} \quad (\text{C.7})$$

$$B_{f_0}^{S\chi PT}(p) = \frac{B_0^2}{n_r} \sum_k \left\{ -\frac{1}{(k+p)^2 + M_{U_I}^2} \frac{1}{k^2 + M_{U_I}^2} + \frac{1}{9} \frac{1}{(k+p)^2 + M_{\eta_I}^2} \frac{1}{k^2 + M_{\eta_I}^2} + C_{V_\eta}^2 \frac{1}{(k+p)^2 + M_{\eta_V}^2} \frac{1}{k^2 + M_{\eta_V}^2} + C_{V_{\eta'}}^2 \frac{1}{(k+p)^2 + M_{\eta'_V}^2} \frac{1}{k^2 + M_{\eta'_V}^2} \right\},$$

$$\begin{aligned}
& +C_{A_\eta}^2 \frac{1}{(k+p)^2 + M_{\eta A}^2} \frac{1}{k^2 + M_{\eta A}^2} + C_{A_{\eta'}}^2 \frac{1}{(k+p)^2 + M_{\eta' A}^2} \frac{1}{k^2 + M_{\eta' A}^2} \\
& -C_{V_\eta} C_{V_{\eta'}} \left[ \frac{1}{(k+p)^2 + M_{\eta V}^2} \frac{1}{k^2 + M_{\eta' V}^2} + \frac{1}{(k+p)^2 + M_{\eta' V}^2} \frac{1}{k^2 + M_{\eta V}^2} \right] \\
& -C_{A_\eta} C_{A_{\eta'}} \left[ \frac{1}{(k+p)^2 + M_{\eta A}^2} \frac{1}{k^2 + M_{\eta' A}^2} + \frac{1}{(k+p)^2 + M_{\eta' A}^2} \frac{1}{k^2 + M_{\eta A}^2} \right] \\
& -4 \frac{1}{(k+p)^2 + M_{U_V}^2} \frac{1}{k^2 + M_{U_V}^2} - 4 \frac{1}{(k+p)^2 + M_{U_A}^2} \frac{1}{k^2 + M_{U_A}^2} \\
& + n_r^2 \sum_{b=1}^{16} \left[ 4 \frac{1}{(k+p)^2 + M_{U_b}^2} \frac{1}{k^2 + M_{U_b}^2} + \frac{1}{(k+p)^2 + M_{K_b}^2} \frac{1}{k^2 + M_{K_b}^2} \right] \Big\}, \quad (C.8)
\end{aligned}$$

where  $\delta_V$ ,  $M_{\eta I}$ ,  $M_{\eta V}^2$ ,  $M_{\eta' V}^2$ ,  $\delta_A$ ,  $M_{\eta A}^2$ ,  $M_{\eta' A}^2$ ,  $C_{V_\eta}$ ,  $C_{V_{\eta'}}$ ,  $C_{A_\eta}$ ,  $C_{A_{\eta'}}$  are denoted in Appendix B. The Fourier Transform of Eq. (C.8) (1+1+1+1 theory) is

$$\begin{aligned}
B_{f_0}^{S\chi^{PT}}(t, \mathbf{p}) = & B_1^2 \sum_{\mathbf{k}} \left\{ \frac{1}{9} \frac{e^{-\left(\sqrt{(\mathbf{p}+\mathbf{k})^2 + M_{\eta I}^2} + \sqrt{\mathbf{k}^2 + M_{\eta I}^2}\right)t}}{\sqrt{(\mathbf{p}+\mathbf{k})^2 + M_{\eta I}^2} \sqrt{\mathbf{k}^2 + M_{\eta I}^2}} - \frac{e^{-\left(\sqrt{(\mathbf{p}+\mathbf{k})^2 + M_{U_I}^2} + \sqrt{\mathbf{k}^2 + M_{U_I}^2}\right)t}}{\sqrt{(\mathbf{p}+\mathbf{k})^2 + M_{U_I}^2} \sqrt{\mathbf{k}^2 + M_{U_I}^2}} \right. \\
& + C_{V_\eta}^2 \frac{e^{-\left(\sqrt{(\mathbf{p}+\mathbf{k})^2 + M_{\eta V}^2} + \sqrt{\mathbf{k}^2 + M_{\eta V}^2}\right)t}}{\sqrt{(\mathbf{p}+\mathbf{k})^2 + M_{\eta V}^2} \sqrt{\mathbf{k}^2 + M_{\eta V}^2}} + C_{V_{\eta'}}^2 \frac{e^{-\left(\sqrt{(\mathbf{p}+\mathbf{k})^2 + M_{\eta' V}^2} + \sqrt{\mathbf{k}^2 + M_{\eta' V}^2}\right)t}}{\sqrt{(\mathbf{p}+\mathbf{k})^2 + M_{\eta' V}^2} \sqrt{\mathbf{k}^2 + M_{\eta' V}^2}} \\
& + C_{A_\eta}^2 \frac{e^{-\left(\sqrt{(\mathbf{p}+\mathbf{k})^2 + M_{\eta A}^2} + \sqrt{\mathbf{k}^2 + M_{\eta A}^2}\right)t}}{\sqrt{(\mathbf{p}+\mathbf{k})^2 + M_{\eta A}^2} \sqrt{\mathbf{k}^2 + M_{\eta A}^2}} + C_{A_{\eta'}}^2 \frac{e^{-\left(\sqrt{(\mathbf{p}+\mathbf{k})^2 + M_{\eta' A}^2} + \sqrt{\mathbf{k}^2 + M_{\eta' A}^2}\right)t}}{\sqrt{(\mathbf{p}+\mathbf{k})^2 + M_{\eta' A}^2} \sqrt{\mathbf{k}^2 + M_{\eta' A}^2}} \\
& - C_{V_\eta} C_{V_{\eta'}} \left[ \frac{e^{-\left(\sqrt{(\mathbf{p}+\mathbf{k})^2 + M_{\eta V}^2} + \sqrt{\mathbf{k}^2 + M_{\eta' V}^2}\right)t}}{\sqrt{(\mathbf{p}+\mathbf{k})^2 + M_{\eta V}^2} \sqrt{\mathbf{k}^2 + M_{\eta' V}^2}} + \frac{e^{-\left(\sqrt{(\mathbf{p}+\mathbf{k})^2 + M_{\eta' V}^2} + \sqrt{\mathbf{k}^2 + M_{\eta V}^2}\right)t}}{\sqrt{(\mathbf{p}+\mathbf{k})^2 + M_{\eta' V}^2} \sqrt{\mathbf{k}^2 + M_{\eta V}^2}} \right] \\
& - C_{A_\eta} C_{A_{\eta'}} \left[ \frac{e^{-\left(\sqrt{(\mathbf{p}+\mathbf{k})^2 + M_{\eta A}^2} + \sqrt{\mathbf{k}^2 + M_{\eta' A}^2}\right)t}}{\sqrt{(\mathbf{p}+\mathbf{k})^2 + M_{\eta A}^2} \sqrt{\mathbf{k}^2 + M_{\eta' A}^2}} + \frac{e^{-\left(\sqrt{(\mathbf{p}+\mathbf{k})^2 + M_{\eta' A}^2} + \sqrt{\mathbf{k}^2 + M_{\eta A}^2}\right)t}}{\sqrt{(\mathbf{p}+\mathbf{k})^2 + M_{\eta' A}^2} \sqrt{\mathbf{k}^2 + M_{\eta A}^2}} \right] \\
& - 4 \frac{e^{-\left(\sqrt{(\mathbf{p}+\mathbf{k})^2 + M_{U_V}^2} + \sqrt{\mathbf{k}^2 + M_{U_V}^2}\right)t}}{\sqrt{(\mathbf{p}+\mathbf{k})^2 + M_{U_V}^2} \sqrt{\mathbf{k}^2 + M_{U_V}^2}} - 4 \frac{e^{-\left(\sqrt{(\mathbf{p}+\mathbf{k})^2 + M_{U_A}^2} + \sqrt{\mathbf{k}^2 + M_{U_A}^2}\right)t}}{\sqrt{(\mathbf{p}+\mathbf{k})^2 + M_{U_A}^2} \sqrt{\mathbf{k}^2 + M_{U_A}^2}} \\
& \left. \frac{1}{16} \sum_{b=1}^{16} \left[ 4 \frac{e^{-\left(\sqrt{(\mathbf{p}+\mathbf{k})^2 + M_{U_b}^2} + \sqrt{\mathbf{k}^2 + M_{U_b}^2}\right)t}}{\sqrt{(\mathbf{p}+\mathbf{k})^2 + M_{U_b}^2} \sqrt{\mathbf{k}^2 + M_{U_b}^2}} + \frac{e^{-\left(\sqrt{(\mathbf{p}+\mathbf{k})^2 + M_{K_b}^2} + \sqrt{\mathbf{k}^2 + M_{K_b}^2}\right)t}}{\sqrt{(\mathbf{p}+\mathbf{k})^2 + M_{K_b}^2} \sqrt{\mathbf{k}^2 + M_{K_b}^2}} \right] \right\}, \quad (C.9)
\end{aligned}$$

where  $B_1^2 = \frac{B_0^2}{4n_r L^3}$ .

# APPENDIX D

## LBO TREATMENT OF DECAY CHANNEL FOR HYBRID

In this dissertation, we are interested in the decay of a hybrid exotic quarkonium  $1^{-+}$  state  $H$  to  $\chi_b$  state with the emission of a pair of pseudoscalar mesons in a scalar channel ( $\pi\pi$ ). To make the problem simple we assume that the scalar meson ( $\pi\pi$ ) in the final state does not interact with the  $\chi_b$  final state. The lattice calculation is performed by the LBO approximation, and the wave functions of the initial and final state are easily described in the rest frame of the heavy quarks. We call it the “body-fixed frame.” The displacement vector  $\mathbf{R}$  of the heavy quarks specifies the  $z$  axis of the body-fixed frame. The exotic hybrid state (H) is  $\Pi_u$  and the final quarkonium state is  $\Sigma_g^+$  state ( $\chi_b$ ).

As discussed in Chapter 4, the potentials are computed in the static approximation. The wave function of the hybrid exotic in lab frame is <sup>1</sup>

$$\Psi_H(R, \phi, \theta, \alpha) = \rho_H(R) \frac{\tilde{D}_{m,1}^1(\phi, \theta, \alpha) + \tilde{D}_{m,-1}^1(\phi, \theta, \alpha)}{\sqrt{2}}, \quad (\text{D.1})$$

where we ignore the spin degrees of freedom,  $m$  is the projection of the total angular momentum (excluding spin) on the lab  $z$  axis, and  $\pm 1$  is its projection on the body-fixed axis. The Euler angle  $\alpha$  specifies a rotation about the body-fixed axis and it is an internal coordinate for the excited flux tube.

---

<sup>1</sup> **$L^2$ -normalized** Wigner D-functions  $\tilde{D}_{M,M'}^J(\phi, \theta, \alpha)$  and ordinary Wigner D-functions  $D_{M,M'}^J(\phi, \theta, \alpha)$  have relationship,  $\tilde{D}_{M,M'}^J(\phi, \theta, \alpha) = \sqrt{\frac{2J+1}{8\pi^2}} D_{M,M'}^J(\phi, \theta, \alpha)$ . Hence

$$\int_0^{2\pi} d\alpha \int_0^\pi \sin \theta d\theta \int_0^{2\pi} d\phi \tilde{D}_{M_1, M_1'}^{J_1*}(\phi, \theta, \alpha) \tilde{D}_{M_2, M_2'}^{J_2}(\phi, \theta, \alpha) = \delta_{J_1 J_2} \delta_{M_1 M_2} \delta_{M_1' M_2'}.$$

In lab frame the state  $H$  can be described by

$$|H\rangle = \int d^3\mathbf{R} d^3\mathbf{r} \int d\alpha \frac{e^{i\mathbf{P}_H \cdot \mathbf{r}}}{(2\pi)^{3/2}} \Psi_H(R, \phi, \theta, \alpha) \mathcal{C}_Q^\dagger(\mathbf{r}_1) \mathcal{C}_{\bar{Q}}^\dagger(\mathbf{r}_2) A(\alpha) |0\rangle, \quad (\text{D.2})$$

where  $\mathbf{r}_1 = (\mathbf{R} - \mathbf{r})/2$ ,  $\mathbf{r}_2 = (\mathbf{R} + \mathbf{r})/2$ , and

$$A(\alpha) = \sum_{\Lambda} \left[ a_{g\Lambda} \frac{e^{i\Lambda\alpha}}{\sqrt{2\pi}} + a_{g\Lambda}^\dagger \frac{e^{-i\Lambda\alpha}}{\sqrt{2\pi}} \right], \quad (\text{D.3})$$

here the  $a_{g\Lambda}$  is the creation operator of gluon.

By convention the wave function of the  $\chi_b$  state in rest frame is

$$\Psi_{\chi_b}(R, \phi, \theta) = \rho_{\chi_b}(R) Y_{1m_b}(\theta, \phi). \quad (\text{D.4})$$

In lab frame the state  $A$  can be described by

$$|A\rangle = \int d^3\mathbf{R} d^3\mathbf{r} \frac{e^{i\mathbf{P}_A \cdot \mathbf{r}}}{(2\pi)^{3/2}} \Psi_{\chi_b}(R, \phi, \theta) \mathcal{C}_Q^\dagger(\mathbf{r}_1) \mathcal{C}_{\bar{Q}}^\dagger(\mathbf{r}_2) |0\rangle. \quad (\text{D.5})$$

In the body-fixed frame with  $\mathbf{R}$  fixed the initial hybrid exotic state has only the internal gluonic degree of freedom with a wave function  $\cos \alpha / \sqrt{\pi}$  corresponding to the choice  $\Lambda = \pm 1$ . We can model this transition in the lab frame through an interaction potential

$$V_I^{\text{lab}} = \int d^3\mathbf{R} d^3\mathbf{r} \int d^3\mathbf{r}'_s \bar{x}(\mathbf{R}') \mathcal{C}_Q^\dagger(\mathbf{r}_1) \mathcal{C}_{\bar{Q}}^\dagger(\mathbf{r}_2) \mathcal{C}_Q(\mathbf{r}_1) \mathcal{C}_{\bar{Q}}(\mathbf{r}_2) \times \\ \bar{\psi}\psi(\mathbf{r}_s + \mathbf{r}) [w_{I,1}(\mathbf{r}'_s) a_{g,1} + w_{I,-1}(\mathbf{r}'_s) a_{g,-1}], \quad (\text{D.6})$$

where the primed coordinates are the coordinates of the scalar meson in the body-fixed frame,  $w_I$  is the wave function of the scalar meson in the body-fixed frame as determined by the dynamics of the transition, and  $x(R)$  controls the transition amplitude. Since final state  $\chi_b$  has  $\Lambda = 0$ , the scalar meson must carry off the nonzero  $z$ -component of the angular momentum in the body-fixed frame.

The wave function of the scalar meson is a free spherical wave with an appropriate angular momentum ( $L = 1$ ). Hence, its wave function in rest frame is

$$\psi_s(r_s, \theta_s, \phi_s) = N_s j_1(pr) Y_{1,m_s}(\theta_s, \phi_s), \quad (\text{D.7})$$

where  $N_s$  is a normalization factor,  $j_1(pr)$  is the spherical Bessel function, and  $Y_{1,m_s}(\theta_s, \phi_s)$  is the spherical harmonic function, and  $p$  is the magnitude of the angular momentum.

In this notation we evaluate the transition amplitude in lab frame by

$$\begin{aligned} \langle A, \pi(\mathbf{p}_1)\pi(\mathbf{p}_2) | V_I^{\text{lab}} | H \rangle &= \int d^3\mathbf{R} \int r_s^2 dr_s d\Omega_s d\alpha \Psi_H(R, \phi, \theta, \alpha) \Psi_{\chi_b}^*(R, \theta, \phi) \\ &\quad \times \psi_s^*(r_s, \theta_s, \phi_s) \frac{\cos(\alpha - \phi'_s)}{\sqrt{2\pi}} x(\mathbf{R}) w_I(\mathbf{r}'_s) \\ &\quad \times \langle \pi(\mathbf{p}_1)\pi(\mathbf{p}_2) | \bar{\psi}\psi(0) | 0 \rangle \delta^{(3)}(\mathbf{P}_H - \mathbf{P}_A - \mathbf{p}), \end{aligned} \quad (\text{D.8})$$

where  $|\pi(\mathbf{p}_1)\pi(\mathbf{p}_2)\rangle = a_{\mathbf{p}_1}^\dagger a_{\mathbf{p}_2}^\dagger |0\rangle$  (namely,  $a_{\mathbf{p}_1}^\dagger a_{\mathbf{p}_2}^\dagger$  is the creation operator for  $\pi\pi$ ),  $\mathbf{p} = \mathbf{p}_1 + \mathbf{p}_2$ , and the  $p$  is the magnitude of the angular momentum  $\mathbf{p}$ . For brevity, we divide  $\langle A, \pi(\mathbf{p}_1)\pi(\mathbf{p}_2) | V_I^{\text{lab}} | H \rangle$  into two parts, that is,

$$\langle A, \pi(\mathbf{p}_1)\pi(\mathbf{p}_2) | V_I^{\text{lab}} | H \rangle \equiv x_{\pi\pi}(p_1, p_2) \delta^{(3)}(\mathbf{P}_H - \mathbf{P}_A - \mathbf{p}), \quad (\text{D.9})$$

where

$$\begin{aligned} x_{\pi\pi}(p_1, p_2) &= \int d^3\mathbf{R} \int r_s^2 dr_s d\Omega_s d\alpha \Psi_H(R, \phi, \theta, \alpha) \Psi_{\chi_b}^*(R, \theta, \phi) \psi_s^*(r_s, \theta_s, \phi_s) \\ &\quad \times \frac{\cos(\alpha - \phi'_s)}{\sqrt{2\pi}} x(\mathbf{R}) w_I(\mathbf{r}'_s) \langle \pi(\mathbf{p}_1)\pi(\mathbf{p}_2) | \bar{\psi}\psi(0) | 0 \rangle. \end{aligned} \quad (\text{D.10})$$

The integration over scalar meson coordinates is carried out in body-fixed frame. To this goal we use the rotation property of the spherical harmonic function

$$Y_{1,m_s}(\theta_s, \phi_s) = \sum_{\Lambda} D_{m_s, \Lambda}^1(\phi, \theta) Y_{1, \Lambda}(\theta'_s, \phi'_s) \quad (\text{D.11})$$

Because the volume element is rotationally invariant, we have

$$\begin{aligned} x_{\pi\pi}(p_1, p_2) &= \int R^2 dR d\Omega \int r_s'^2 dr_s' d\Omega'_s \sum_{\Lambda} D_{m_s, \Lambda}^{1*}(\phi, \theta) x(R) \rho_{\chi_b}(R) \rho_H(R) N_s j_1(pr'_s) \\ &\quad \times Y_{1, \Lambda}(\theta'_s, \phi'_s) Y_{1m_b}^*(\theta, \phi) x(R) w_I(r'_s, \theta'_s, \phi'_s) \langle \pi(\mathbf{p}_1)\pi(\mathbf{p}_2) | \bar{\psi}\psi(0) | 0 \rangle \\ &\quad \times \int d\alpha \frac{\cos(\alpha - \phi'_s)}{\sqrt{\pi}} \frac{\tilde{D}_{m,1}^1(\phi, \theta, \alpha) + \tilde{D}_{m,-1}^1(\phi, \theta, \alpha)}{\sqrt{2}}. \end{aligned} \quad (\text{D.12})$$

After integrating out the  $\alpha$  and rearranging terms, we obtain <sup>2</sup>

$$\begin{aligned} x_{\pi\pi}(p_1, p_2) &= \int R^2 dR d\Omega \int r_s'^2 dr_s' d\Omega'_s \sum_{\Lambda} D_{m_s, \Lambda}^{1*}(\phi, \theta) \rho_{\chi_b}(R) \rho_H(R) N_s j_1(pr'_s) \\ &\quad \times Y_{1, \Lambda}(\theta'_s, \phi'_s) Y_{1m_b}^*(\phi, \theta) x(R) w_I(r'_s, \theta'_s, \phi'_s) \langle \pi(\mathbf{p}_1)\pi(\mathbf{p}_2) | \bar{\psi}\psi(0) | 0 \rangle \end{aligned}$$

---

<sup>2</sup>Here we use the convention that  $D_{m,n}^j(\phi, \theta, \alpha) = e^{im\phi} d_{m,n}^j(\phi, \theta, \alpha) e^{in\alpha}$ .

$$\times \sqrt{\frac{3}{4\pi}} [e^{im\phi} d_{m,1}(\theta) e^{-i\phi'_s} + e^{im\phi} d_{m,-1}(\theta) e^{i\phi'_s}]. \quad (\text{D.13})$$

When carrying out the  $\phi'_s$  integration and rearranging terms, we can omit the summation over  $\Lambda$ . In order to normalize correctly later, we here still keep the integral over  $\phi'_s$ , that is,

$$\begin{aligned} x_{\pi\pi}(p_1, p_2) &= \int R^2 \rho_{\chi_b}(R) x(p, R) \rho_H(R) dR \times \langle \pi(\mathbf{p}_1) \pi(\mathbf{p}_2) | \bar{\psi}\psi(0) | 0 \rangle \\ &\times \int d\Omega D_{m_s,1}^{1*}(\phi, \theta) Y_{1m_b}^*(\phi, \theta) e^{im\phi} \sqrt{\frac{3}{4\pi}} [d_{m,1}(\theta) - d_{m,-1}(\theta)], \end{aligned} \quad (\text{D.14})$$

where

$$x(p, R) = x(R) \int r_s'^2 dr_s' \cos \theta'_s d\theta'_s N_s j_1(pr_s') Y_{11}(\theta'_s, \phi'_s) w_I(r'_s, \theta'_s, \phi'_s). \quad (\text{D.15})$$

We can divide Eq. (D.14) into three parts, that is,

$$x_{\pi\pi}(p_1, p_2) = \int R^2 \rho_H(R) x(p, R) \rho_{\chi_b}(R) dR \times F(m, m_s, m_b), \quad (\text{D.16})$$

where

$$F(m, m_s, m_b) = \sqrt{\frac{3}{4\pi}} \int d\Omega D_{m_s,1}^{1*}(\phi, \theta) Y_{1m_b}^*(\phi, \theta) e^{im\phi} [d_{m,1}(\theta) - d_{m,-1}(\theta)]. \quad (\text{D.17})$$

We choose the right measurement choice of spherical harmonics function  $Y$  and Wigner  $D$  function, that is,

$$Y_{11}(\phi, \theta) = -\sqrt{\frac{3}{8\pi}} \sin \theta e^{i\phi} \quad (\text{D.18})$$

$$Y_{10}(\phi, \theta) = \sqrt{\frac{3}{4\pi}} \cos \theta \quad (\text{D.19})$$

$$Y_{1-1}(\phi, \theta) = \sqrt{\frac{3}{8\pi}} \sin \theta e^{-i\phi}, \quad (\text{D.20})$$

and

$$D_{1,1}^1(\phi, \theta) = \frac{1 + \cos \theta}{2} e^{-i\phi} \quad D_{1,-1}^1(\phi, \theta) = \frac{1 - \cos \theta}{2} e^{-i\phi} \quad (\text{D.21})$$

$$D_{-1,1}^1(\phi, \theta) = \frac{1 - \cos \theta}{2} e^{i\phi} \quad D_{-1,-1}^1(\phi, \theta) = \frac{1 + \cos \theta}{2} e^{i\phi} \quad (\text{D.22})$$

$$D_{0,1}^1(\phi, \theta) = \frac{\sin \theta}{\sqrt{2}} \quad D_{0,-1}^1(\phi, \theta) = -\frac{\sin \theta}{\sqrt{2}}. \quad (\text{D.23})$$

We can show only when

$$m = m_s + m_b, \quad (\text{D.24})$$

$F(m, m_s, m_b)$  is nonzero. Here we list all the cases, that is,

- Case 1)  $m = 1, m_s = 1, m_b = 0$ :  $F(m, m_s, m_b) = \frac{1}{2}$   
Case 2)  $m = 1, m_s = 0, m_b = 1$ :  $F(m, m_s, m_b) = \frac{1}{2}$   
Case 3)  $m = 0, m_s = 1, m_b = -1$ :  $F(m, m_s, m_b) = \frac{1}{2}$   
Case 4)  $m = 0, m_s = 0, m_b = 0$ :  $F(m, m_s, m_b) = 0$   
Case 5)  $m = 0, m_s = -1, m_b = 1$ :  $F(m, m_s, m_b) = \frac{1}{2}$   
Case 6)  $m = -1, m_s = -1, m_b = 0$ :  $F(m, m_s, m_b) = \frac{1}{2}$   
Case 7)  $m = -1, m_s = 0, m_b = -1$ :  $F(m, m_s, m_b) = \frac{1}{2}$ .

Finally, we obtain

$$x_{\pi\pi}(p_1, p_2) = \frac{1}{2} \int R^2 \rho_H(R) x(p, R) \rho_{\chi_b}(R) dR \times \langle \pi(\mathbf{p}_1) \pi(\mathbf{p}_2) | \bar{\psi} \psi(0) | 0 \rangle. \quad (\text{D.25})$$

If we introduce the reduced radial wave function  $u_H(R) = R\rho_H(R)$ , and the reduced radial wave function  $u_{\chi_b}(R) = R\rho_{\chi_b}(R)$ , we rewrite above equation as

$$x_{\pi\pi}(p_1, p_2) = \frac{1}{2} \int u_H(R) x(p, R) u_{\chi_b}(R) dR \times \langle \pi(\mathbf{p}_1) \pi(\mathbf{p}_2) | \bar{\psi} \psi(0) | 0 \rangle. \quad (\text{D.26})$$

If we denote

$$x(p) = \frac{1}{2} \int u_H(R) x(p, R) u_{\chi_b}(R) dR, \quad (\text{D.27})$$

we have

$$x_{\pi\pi}(p) = x(p_1, p_2) \langle \pi(\mathbf{p}_1) \pi(\mathbf{p}_2) | \bar{\psi} \psi(0) | 0 \rangle. \quad (\text{D.28})$$

In Chapter 8, we use Eq. (D.26) to calculate the  $x_{\pi\pi}(p)$ .

The integration is done in the body-fixed frame. Since the transition amplitude is computed on the lattice, we replace the continuous integration with a lattice sum. The wave function is measured in lattice momentum space for a lattice of spatial size  $a^3 L^3$  through the expansion

$$w_I(x, y, z) = \sum_{k_x \neq 0, k_y, k_z} w_I(k_x, k_y, k_z) \sin(k_x x) \cos(k_y y) \cos(k_z z), \quad (\text{D.29})$$

In this approximation

$$x(p, R) = \frac{1}{L^3} \sum_{k_x \neq 0, k_y, k_z} \sum_{x, y, z} a^3 N_s j_1(pr'_s) Y_{11}(\theta'_s, \phi'_s) x(\mathbf{k}, R) \sin(k_x x) \cos(k_y y) \cos(k_z z). \quad (\text{D.30})$$

With a sufficiently large lattice volume the overlap sum over coordinates  $(x, y, z)$  recovers the continuum momentum conservation constraint  $p = |\mathbf{k}|$ . Here we use Eq. (7.22).



Now we discuss how to calculate the above equation numerically. First we calculate the  $N_s$ , this number come from the normalized condition

$$\sum_{x,y,z} N_s^2 |j_1(pr)Y_{11}(\theta, \phi)|^2 = 1, \quad (\text{D.31})$$

where

$$Y_{11}(\theta, \phi) = \frac{x + iy}{r} \quad (\text{D.32})$$

$$j_1(pr) = \frac{\sin(pr)}{p^2 r^2} - \frac{\cos(pr)}{pr}, \quad (\text{D.33})$$

here  $r = \sqrt{x^2 + y^2 + z^2}$ . Then we can use Eq. (D.30) to calculate  $x(p, R)$  at any given momentum  $p$ .

In practice, we can rewrite Eq. (D.25) as

$$\begin{aligned} x_{\pi\pi}(p_1, p_2) &= \frac{1}{L^3} \sum_{k_x \neq 0, k_y, k_z} \sum_{x,y,z} a^3 N_s j_1(pr'_s) Y_{11}(\theta'_s, \phi'_s) \\ &\times \tilde{x}(\mathbf{k}) \langle \pi(\mathbf{p}_1) \pi(\mathbf{p}_2) | \bar{\psi} \psi(0) | 0 \rangle \sin(k_x x) \cos(k_y y) \cos(k_z z), \end{aligned} \quad (\text{D.34})$$

where

$$\tilde{x}(\mathbf{k}) = \frac{1}{2} \int u_H(R) x(\mathbf{k}, R) u_{\chi_b}(R) dR. \quad (\text{D.35})$$

From Chapter 7, we know,

$$\langle \pi(\mathbf{p}_1) \pi(\mathbf{p}_2) | \bar{\psi} \psi(0) | 0 \rangle = \hat{b}_{\pi\pi} \frac{1}{\sqrt{2E_\pi(\mathbf{p}_1)} \sqrt{2E_\pi(\mathbf{p}_2)}}, \quad (\text{D.36})$$

where  $b_{\pi\pi}$  is denoted in Eq. (7.42). For notational simplicity, we define

$$\hat{x}(\mathbf{k}) \equiv \tilde{x}(\mathbf{k}) \hat{b}_{\pi\pi}. \quad (\text{D.37})$$

If we define

$$\hat{x}_{\pi\pi}(p) = \frac{1}{L^3} \sum_{k_x \neq 0, k_y, k_z} \sum_{x,y,z} a^3 N_s j_1(pr'_s) Y_{11}(\theta'_s, \phi'_s) \hat{x}(\mathbf{k}) \sin(k_x x) \cos(k_y y) \cos(k_z z), \quad (\text{D.38})$$

then

$$x_{\pi\pi}(p_1, p_2) = \hat{x}_{\pi\pi}(p) \frac{1}{\sqrt{2E_\pi(\mathbf{p}_1)} \sqrt{2E_\pi(\mathbf{p}_2)}}. \quad (\text{D.39})$$

## APPENDIX E

### THREE-BODY PHASE SPACE

In this dissertation, we are interested in the decay

$$H \rightarrow \chi_b + \pi + \pi, \quad (\text{E.1})$$

where two-pion final state is in an scalar singlet channel. In Appendix D, we calculated the transition amplitude  $x_{\pi\pi}(p)$  for two-pion production as a function of the momentum  $p$  of the two-pion system in the rest frame of the  $H$ .

The starting point is the Fermi's Golden rule, that is,

$$d\Gamma = \frac{1}{(2\pi)^3} |\langle f|V_I|i\rangle|^2 (2\pi)^4 \delta^4(p_f - p_i) df, \quad (\text{E.2})$$

where  $\langle f|V_I|i\rangle$  is the transition amplitude from initial state  $i$  to the final state  $f$ ,  $df$  is the phase space factor.

The general rule is that the various factors in the phase space are determined by the normalization of the states. From the definition in Eq. (D.2), we can show that the initial state  $|H\rangle$  is normalized as

$$\int d^3\mathbf{p}_H |\mathbf{p}_H\rangle \langle \mathbf{p}_H| = 1, \quad (\text{E.3})$$

and from the definition in Eq. (D.5), the final state  $|A\rangle$  is normalized as

$$\int d^3\mathbf{p}_A |\mathbf{p}_A\rangle \langle \mathbf{p}_A| = 1, \quad (\text{E.4})$$

Hence, they should not give a factor in the phase space formula. There are two other momentum factors in our phase space formula, called  $p_1$  and  $p_2$ . From the Ref. [64], they are normalized as

$$\sum_{\mathbf{p}_1} \sum_{\mathbf{p}_2} |\mathbf{p}_1 \mathbf{p}_2\rangle \langle \mathbf{p}_1 \mathbf{p}_2| = 1, \quad (\text{E.5})$$

They are replaced by  $p = p_{12}$ , the total momentum of the two pions and  $p_1 = k$ , the momentum of one of the pions. In the analysis of the bubble diagram the momenta  $p$  and  $k$  are quantized in a box and summed. Hence the phase space factor

$$df = d^3\mathbf{p}_A \frac{L^3 a^3}{(2\pi)^3 2E_1} d^3\mathbf{p}_1 \frac{L^3 a^3}{(2\pi)^3 2E_2} d^3\mathbf{p}_2, \quad (\text{E.6})$$

where  $E_1, E_2$  are the energies of two pions. Hence, according to Fermi's Golden rule, we obtain transition rate ( $\Gamma$ ) by

$$\begin{aligned} \Gamma = & \frac{1}{(2\pi)^3} \int dp \int d^3\mathbf{p}_A \frac{L^3 a^3}{(2\pi)^3 2E_1} d^3\mathbf{p}_1 \frac{L^3 a^3}{(2\pi)^3 2E_2} d^3\mathbf{p}_2 (2\pi)^4 \delta^4(p_A + p_1 + p_2 - p_H) \\ & \delta(|\mathbf{p}_{12}| - p) \hat{x}_{\pi\pi}(p)^2, \end{aligned} \quad (\text{E.7})$$

where  $p_H$  is the four momentum of initial hybrid exotic state  $H$ ,  $p_A$  is the four momentum of  $\chi_b$  final state,  $p_1$  is the four momentum of one pion final state,  $p_2$  is the four momentum of other pion final state, we denote  $p_{12} \equiv p_1 + p_2$ , and where  $\hat{x}_{\pi\pi}(p)$  is denoted in Eq. (7.40), which is the transition amplitude from initial state to the final state.

To simplify the integration in Eq. (E.7), we introduce the integral over the intermediate four momentum  $p_{12}$  and its invariant mass  $s \equiv p_{12}^2 = E_{12}^2 - |\mathbf{p}_{12}|^2$ . We rewrite the Eq. (E.7) as

$$\begin{aligned} \Gamma = & \frac{1}{(2\pi)^3} \left( \frac{La}{2\pi} \right)^6 \int dp dE_{12} d^3\mathbf{p}_A d^3\mathbf{p}_{12} (2\pi)^4 \delta^4(p_A + p_1 + p_2 - p_H) \\ & \times F_{12}(s) \delta(|\mathbf{p}_{12}| - p) \hat{x}_{\pi\pi}(p)^2, \end{aligned} \quad (\text{E.8})$$

where  $d^3\mathbf{p}_A = |\mathbf{p}_A|^2 d|\mathbf{p}_A| \sin\theta d\theta d\phi$ , and  $F_{12}(s)$  is the two-body phase space factor for two-pion system, that is,

$$F_{12}(s) = \int \frac{d^3\mathbf{p}_1}{2E_1} \frac{d^3\mathbf{p}_2}{2E_2} \delta^4(p_{12} - p_1 - p_2), \quad (\text{E.9})$$

where  $d^3\mathbf{p}_1 = |\mathbf{p}_1|^2 d|\mathbf{p}_1| \sin\theta d\theta d\phi$ . This phase space factor is a Lorentz invariant. Thus we can easily evaluate it in the rest frame of two-pion system, that is,

$$F_{12}(s) = 4\pi \int \frac{|\mathbf{p}_1|^2}{2E_1 2E_2} d|\mathbf{p}_1| \delta(E_1 + E_2 - \sqrt{s})$$

$$= \pi \sqrt{\frac{1}{4} - \frac{m_\pi^2}{s}}, \quad (\text{E.10})$$

where  $m_\pi$  is the mass of the pion meson. Therefore, we obtain

$$\begin{aligned} \Gamma &= 2\pi^2 \left(\frac{La}{2\pi}\right)^6 \int dp dE_{12} d^3\mathbf{p}_A d^3\mathbf{p}_{12} \delta^4(p_A + p_1 + p_2 - p_H) \\ &\times \sqrt{\frac{1}{4} - \frac{m_\pi^2}{s}} \delta(|\mathbf{p}_{12}| - p) \hat{x}_{\pi\pi}(p)^2. \end{aligned} \quad (\text{E.11})$$

In the rest frame of the  $H$  we integrate above equation, and we obtain

$$\Gamma = 8\pi^3 \left(\frac{La}{2\pi}\right)^6 \int dp dE_{12} |\mathbf{p}_A|^2 d|\mathbf{p}_A| \delta(E_A + E_{12} - M_H) \sqrt{\frac{1}{4} - \frac{m_\pi^2}{s}} \delta(|\mathbf{p}_A| - p) \hat{x}_{\pi\pi}(p)^2, \quad (\text{E.12})$$

In the rest frame of the  $H$  we integrate over  $|\mathbf{p}_A| = p$  and  $s$  to get

$$\Gamma = 8\pi^3 \left(\frac{La}{2\pi}\right)^6 \int_0^{p_{\max}} dp p^2 \hat{x}_{\pi\pi}(p)^2 \sqrt{\frac{1}{4} - \frac{m_\pi^2}{(\Delta M)^2 - p^2}}, \quad (\text{E.13})$$

where we approximate  $E_A = M_A$ , and define  $\Delta M = M_H - M_A$ . If we consider  $(\Delta M)^2 - p^2 \geq 4m_\pi^2$ , we have

$$p_{\max} = \sqrt{(\Delta M)^2 - 4m_\pi^2}. \quad (\text{E.14})$$

## REFERENCES

- [1] D. Besson et al. Observation of new structure in the  $e^+e^-$  annihilation cross-section above  $b\bar{b}$  threshold. *Phys. Rev. Lett.*, 54:381, 1985.
- [2] D. M. J. Lovelock et al. Masses, widths, and leptonic widths of the higher  $\Upsilon$  resonances. *Phys. Rev. Lett.*, 54:377–380, 1985.
- [3] J. Kuti. Exotica and the confining flux. *Nucl. Phys. Proc. Suppl.*, 73:72–85, 1999.
- [4] C. McNeile, C. Michael, and P. Pennanen. Hybrid meson decay from the lattice. *Phys. Rev.*, D65:094505, 2002.
- [5] K. J. Juge, J. Kuti, and C. J. Morningstar. Ab initio study of hybrid  $\bar{b}gb$  mesons. *Phys. Rev. Lett.*, 82:4400–4403, 1999.
- [6] Gunnar S. Bali et al. Static potentials and glueball masses from QCD simulations with wilson sea quarks. *Phys. Rev.*, D62:054503, 2000.
- [7] P. Hasenfratz, R. R. Horgan, J. Kuti, and J. M. Richard. The effects of colored glue in the QCD motivated bag of heavy quark-antiquark systems. *Phys. Lett.*, B95:299, 1980.
- [8] D. Horn and J. Mandula. A model of mesons with constituent gluons. *Phys. Rev.*, D17:898, 1978.
- [9] Kostas Orginos, Doug Toussaint, and R. L. Sugar. Variants of fattening and flavor symmetry restoration. *Phys. Rev.*, D60:054503, 1999.
- [10] C. Aubin et al. Light hadrons with improved staggered quarks: Approaching the continuum limit. *Phys. Rev.*, D70:094505, 2004.
- [11] Steven A. Gottlieb, W. Liu, D. Toussaint, R. L. Renken, and R. L. Sugar. Hybrid molecular dynamics algorithms for the numerical simulation of quantum chromodynamics. *Phys. Rev.*, D35:2531–2542, 1987.
- [12] K. Hagiwara et al. Review of particle physics. *Phys. Rev.*, D66:010001, 2002.
- [13] David J. Griffiths. *Introduction to Elementary Particles*. Wiley, New York, 1987.
- [14] D. H. Perkins. *Introduction to High Energy Physics*. Addison-wesley, Reading, USA, 1982.

- [15] I. Montvay and G. Munster. Quantum fields on a lattice. Cambridge, UK: Univ. Pr. (1994) 491 p. (Cambridge monographs on mathematical physics).
- [16] H. J. Rothe. Lattice gauge theories: An introduction. *World Sci. Lect. Notes Phys.*, 43:1–381, 1992.
- [17] G. Mack. Physical principles, geometrical aspects, and locality properties of gauge field theories. *Fortschr. Phys.*, 29:135, 1981.
- [18] Tai Tsun Wu and Chen Ning Yang. Concept of nonintegrable phase factors and global formulation of gauge fields. *Phys. Rev.*, D12:3845–3857, 1975.
- [19] Chen-Ning Yang. Integral formalism for gauge fields. *Phys. Rev. Lett.*, 33:445–447, 1974.
- [20] F. J. Dyson. The S matrix in quantum electrodynamics. *Phys. Rev.*, 75:1736–1755, 1949.
- [21] R. P. Feynman. Space-time approach to nonrelativistic quantum mechanics. *Rev. Mod. Phys.*, 20:367–387, 1948.
- [22] J. F. Donoghue, E. Golowich, and Barry R. Holstein. Dynamics of the standard model. *Camb. Monogr. Part. Phys. Nucl. Phys. Cosmol.*, 2:1–540, 1992.
- [23] L. Maiani and M. Testa. Final state interactions from Euclidean correlation functions. *Phys. Lett.*, B245:585–590, 1990.
- [24] Thomas DeGrand. Lattice QCD at the end of 2003. *Int. J. Mod. Phys.*, A19:1337–1394, 2004.
- [25] Claude W. Bernard et al. Continuum limit of lattice QCD with staggered quarks in the quenched approximation: A critical role for the chiral extrapolation. *Phys. Rev. Lett.*, 81:3087–3090, 1998.
- [26] Kenneth G. Wilson. Confinement of quarks. *Phys. Rev.*, D10:2445–2459, 1974.
- [27] K. Symanzik. Continuum limit and improved action in lattice theories. 1. principles and  $\phi^4$  theory. *Nucl. Phys.*, B226:187, 1983.
- [28] Claude W. Bernard et al. Quenched hadron spectroscopy with improved staggered quark action. *Phys. Rev.*, D58:014503, 1998.
- [29] John B. Kogut. A review of the lattice gauge theory approach to quantum chromodynamics. *Rev. Mod. Phys.*, 55:775, 1983.
- [30] Rajan Gupta, Gerald Guralnik, Gregory W. Kilcup, and Stephen R. Sharpe. The quenched spectrum with staggered fermions. *Phys. Rev.*, D43:2003–2026, 1991.
- [31] H. Kluberg-Stern, A. Morel, O. Napoly, and B. Petersson. Flavors of lagrangian

- susskind fermions. *Nucl. Phys.*, B220:447, 1983.
- [32] K. C. Bowler, C. B. Chalmers, R. D. Kenway, D. Roweth, and D. Stephenson. Quenched hadron mass calculations using staggered fermions at  $\beta = 6.15$  and 6.3. *Nucl. Phys.*, B296:732, 1988.
  - [33] Joel Giedt. Toward a systematic analysis of the fourth-root trick. 2005. *hep-lat/0507002*.
  - [34] J. Polonyi, H. W. Wyld, J. B. Kogut, J. Shigemitsu, and D. K. Sinclair. Finite temperature phase transitions in SU(3) lattice gauge theory with dynamical, light fermions. *Phys. Rev. Lett.*, 53:644, 1984.
  - [35] Simon Duane and John B. Kogut. Hybrid stochastic differential equations applied to quantum chromodynamics. *Phys. Rev. Lett.*, 55:2774, 1985.
  - [36] S. Duane and J. B. Kogut. The theory of hybrid stochastic algorithms. *Nucl. Phys.*, B275:398, 1986.
  - [37] G. G. Batrouni et al. Langevin simulations of lattice field theories. *Phys. Rev.*, D32:2736, 1985.
  - [38] Claude W. Bernard et al. The QCD spectrum with three quark flavors. *Phys. Rev.*, D64:054506, 2001.
  - [39] David J. Griffiths. *Introduction to Quantum Mechanics*. A Simon Schuster Company, Englewood Cliffs, New Jersey 07632, 1994.
  - [40] M. Falcioni, M. L. Paciello, G. Parisi, and B. Taglienti. Again on  $SU(3)$  glueball mass. *Nucl. Phys.*, B251:624–632, 1985.
  - [41] G. Parisi, R. Petronzio, and F. Rapuano. A measurement of the string tension near the continuum limit. *Phys. Lett.*, B128:418, 1983.
  - [42] C Legeland, M Lutgemeier, and T Scheideler. Smearing and the string tension. *BI-TP 96/30*.
  - [43] C. Legeland, B. Beinlich, M. Lutgemeier, A. Peikert, and T. Scheideler. The string tension in SU(N) gauge theory from a careful analysis of smearing parameters. *Nucl. Phys. Proc. Suppl.*, 63:260–262, 1998.
  - [44] J. Engels et al. A study of finite temperature gauge theory in (2+1) dimensions. *Nucl. Phys. Proc. Suppl.*, 53:420–422, 1997.
  - [45] M. Albanese et al. Glueball masses and string tension in lattice QCD. *Phys. Lett.*, B192:163, 1987.
  - [46] Tom Blum et al. Improving flavor symmetry in the kogut-susskind hadron spectrum. *Phys. Rev.*, D55:1133–1137, 1997.

- [47] William H. Press, Saul A. Teukolsky, William T. Vetterling, and Brian P. Flannery. *Numerical Recipes in C++*. Cambridge University Press, The Pitt Building, Trumpington Street, Cambridge, United Kingdom, 2002.
- [48] Claude W. Bernard et al. The static quark potential in three flavor QCD. *Phys. Rev.*, D62:034503, 2000.
- [49] S. P. Booth et al. The running coupling from SU(3) lattice gauge theory. *Phys. Lett.*, B294:385–390, 1992.
- [50] P. Weisz. Continuum limit improved lattice action for pure Yang-Mills theory. 1. *Nucl. Phys.*, B212:1, 1983.
- [51] Frederic D. R. Bonnet, Patrick O. Bowman, Derek B. Leinweber, Anthony G. Williams, and James M. Zanotti. Infinite volume and continuum limits of the landau-gauge gluon propagator. *Phys. Rev.*, D64:034501, 2001.
- [52] Nora Brambilla, Antonio Pineda, Joan Soto, and Antonio Vairo. Potential NRQCD: An effective theory for heavy quarkonium. *Nucl. Phys.*, B566:275, 2000.
- [53] Landau, L. D. and Lifshitz. *Quantum Mechanics*. Pergamon Press, New York, USA, 1965.
- [54] Colin J. Morningstar. The heavy quark selfenergy in nonrelativistic lattice QCD. *Phys. Rev.*, D48:2265–2278, 1993.
- [55] Aida X. El-Khadra, Andreas S. Kronfeld, Paul B. Mackenzie, Sinead M. Ryan, and James N. Simone. B and d meson decay constants in lattice QCD. *Phys. Rev.*, D58:014506, 1998.
- [56] Paul Geiger and Eric S. Swanson. Distinguishing among strong decay models. *Phys. Rev.*, D50:6855–6862, 1994.
- [57] Philip R. Page, Eric S. Swanson, and Adam P. Szczepaniak. Hybrid meson decay phenomenology. *Phys. Rev.*, D59:034016, 1999.
- [58] Chris Michael. Quarkonia and hybrids from the lattice. 1999. *hep-ph/9911219*.
- [59] Philip R. Page. Symmetrization selection rules. ii. *Phys. Lett.*, B402:183–188, 1997.
- [60] C. Aubin and C. Bernard. Pion and kaon masses in staggered chiral perturbation theory. *Phys. Rev.*, D68:034014, 2003.
- [61] S. F. Edwards and P. Anderson. Theory of spin glasses. *J. Phys.*, F 5:965, 1975.
- [62] K. Splittorff and J. J. M. Verbaarschot. Replica limit of the toda lattice equation. *Phys. Rev. Lett.*, 90:041601, 2003.



- [63] S. Prelovsek. Effects of staggered fermions and mixed actions on the scalar correlator. *Phys. Rev.*, D73:014506, 2006.
- [64] C. Bernard, C. DeTar, Ziwen Fu, and Sasa Prelovsek. Scalar meson spectroscopy with lattice staggered fermions, University of Utah, 2006, in preparation.
- [65] Keiji Igi and Kenichi Hikasa. Another look at  $\pi\pi$  scattering in the scalar channel. *Phys. Rev.*, D59:034005, 1999.
- [66] C. Aubin et al. Light pseudoscalar decay constants, quark masses, and low energy constants from three-flavor lattice QCD. *Phys. Rev.*, D70:114501, 2004.
- [67] Anthony M. Green, C. Michael, and P. S. Spencer. The structure of flux-tubes in SU(2). *Phys. Rev.*, D55:1216–1225, 1997.
- [68] T. Hatsuda and T. Kunihiro. The  $\sigma$ -meson and  $\pi\pi$  correlation in hot/dense medium: Soft modes for chiral transition in QCD. 2001. *nucl-th/0112027*.
- [69] E. M. Aitala et al. Dalitz plot analysis of the decay  $D^+ \rightarrow K^- \pi^+ \pi^+$  and study of the  $K\pi$  scalar amplitudes. *Phys. Rev. Lett.*, 89:121801, 2002.
- [70] J. E. Augustin et al. Study of the  $J/\psi$  decay into five pions. *Nucl. Phys.*, B320:1, 1989.
- [71] C. Amsler et al. High statistics study of  $f_0$  (1500) decay into  $\eta\eta$ . *Phys. Lett.*, B353:571–577, 1995.
- [72] F. Antinori et al. A further study of the centrally produced  $\pi^+\pi^-$  and  $\pi^+\pi^-\pi^+\pi^-$  channels in  $pp$  interactions at 300 GeV/c and 450 GeV/c. *Phys. Lett.*, B353:589–594, 1995.
- [73] Shin Ishida et al. An analysis of  $\pi\pi$  scattering phase shift and existence of  $\sigma(555)$  particle. *Prog. Theor. Phys.*, 95:745–766, 1996.
- [74] Muneyuki Ishida, Shin Ishida, Taku Ishida, Kunio Takamatsu, and Tsuneaki Tsuru. Observed properties of  $\sigma$ -particle. 1999. *hep-ph/9905261*.
- [75] P. Lacock, C. Michael, P. Boyle, and P. Rowland. Hybrid mesons from quenched QCD. *Phys. Lett.*, B401:308–312, 1997.
- [76] P. Lacock and K. Schilling. Hybrid and orbitally excited mesons in full QCD. *Nucl. Phys. Proc. Suppl.*, 73:261–263, 1999.
- [77] Zhong-Hao Mei and Xiang-Qian Luo. Exotic mesons from quantum chromodynamics with improved gluon and quark actions on the anisotropic lattice. *Int. J. Mod. Phys.*, A18:5713, 2003.
- [78] C. Bernard et al. Lattice calculation of  $1^{-+}$  hybrid mesons with improved kogut-susskind fermions. *Phys. Rev.*, D68:074505, 2003.

- [79] Daniel S. Carman. Gluex: The search for gluonic excitations at Jefferson laboratory. *AIP Conf. Proc.*, 814:173–182, 2006.
- [80] G. M. Beladidze et al. Study of  $\pi^- n \rightarrow \eta \pi^- n$  and  $\pi^- n \rightarrow \eta' \pi^- n$  reactions at 37 GeV/c. *Phys. Lett.*, B313:276–282, 1993.
- [81] D. R. Thompson et al. Evidence for exotic meson production in the reaction  $\pi^- p \rightarrow \eta \pi^- p$  at 18 GeV/c. *Phys. Rev. Lett.*, 79:1630–1633, 1997.
- [82] A. Abele et al. Exotic  $\eta\pi$  state in  $\bar{p}d$  annihilation at rest into  $\pi^- \pi^0 \eta p$ (spectator). *Phys. Lett.*, B423:175–184, 1998.
- [83] S. Eidelman et al. Review of particle physics. *Phys. Lett.*, B592:1, 2004.
- [84] G. S. Adams et al. Observation of a new  $J^{PC} = 1^{-+}$  exotic state in the reaction  $\pi^+ p \rightarrow \pi^+ \pi^+ \pi^+ p$  at 18 GeV/c. *Phys. Rev. Lett.*, 81:5760–5763, 1998.
- [85] E. I. Ivanov et al. Observation of exotic meson production in the reaction  $\pi + p \rightarrow \eta' + \pi + p$  at 18 GeV/c. *Phys. Rev. Lett.*, 86:3977–3980, 2001.
- [86] J. Kuhn et al. Exotic meson production in the  $f_1(1285)\pi^-$  system observed in the reaction  $\pi + p \rightarrow \eta + \pi + \pi + \pi + p$  at 18 GeV/c. *Phys. Lett.*, B595:109–117, 2004.
- [87] M. Lu et al. Exotic meson decay to omega  $\pi^0 \pi^-$ . *Phys. Rev. Lett.*, 94:032002, 2005.
- [88] N. Brambilla et al. Heavy quarkonium physics. 2004. *hep-ph/0412158*.
- [89] Frank E. Close, Isard Dunietz, Philip R. Page, Sinisa Veseli, and Hitoshi Yamamoto. Gluonic hadrons and charmless b decays. *Phys. Rev.*, D57:5653–5657, 1998.
- [90] George Chiladze, Adam F. Falk, and Alexey A. Petrov. Hybrid charmonium production in b decays. *Phys. Rev.*, D58:034013, 1998.
- [91] D. Acosta et al. Observation of the narrow state  $x(3872) \rightarrow J/\psi \pi^+ \pi^-$  in  $\bar{p}p$  collisions at  $s^{**}(1/2) = 1.96$  GeV. *Phys. Rev. Lett.*, 93:072001, 2004.
- [92] V. M. Abazov et al. Observation and properties of the X(3872) decaying to  $J/\psi \pi^+ \pi^-$  in  $p\bar{p}$  collisions at  $s^{**}(1/2) = 1.96$  TeV. *Phys. Rev. Lett.*, 93:162002, 2004.
- [93] B. Aubert et al. Study of the  $b \rightarrow J/\psi k^- \pi^+ \pi^-$  decay and measurement of the  $b \rightarrow x(3872)$  k-branching fraction. *Phys. Rev.*, D71:071103, 2005.
- [94] William A. Bardeen, A. Duncan, E. Eichten, Nathan Isgur, and H. Thacker. Chiral loops and ghost states in the quenched scalar propagator. *Phys. Rev.*, D65:014509, 2002.